ELUCIDATING THE SPATIAL AND TEMPORAL IMMUNE RESPONSE TO IMMUNOMODULATORY MATERIALS

A Dissertation
Presented to
The Academic Faculty

by

Nusaiba Fatemah Baker

In Partial Fulfillment
of the Requirements for the Degree
Doctor of Philosophy in the
Wallace H. Coulter Department of Biomedical Engineering

Georgia Institute of Technology
May 2020

ELUCIDATING THE SPATIAL AND TEMPORAL IMMUNE RESPONSE TO IMMUNOMODULATORY MATERIALS

Approved by:

Dr. Edward Botchwey, PhD, Co-Advisor
School of Biomedical Engineering
Georgia Institute of Technology

Dr. Gabriel Kwong, PhD
School of Biomedical Engineering
Georgia Institute of Technology

Dr. Andrew Neish, MD, Co-Advisor
Department of Pathology
Emory University School of Medicine

Dr. Robert Gross, MD, PhD
School of Biomedical Engineering
Georgia Institute of Technology

Dr. Julie Champion, PhD
School of Chemical and Biomolecular Engineering
Georgia Institute of Technology

Date Approved: March 10, 2020

In memory of Kobe Bean Bryant

ACKNOWLEDGEMENTS

When I started MD/PhD at Emory, I had no idea what was to come. Graduate school has been the biggest challenge of my life, and I have learned so much more than just science over these last few years. That being said, none of this was possible without the incredible support and amazing people I have met along the way. There are so many people who helped and encouraged me, who taught me techniques and skills, and who simply were kind to me during my time of need. I wrote this section of my thesis at the same time that the legendary Kobe Bryant passed away, and it made me reflect on the importance of life and its fragility. I am so thankful to everyone who supported me, who inspired me, and who pushed me to complete both my MD and PhD. This work is dedicated to Kobe, whose Mamba Mentality taught me to work hard and chase my dreams.

First, I have to thank my family. I am so thankful to my parents, who have been the most supportive and most caring people throughout this journey. Without their hard work, dedication, passion, and drive, Hanan and I wouldn't be who we are or where we are today. I am also thankful to my sister, Hanan, whose fearlessness and intelligence earned her a spot at the Weill Cornell MD/PhD program, and who defended her PhD before me. Her thoughtfulness as a scientist and human being inspires me beyond anyone I have ever met.

I am also extremely thankful to my advisors, Dr. Andrew Neish and Dr. Edward Botchwey. Dr. Neish has been an incredibly supportive advisor, who was always there when I needed science advice or personal advice. Dr. Neish was always in my corner, whether it was moving my projects forward, or supporting my career aspirations. Dr. Neish is a great listener and is the reason why I stayed in science when times were hard. His dedication to making sure I was doing my best inspired me to make him proud. I cannot thank him enough for welcoming me into his lab and making sure I graduated with both an MD and a PhD.

Dr. Edward Botchwey has been an incredible mentor and source of inspiration. Joining his lab was one of the biggest blessings that could have happened in my career. Beyond immunology and biomaterials, I was fortunate to be exposed to computational techniques that added more depth to my graduate training than I thought possible. Dr. Botchwey's suggestions and advice were always invaluable, and he was always thinking ahead on how to best represent and characterize our data. His influence will always be with me, even as I move onto a career in surgery.

I owe my utmost gratitude to my thesis committee, which includes Dr. Julie Champion, Dr. Gabriel Kwong and Dr. Robert Gross. Their support and insight has been invaluable and truly changed the trajectory of my graduate career for the better. Their feedback at my thesis proposal was instrumental to helping me identify areas where I needed to improve. Every suggestion was monumental to helping me develop a framework for asking questions and focus my thesis work. Without them, it is unlikely that this document would have been written.

I owe much of my gratitude to Arielle, Amanda, and Stephanie. I never imagined I would meet a group of women in MD/PhD who are so much like me. I am so thankful to have friends who understood every aspect of what I was going through. I could not imagine a better group of friends with whom to take on these eight years.

I am also indebted to the incredible mentors I have had over the years. Kornelia Galior was my first mentor, and she was beyond inspirational. She was able to do anything she put her mind towards, and her infectious smile and joy for life made going to lab so worth it. Kim Clarke was also a close friend and advisor, who spent countless hours helping me organize my thoughts and guiding me in creating powerful presentations. Bridgette Peake was also a huge source of inspiration, and I am so grateful to have worked alongside such a strong and confident woman so early in my career.

I am very grateful to have the opportunity to pursue my graduate career at a school like Georgia Tech. The Biomedical Engineering program is unrivaled in the quality of research and

the opportunity to collaborate. There are many people who helped me along the way, whose kindness and responsiveness helped me gain the confidence in techniques to move my project forward.

My labmates and close friends in the Botchwey lab, Claire McClain, Lauren Hymel, Dre Deveaux, and Thomas Turner are some of the most inspiring, talented, intelligent people I have ever met. I am so excited to see what amazing things they accomplish, how many accolades they all receive, and what high-impact papers they publish. I am so blessed to have spent time with and learn from them. Spending every day in their company brought me so much joy. I wish I could capture that feeling forever.

The Neish lab has the kindest, most incredible friends and scientists I have ever had the pleasure of working with. Bejan Saeedi, Josh Owens, Brian Robinson, Sarah Hunter-Chang, and Huixia Wu are, by far, the most creative, most innovative people I have ever met. Bejan, Josh, Sarah, and Brian were always willing to help me out, listen to my science ideas (even when my ideas involved giving traumatic brain injury to *Drosophila*), and do whatever it took to move science forward. These individuals will be the great PIs of the future, and I am so excited to see what they accomplish.

I am also eternally grateful to Ian Miller and Elda Treviño, whose passions for life and science influenced me daily. Our weekly lunches were one of the main drivers for getting me through the last year of my PhD.

I am also thankful for everyone at Georgia Tech who was willing to go out of their way to show me how to use equipment or teach me new techniques. Sommer Durham is one of the kindest people that I have the pleasure of working with, and she was always responsive and willing to help me in my time of need. Dr. Laura O'Farrell and Dr. Richard Noel were also very understanding, and their passion for their work inspired me with mine. I particularly appreciate Dr. O'Farrell going out of her way to teach me how to collect blood from a rat jugular vein. Her guidance will stay with me as I complete my PhD and return to medical school.

I would also like to thank my PSRC mentor, Dr. Justine Lee, whose influence as a successful surgeon-scientist inspires my career in science. I felt motivated by her successes, and her guidance and support along the way kept me excited about my future career in surgery, and in science.

TABLE OF CONTENTS

LIST OF TABLES

LIST OF FIGURES

LIST OF SYMBOLS AND ABBREVIATIONS

ANOVA	Analysis of Variance
BSA	Bovine serum albumin
CO_2	Carbon dioxide
CXCL	C-X-C ligand
CXCR4	C-X-C chemokine receptor 4
DC	Dendritic cell
DMEM	Dulbecco's Modified Eagle Media
DSWC	Dorsal skinfold window chamber
ECM	Extracellular matrix
FBS	Fetal bovine serum
FGF	Fibroblast growth factor
FSC	Forward scatter
IACUC	Institutional Animal Care and Use Committee
IEL	Intraepithelial lymphocytes
IHC	Immunohistochemistry
IL	Interleukin
IFN	Interferon
i.p	Intraperitoneal
LPS	Lipopolysaccharide
MerTK	Mer receptor tyrosine kinase
Mg/kg	Milligram per kilogram
MMP	Matrix metalloprotease
M1	Classically activated inflammatory macrophage
M2	Alternatively activated macrophages
NIH	National Institutes of Health

PBS	Phosphate buffered saline
PEG	Poly(ethylene glycol)
PEG-MAL	4-arm poly(ethylene glycol)-maleimide
PLGA	Poly(lactic-co-glycolic acid)
PP	Peyer's patches
ROS	Radical oxygen species
SSC	Side scatter
SEM	Standard error of the mean
SI	Small intestine
T_H	T-helper
TNF	Tumor necrosis factor
VEGF	Vascular endothelial growth factor
VPM	Valine-proline-methionine peptide

SUMMARY

Immune pathology is characterized by the dysregulation of cellular homeostasis. The immune system works as complex network between effector and regulatory pathways that balance pro- and anti-inflammatory signals to maintain homeostasis within the body. In normal inflammatory processes, the transition between the initial inflammatory response to the subsequent proliferative phase is an important one, and dysregulation of this process can lead to poor clinical outcomes. When immune cells are unable to mount an appropriate immune response, particularly to a self-antigen, inflammatory disorders and autoimmunity can ensue.

Immune modulation therapy has come to the forefront of basic science and clinical research to either interrupt immune dysregulation or induce a specific immune response. In order to develop novel therapies for targeting the underlying immune processes of inflammatory conditions, it is necessary to elucidate the disease etiology and cellular signals involved in disease progression. The purposeful manipulation of immune cell fates could therefore be useful for promoting an immune response or inhibiting inflammation and promoting healing. Biomaterial-based delivery of therapeutics is one method to enable localized and targeted modulation of the immune system.

This dissertation presents the results of using biomaterials delivery of therapeutic factors to exploit endogenous mechanisms of innate and adaptive immunity to alleviate inflammation and promote the healing response. We hypothesized that biomaterial-based delivery of therapeutics are effective treatments to induce local immunomodulation in both acute and chronic models of inflammation. First, we used flow cytometry to

characterize the spatial and temporal cellular responses to these materials. The analysis of flow cytometry data, however, is subject to some bias, and requires detailed knowledge of underlying cellular phenotypes. Thus, we next employed Spanning-tree Progression Analysis of Density-normalized Events (SPADE), a computational technique for the elucidation of multi-dimensional data. SPADE is able to create a 2D visualization of complex datasets in a branched "tree" without much needed oversight from the user. The usage of this technique allows for the identification of cellular hierarchy, as well as rare events, among subpopulations of immune cells. We identified the unexpected involvement of adaptive immune cell populations in response to immunomodulatory therapeutics. Investigation of the spatial and temporal distribution of innate and adaptive immunity at different stages of immunomodulation reveals variations in the local microenvironment that may be manipulated to enhance therapeutic development. These data suggest that the importance of local biomaterial influence of specific cellular subsets and demonstrated the importance of analytical techniques like SPADE for elucidating cellular heterogeneity.

CHAPTER 1. INTRODUCTION AND SPECIFIC AIMS

1.1 Introduction

Normal healing consists of three main phages: the inflammatory phase, the proliferative phase, and the remodeling phase(1). The inflammatory phase begins with the recruitment of innate immune cells, such as macrophages and neutrophils, to clear debris and prevent infection(2). The transition to the proliferative phase is an important one, with macrophages taking on a pro-regenerative phenotype, characterized as M2 “alternatively-activated” macrophages, and increased expression of anti-inflammatory cytokines(3). Dysregulation of immune homeostasis leads to inflammatory disorders and autoimmune disease. Such diseases, including rheumatoid arthritis, systemic lupus erythematosus, and ulcerative colitis, are a burden to humans because of debilitating illness, high costs for medication, and increased risk of mortality. Current treatments, including small molecule inhibitors and steroids, are often administered systemically by injection, reducing patient compliance. Additionally, these medications are non-specific and frequently result in off-target effects(4).

The immune system is a finely regulated and controlled interplay between activators and inhibitors. In response to an external stimulus, the innate immune system responds to get rid of the pathogen. Tissue engineering as a field has developed biomaterials as scaffolds to modulate or influence the immune response. These scaffolds are carefully selected with ideal chemical and mechanical properties, as well as their biocompatibility with the system of interest(5, 6). Our approach is to engineer biocompatible, yet degradable biomaterial scaffolds to temporally and spatially target the immune system. Moreover, we will use dimensionality reduction techniques to elucidate and better understand the contributions from individual cell populations of the innate and adaptive immune systems.

1.2 Specific Aims

Aim 1. Evaluation of pro-regenerative innate and adaptive immune cell recruitment to areas of injury following administration of dual-loaded immunomodulatory hydrogels.

Aim 1 aims to quantify in vivo changes in the recruitment dynamics and differentiation status of immune cells after delivery of hydrogels. Here, we develop*ed* a PEG-hydrogel system that releases IL-10 and AT-RvD1 at the site of injury using the dorsal skinfold window chamber mouse model. Following delivery, we characterize the spatial and temporal changes in the immune response. We hypothesize that combined delivery of IL-10 and AT-RvD1 can tune the immune response after injury and recruit and polarize anti-inflammatory, pro-regenerative subsets of macrophages and dendritic cells. In Aim 1A, we characterize the manufacturing of AT-RvD1 and IL-10 dual hydrogels. In Aim 1B, we implant hydrogels using the dorsal skinfold window chamber mouse model and isolate individual cell populations by flow cytometry at day 1, day 3, and day 7 following hydrogel delivery. Importantly, control and therapeutic hydrogels are delivered into the same mouse; thus, each therapeutic has its own internal control for comparison. In Aim 1C, we assess cell phenotypes recruited to the hydrogel by SPADE analysis. This dimensionality reduction technique was selected to elucidate the roles of both innate and adaptive immunity in the healing response to hydrogels.

Aim 2. Elucidation of the local and systemic effects on the immune response following oral gavage of immunomodulatory microparticles

Inflammatory bowel diseases (IBD) affect five million people worldwide. IBD includes Crohn's disease and ulcerative colitis, two inflammatory disorders that can range from mild to severe. If IBD is poorly controlled, it can progress lead to a more severe disease, which can cause debilitating pain, bleeding, and in the case of ulcerative colitis, patients have a high likelihood of developing cancer. Areas of chronic gastrointestinal inflammation are driven by hyper reactive

autoimmune cells producing inflammatory cytokines that can lead to damage of the local tissue(7). In this aim, we use previously developed alginate and chitosan microparticles to deliver Salmonella AvrA to the site of inflammation(8). AvrA is an effector protein utilized by Salmonella to modify and block activation of transcriptional activation of a number of inflammatory effector genes(9). The anti-inflammatory properties make AvrA a promising therapeutic for the amelioration of inflammation. We hypothesize that microparticle treatment will result in inhibition of innate immunity in the Peyer's patches.

Specific aim 2A is to elucidate the immune response to AvrA microparticles locally in both small intestine and in gastrointestinal lymphoid tissue (GALT). Specific Aim 2B is to utilize SPADE to identify characteristic leukocyte populations, as well as rare subsets. Aim 2C is to investigate the systemic effects of AvrA microparticles. These data will allow us to determine the spatial response to treatment with AvrA particles in an acute model of systemic inflammation.

Aim 3. Development of nanoparticle-based immune modifiers for the treatment of Th2-mediated disease

A main cause of inflammatory symptoms is the release of cytokines by circulating immune cells from both the innate and adaptive immune systems in response to a stimulus. In some cases, dysregulation of the adaptive immune response can be the major driver of disease. The T-helper cells (Th cells), also known as CD4+ cells, are a type of cell involved in the adaptive immune response, depending on which helper subtype is activated(10). Th1 polarized cells are responsible for intracellular pathogens. Th2 cells are important in the defense against helminths and some allergic reactions. Th17 cells are a subset that have been linked to several inflammatory conditions(10). The production of cytokines by Th2 cells underlies the inappropriate immune response found in some inflammatory and autoimmune disorders, such as ulcerative colitis(11). GATA3 is a transcription factor that is a major factor involved in Th2 differentiation and

activation (12) and has been found to be upregulated in biopsies and serum from patients with inflammatory diseases (13). Therefore, methods to suppress GATA3 expression are being actively pursued as a potential therapy to ameliorate chronic inflammation. We *hypothesize* that DzNPs are an effective method of regulating intracellular GATA3, leading to reduction of Th2-specific cytokines. Aim 3A will investigate DzNP-mediated GATA3 regulation in a Th2 asthma model. Aim 3B will determine efficacy of orally delivered DzNP using an alginate hydrogel delivery method. Using a mouse model of colitis, we will evaluate efficacy of orally delivering GATA3 and TNF-α DzNPs.

1.3 Significance

The use of biomaterials for the local delivery of immunomodulatory factors in an unexplored area that has the potential to be applied to a number of different fields. Our proposed research uses different biomaterials to specifically deliver therapeutics to the site of injury. In the case of aim 1, the combination of IL-10 and AT-RvD1 aims to not only resolve inflammation but polarize the local immune microenvironment into anti-inflammatory phenotypes. Moreover, aim 2 utilizes a bacterial protein to specifically target the inflamed gastrointestinal tract, and locally reduce inflammation at the cellular level. Finally, aim 3 employs a DNA-based technology to inhibit a pro-inflammatory transcription factor and alleviate the actions of a specific subtype of T-cell. Moreover, this work is benefitted by the usage of SPADE, a dimensionality reduction technique that allowed for the characterization of the local and systemic immune response to treatment. SPADE was instrumental in creating a big-picture view of how the therapeutic was influencing the immune system at a cellular level, but also in elucidating the role of some cell populations that we would not have found by traditional flow cytometry techniques.

CHAPTER 2. BACKGROUND

2.1 Roles of the Immune System in Healing and Disease

The immune system detects and eliminates foreign pathogens, tumor cells, and other invading factors, in order to maintain homeostasis(14). The immune system is a network of cells and signaling pathways that eliminate pathogens and infected cells and keep effector cells under control under physiological conditions(15). In order to contain infection by a pathogen, the initial response by the innate immune cells results in an inflammatory response to activate and recruit the appropriate types of cells to eliminate it(16). In the event that inflammatory signaling becomes dysregulated, however, the cellular signals can result in damage to the body's own tissues. In fact, inflammation is a major problem in human diseases, such as rheumatoid arthritis and inflammatory bowel disorders (IBD), wound healing, infection, and cancer(17, 18). Impaired wound healing after surgical procedures is one of the most common complications arising from impaired immune function due to systemic immunosuppression(19, 20). Any environment with excessive cytokine and chemokine production can lead to a persistent immune response and subsequent impaired wound healing in the context of injury or infection. Moreover, this type of environment may potentially lead to the development of inflammatory syndromes or autoimmune disease. The management of chronic wounds and chronic inflammatory conditions poses an enormous economic burden on patients and the healthcare system. Thus, it is imperative to develop novel therapeutic techniques to reduce inflammation and redirect the immune cells towards resolution(21, 22).

2.1.1 Phases of wound healing

Wound healing involves a careful cascade of cells and signals following injury. Wound healing is broken up into three main phases: the inflammatory phase, the proliferative phase, and the maturation/remodeling phase(23-27). Following initial injury, coagulation pathways are activated and result in stopping the outpouring of blood(28). Specific coagulation factors also signal to platelets, causing platelet clotting and subsequent thrombosis(29). Initial vasoconstriction is quickly followed by vasodilation in order to allow for leukocyte recruitment and entry to the site of injury(30).

The inflammatory phase begins as white blood cells and thrombocytes are recruited and begin to secrete inflammatory mediators and cytokines(31). These factors include platelet-derived growth factor (PDGF), serotonin, histamine, fibroblast-growth factor (FGF), among others(32, 33). PDGF attracts fibroblasts, and, with transforming growth factor (TGF) enhances the proliferation of fibroblasts, which are then able to produce collagen to replenish the damaged ECM(29, 34). Crucial to the inflammatory phase is the immediate response by cells from the innate immune system. Neutrophils, monocytes, and endothelial cells adhere to the fibrin scaffold that is set by platelet activation following tissue injury(35). This allows for neutrophils and macrophages to phagocytose cellular debris, preventing infection of the wound(36). Interestingly, some studies have suggested that the adaptive immune system may also play a more significant role in the healing process(19). Because of the contributions of different immune cell types at different phases of the healing cascade, there exists an opportunity to exploit the intrinsic mechanisms of repair in a variety of contexts.

The proliferative phase begins after 6-7 days, and by a week following injury, fibroblasts have begun to lay down new collagen and glycosaminoglycans(37). Re-

epithelialization and neovascularization begin to occur, forming new vessels and cells to bridge the wound. As the wound matures, and more collagen is deposited, the wound starts to contract. The maturation phase starts by week 3, and the wound undergoes progressive remodeling, which can continue for many years. Matrix metalloproteases (MMPs) and tissue inhibitor of metalloproteinase (TIMPs) play important roles in developing and remodeling the ECM(38). Collagen type III is eventually replaced by collagen type I, which is more oriented and reorganized into a lattice made up of glyocsaminoglycans and proteoglycans(39).

2.1.2 Intestinal damage and healing

Damage and impairment of the intestinal barrier are observed in a number of diseases. The integrity of the intestinal barrier allows for luminal bacteria to communicate with the immune system(40). Permeation of the epithelial barrier results in the absorption of toxic and immunogenic factors that cause inflammation and disequilibrium of host homeostasis(41). The gastrointestinal tract is constantly exposed to various antigens, such as enteric bacteria and food. Following injury, the intestinal epithelium undergoes a wound healing process(42). Intestinal wound healing depends on the migration and proliferation of epithelial cells at the site of injury (43). Previous studies have shown that growth factors, cytokines, and the activation of specific signaling pathways are involved in intestinal epithelial wound healing(41, 44, 45).

The etiology of IBD remains unknown, but it has been suggested that disruption of the intestinal barrier and repeated intestinal epithelial damage are highly implicated to be involved in disease pathogenesis and severity(41, 46). As a result, the integrity of the epithelial layer is damaged, which results in aberrant immune cell activation. In both

innate and adaptive immunity, the disruption of mechanisms of regulation may lead to abnormal immune responses to foreign antigens and result in chronic inflammation. In this context, it has been suggested that therapeutic strategies should focus on improving the wound healing response of the intestinal epithelium or reducing the inflammation caused by the immune system(42).

2.2 Role of the Innate Immune System

The innate immune system plays an important role in maintaining homeostasis and restoring homeostasis following tissue injury or infection. In the context of infection, the immediate response of the innate immune system is to mount a rapid, non-specific defense to foreign pathogens(5, 19). Typically found on such pathogens are molecular patterns that stimulate individual cells to identify a target as foreign, and either immediately remove it, or signal to the adaptive immune system to activate a more specific immune response(16, 47).

Infections and similar inflammatory mechanisms are first accompanied by a rapid influx of neutrophils from the periphery to the site of inflammation(48). These cells kill microorganisms, clear infections, and recruit the necessary immune cells. Their ability to kill and clear infections depends on different mechanisms, such as chemotaxis, phagocytosis, and release of reactive oxygen species (ROS) (49, 50).

2.2.1 Neutrophils play several roles in the inflammatory cascade

Neutrophils, also known as polymorphonuclear (PMN) leukocytes, are the most abundant cell type in humans, produced in the bone marrow at 10^{11} per day(51). The maintenance of neutrophil homeostasis is achieved by balancing short lifespans with

regular release from bone marrow. These cells enter circulation and complete their functions in various tissues before being removed by macrophages at the end of the day. Interestingly, macrophages take on anti-inflammatory phenotypes after phagocytosing apoptotic neutrophils(52). Their functions include patrolling for signs of infection, following which they trap and eliminate foreign pathogens(53). Neutrophils respond to multiple signals, by causing the production of several cytokines and inflammatory factors that influence inflammation(54, 55).

Neutrophils have three main functions: phagocytosis, degranulation, and release of nuclear material in neutrophil extracellular traps (NETs)(56). Within their granules are several types of proteins, including cytokines to recruit macrophages promote the neutrophil presence(57). Neutrophils from the blood are mobilized to sites of infection or inflammation through the leukocyte adhesion cascade(58, 59). When an injury occurs, chemoattractants called damage-associated molecular patterns (DAMPs) are released from dying cells to recruit circulating neutrophils. In addition, IL-1a and IL-33 are released from cells following necrotic cell death(60, 61). Following injury, endothelial cells close to the affected site are activated, and begin to express adhesion receptors, like E- and P-selectins(62). Neutrophils are able to bind these receptors, initiating their "rolling' on the endothelium. The neutrophil is then activated by chemokines, which results in neutrophil adhesion to the endothelium(63). This allows for the neutrophil to then transmigrate into the nearby peripheral tissues, where they travel along chemoattractant gradients to elicit their response(64). These chemoattractants also signal to the surrounding tissues to increase immune cell chemotaxis. Examples of such signals are C-X-C motif chemokine ligand 8 (CXCL8) and leukotriene B4 (LTB4)(65).

Neutrophils responding to DAMPs can contribute to and perpetuate sterile tissue injury by the release of toxic effectors, such as reactive oxygen species (ROS)(66). Furthermore, the release of NETs can potentially injure the tissue, and has been attributed to the development of some diseases, such as systemic lupus erythematous (SLE), diabetes, and thrombosis(67). NETs are made up of granular and cytosolic proteins, which could potentially present as autoantigens to host immunity(56, 68). This may signal for the additional release of DAMPs that may amplify the ongoing immune response. Thus, many strategies have been used to interfere with NETs before they can cause additional tissue damage(56).

In the gastrointestinal tract, immune homeostasis is particularly important for maintenance of the epithelial barrier, which prevents antigens from permeating and causing an immune response. Normally, the intestinal epithelium is a physical barrier that presents contact between the luminal microbiota and intestinal mucosa. When the epithelial barrier is affected, increased intestinal permeability is increased, and persistent chronic inflammation can occur(42, 69). Neutrophils are then recruited to the infected site to phagocytose and kill pathogens through their many mechanisms of eradicating pathogens: phagocytosis, ROS, lytic enzymes from granules, and NETs(70).

Recent studies have indicated that neutrophils play an important role in the pathogenesis of IBD, but depending on the experimental model utilized, it is unknown whether neutrophils have a beneficial or deleterious role. For example, depletion of anti-neutrophil antibodies ameliorates colitis induced by dextran sulphate sodium (DSS) or trinitrobenzene (TNBS) in rats(71, 72). Other studies utilized a model of dysregulated

immunity, such as the T-cell transfer model, and found that neutrophils actually play the opposite role in UC pathogenesis.

2.2.2 Macrophages are an important mediator between innate and adaptive immunity

Macrophages exhibit a wide range of phenotypic heterogeneity and have a number of effector functions. Macrophages are involved in mediating communication between the innate and adaptive immune systems, killing pathogens and parasites, and promoting tissue repair(73). In response to tissue injury and during the wound healing cascade, macrophages secrete inflammatory cytokines, matrix degrading factors, and growth factors. However, once the inflammation begins to subside, these innate immune cells can become polarized to take on other fates for the promotion of healing. Macrophages exist on a spectrum from M1 “pro-inflammatory” to M2 “anti-inflammatory” or “regenerative” macrophages(49). The heterogeneity of this cell type allows for the development of biomaterial-based therapies that can manipulate the inherent signalling and effector functions of macrophages.

The presence of IFN γ, lipopolysaccharide (LPS), or TNF cause macrophages to take on an M1 phenotype. This subset of cells releases reactive oxygen species and inflammatory cytokines that promote an immune response, with the goal of ultimately clearing necrotic tissue and recruiting additional immune cell populations(49). These cells also secrete growth factors, including VEGF and FGF2(74). This is necessary for the normal healing response, but persistence of the M1 phenotype can lead to increased tissue damage and a perpetuating inflammatory response(75, 76).

M2 macrophages can be polarized by signals such as IL-4, and IL-13. These cells support the deposition of ECM and promote wound closure via arginase-1 (CD206)

expression. This allows for the development and generation of collagen and FGF, and remodeling of the site of injury(77, 78). The dominant presence of M2 versus M1 macrophages determines the activation status of the immune system, and whether a positive or negative healing outcome will occur(76).

Indeed, macrophages have a crucial role in suppressing the neutrophilic response in autoimmune disorders, such as UC. Macrophages have been previously shown to play an important role in forming noncaseous epithelioid granulomas in the intestinal mucosa. These macrophages produce cytokines, such as TNF, interleukins (Il-6, 8), and others when activated, which signal to surrounding tissue and cells(79, 80).

2.3 Role of the Adaptive Immune System

Compared to innate immunity, the adaptive immune system provides a more specific, but delayed response. Adaptive immunity is regulated by T-cells and B-cells, whose cell surface receptors recognize specific “antigens” or molecular fragments of a pathogen presented to them by antigen-presenting cells (APCs). Typically, the innate immune system will process and present antigen to a T-cell specific for that antigen. Next, the innate cell binds to the naïve T-cell using “costimulatory” receptors(81, 82), which are expressed on innate cells after the pathogen is processed. Lastly, the innate cell will release signaling factors, or cytokines, that activate and condition a specific population of adaptive immune cell. This allows for T-cells to take on specific T effector fates (T_{EFF}), which then have the important job of specifically eradicating the pathogen(83).

During development, T-cell progenitors migrate from the bone marrow to the thymus. During this migration, the T-cells begin to express TCR, and once they reach the

medulla, they express either CD4 or CD8(84). CD4+ cells are known as T-helper cells (Th), and are differentiated into Th1, Th2, Treg, and Th17 subtypes, each with individual functions(85, 86). CD8+ T-cells, or cytotoxic T lymphocytes, are important for immune defense against viruses and bacteria, and play a role in tumor surveillance(87). In the event that the signaling factors from innate to adaptive immunity, or adaptive to adaptive immunity, are regulatory or anti-inflammatory, T-cells can take on an immunosuppressive fate(88, 89). Regulatory T-cells (T_{REGs}) suppress the function of T_{EFFs} and drive the immune system towards immune tolerance. This allows for the suppression of the immune response and return to homeostasis. Several types of Tregs have been identified, such as CD4+ cells, Th3 cells, Tr1 cells, and CD8+ Tregs(90-92).

Adaptive immunity plays an important role in inflammatory disease, particularly in the case in IBD. Alteration in the proliferation of T-cell subsets may cause an increase in cytokines and signaling factors, leading to worsened disease(93). The gut-associated lymphoid tissue (GALT) is where antigens come into contact with effector CD4+ (Th1 and Th2) and CD8+ T-cells(94). Tregs are capable of inhibiting other Th subtypes and have become a popular target for immunomodulatory biomaterials. Tregs are able to suppress autoimmune disease and can induce immunological tolerance(93). In fact, reductions in Tregs were found in colonic mucosa in IBD patients, suggesting an important role for Tregs in its pathogenesis(95).

These studies suggest that Tregs are involved in suppressing the adaptive immune system, and potentially also reeling back the innate immune system. Tregs can do so by inhibiting neutrophil and macrophage activation and inducing macrophage polarization towards M2 phenotypes. There is therefore a complex interplay between innate and

adaptive immune systems in normal wound healing and in disease states. This complex signaling network can be manipulated and harnessed to direct tissue responses using a multifactorial approach.

2.4 The interface between biomaterials and immunology

Biomaterials are defined engineered substances to interact with biological systems to either diagnose, treat, or elucidate mechanisms of disease. The first drug delivery system was described in the mid 1960s, when Folkman and Long introduced encapsulated anesthetic within silicone rubber into the myocardium of an animal to show control of the heart rhythm with release of the drug(96). The observation that small molecules could diffuse through polymers sparked the field of controlled-release technology. In the case of drug delivery, selection of the biomaterial is determined by its compatibility with the contained therapeutic(97). Further, the biomaterial must be able to be delivered in a manner that is translatable to patients and arrive at the organ system of interest. These systems aim to target a specific location for a short or extended period of time to achieve an effect. The method of delivery must be able to keep the enclosed therapeutic intact, and once the destination is reached, release drug in either a constant, oscillating, pulsating, or declining fashion(98). For example, gastrointestinal delivery has proven challenging due to the acidity of the gastric system(99).

Notably, Folkman observed that the material induced inflammation after it was implanted into different tissues(100). As such, a main focus of biocompatible materials is to develop therapeutic materials that are compatible with biological systems, without causing immunogenicity. Recent work has focused on creation of novel materials with

the specific focus of harnessing and directing the power of immune system, without generating an undesired immune response.

2.4.1 Novel molecular therapies for IBD

Treatment for IBD depends on the degree of severity and is different for patients with Crohn's or UC. Current drug treatments aim to induce remission and ameliorate symptoms of disease. However, few therapeutics aim to modify or reverse the underlying causes of pathogenesis(101). Corticosteroids, aminosalicylates, and immunosuppressive agents are all involved in caring for patients with IBD(102). New approaches have used humanized monoclonal antibodies, such as antibodies against TNF or IL-6, which have become the standard of care(103). Because many pro-and anti-inflammatory cytokines are generated by the inflamed gut, TNF is a popular target. TNF inhibitors, like Infliximab, target the Th1 immune response of Crohn's disease. Recent studies have suggested that infliximab may actually deplete some populations of intraepithelial inflammatory cells(104).

Though the development of more immune specific drugs and improved biotechnology has aided the development of novel medications, several challenges exist for therapeutic delivery to the gastrointestinal tract. Oral drug delivery would be the ideal mechanism of delivery. However, the absorption of oral drugs is complex. First, oral drugs must be soluble in gastric fluid for absorption into the stomach, small intestine, or large intestine(105). Furthermore, therapeutics must be able to withstand the low pH of the stomach, which ranges from 0.8-5(106). In addition, current therapeutics have a number of side effects, and preventing those side effects adds a layer of difficulty.

Potential side effects include nephrotoxicity, hepatotoxicity, peptic ulcers, infection, and even cancer(107, 108).

IBD treatment in particular necessitates a balance between therapeutic efficacy and reduced side effects. Potential strategies to increase therapeutic efficacy is by using particle carrier systems, which specifically release drug at the inflamed intestine(109). Because the intestinal barrier is disrupted, causing increased permeability(110, 111), alterations in mucus(112), and loss of epithelium(113), targeted drug delivery offer a range of therapeutic benefits, including preventing uptake by non-inflamed tissues, and the ability to deliver smaller doses, leading to reduced side effects.

Biomaterials research has focused on testing the biocompatibility of polymers and developing these materials as therapeutic agents. Hydrogels have been widely studied due to their ability to ability to form in the presence of cells and proteins, their ability to survive and thrive in biological environments(114), and their tunable physicochemical properties. For example, gelation of hydrogels can be induced by changes in pH(115), temperature, covalent or non-covalent bonding(116), or polymerization. Materials to form hydrogels can also be synthetic, such as poly(ethylene glycol) (PEG), poly(hydroxyethyl methacrylate) or naturally derived, such as collagen, hyaluronan, chitosan, or alginate(117). To design successful therapeutic materials, it is necessary to consider the interplay between the cellular environment and biomaterial.

In the case of normal wounding and wound healing, or in chronic inflammatory disorders, biomaterials have played an important role in delivering therapeutic factors to either enhance the healing process or prevent further inflammation. Recent studies have shown that using materials such as silicone or hyaluronic acid, particularly high

molecular weight hyaluronan (HMWHA), alone, inhibit pro-inflammatory cytokines, such as IL-1β and TNF, and recruit factors that promote a healing response (118, 119). Other studies have attempted to use pre-devised therapeutic tools to augment or engineer the local microenvironment to mobilize reparative cell populations to exert their regenerative potential (120, 121).

In the case of chronic inflammatory disease in the gastrointestinal tract, therapeutic strategies have also focused on using biomaterials to suppress or ameliorate the overwhelming immune response to prevent local tissue damage. A recent study found that by functionalizing nanoparticles with poly(ethylene) glycol (PEG), particles were able to specifically translocate and deposit in inflamed tissues(109). Other potential strategies for drug delivery include liposomes(122), polysaccharide-based and PLA-based nanoparticles(123), and NiMOS(124).

Liposomes have been conjugated with ligands on their surface to specifically bind the receptors of enterocytes. A recent study developed integrin B7 antibody-conjugated liposomes that specifically targeted leukocytes in colonic inflammation. Liposomes have also been used as a delivery vehicle for siRNA. Importantly, these liposomes are usually coated with mucoadhesive polymers, such as chitosan, to remain intact through the gastrointestinal tract(125).

2.4.2 Polysaccharide-based materials

One of the most attractive areas in research is designing nanosystems that can deliver drugs exactly to the site of inflammation, at the right dosage and in an appropriate time frame. Polysaccharide-based materials have the ability to improve and increase the duration of the therapy, and prevent drug degradation(126, 127). These materials are

popular drug carriers, based on their biocompatibility, low toxicity, and low cost(128). Some polysaccharides, such as chitosan, alginate, and hyaluronic acid, have the potential for bio-adhesion by forming non-covalent bonds among functional groups and epithelium(129). Chitosan, for example, is a linear cationic polysaccharide derived from the deacetylation of chitin. Chitosan is often used as a mucosal delivery agent due to its ability to interact with anionic molecules or tissues(130).

Alginic acid is derived from *Pseudomonas aeruginosa*, whose biofilms consist of the β-D-mannuronate and a-L-guluronate units, as well as the cell wall of brown algae(131). Alginate can form hydrogels under mild gelation conditions ideal for protein encapsulation. To enhance the hydrogel mechanical properties, a chitosan coating can be used to form a polyelectrolyte complex and prevent the leakage of encapsulated drug(132, 133). In low pH environments, chitosan amine groups become protonated, which strengthens the electrostatic properties of anionic alginate and cationic chitosan. At intestinal pH, alginate gels swell and the charge of chitosan reverses to negative(134, 135). This swelling allows for the release of loaded drug. The encapsulation within alginate and chitosan also prevents the loaded cargo from enzymatic degradation(126).

Alginate and chitosan are two promising biodegradable polymers that already have widespread usage in the pharmaceutical industry(136, 137). Alginate cross-linking alone has low mechanical stability that results in quick release of drug, thus, alginate nanoparticles and microparticles can be coated with polycationic polymers, such as chitosan or poly-L-lysine, that increase mechanical integrity(138-140). Alginate/chitosan microparticles have been developed specifically for M-cell uptake in the gastrointestinal tract(138, 141). M-cells are specialized epithelial cells located in the Peyer's patches, or

GALT. Alginate-gels have been extensively studied, as calcium ions have a specific interaction with G-units in alginate(142, 143). When a polycation and polyanion are mixed when fully charged, they do not form a gel. The amino-groups on chitosan have pK_a-values around 6.5, whereas the carboxyl-groups from alginate have pK_a values at 3.5, indicating that between pH 4-6 is a strong ionic interaction between positively charged chitosans and negatively-charged alginate(142, 143). In order to take advantage of this, Laroui et al designed a hydrogel made of chitosan and alginate that was sensitive to the pH of the intestine and would collapse once arriving to that specific location. Within the hydrogel were nanoparticles (NPs) containing anti-inflammatory peptides. The ability to protect therapeutic NPs through the stomach for specific release in the small intestine allowed for lower drug doses to be delivered, and the study showed reduction of mucosal inflammation in a mouse model of colitis(144). This unique colon drug formulation, called the NP-in microparticle oral delivery (NiMOS) system has been previously used to deliver plasmid DNA in specific regions of the gastriointestinal tract(145). NiMOS systems combine the ability of nanoparticles to passively target inflamed tissue, whereas microparticles (MPs) provide an increased loading capacity for therapeutics (146, 147).

Another synthetic polymer that has been used for the delivery of therapeutics are PEG hydrogels. PEG-4MAL, in particular, has been used due to its ability to be functionalized with adhesive peptides and crosslinked to generate hydrogels(148). Poly(ethylene glycol) (PEG) is a non-toxic, non-immunogenic(149), water soluble polymer that has been approved for a wide range of biomedical applications. PEG polymers have high water solubility, favorable pharmacokinetics, and can be conjugated with biological molecules(150). In addition, the biocompatible properties of PEG gels are

extended to the conjugated substance, including protection against proteases and reduced clearance(151). PEG has been used to modify therapeutic proteins to increase their solubility, lower toxicity, and prolong their half-life(152). Polymeric materials can be modified via the formation of bonds (cross-linking) or bond breaking (controlled degradation/release)(153). Enzymatic degradation of hydrogels usually occurs in proximity to cells. Notably, sequence-specific degradation can occur by incorporating linkages sensitive to matrix metalloproteinase (MMP) degradation(154). For example, the target sequence GCRDVPMSMRGGDRCG (VPM) has been shown to be degraded by proteases such as MMP-1, MMP-2, and collagenase(155). Thus, it is thought to be a model peptide cross-linker for biological applications.

An advantage of using PEG gels is their ability to incorporate various reactive groups. Michael-type addition of 4- or 8-arm PEG macromers with acrylate, vinyl-sulfone, and thiol end-groups have been studied(156). Maleimide ($H_2C_2(CO)_2NH$) is a compound that is often linked to PEG chains to allow for the linking of proteins to the polymer surface. Maleimides have fast reaction kinetics and high specificity towards cysteines at physiological pH, making them desirable for the development and preparation of targeted therapeutics(157). Importantly, 4-arm PEG-MAL hydrogels exhibit improved cross-linking efficiency, bioligand incorporation, and reaction time scales that can be translatable into the clinic(158). Thus, PEG-4MAL is another biomaterial that may be useful in delivering therapeutics and modulating and directing the immune response.

2.5 Using dimensionality reduction techniques to elucidate cellular heterogeneity in data

Techniques that measure single-cell data can offer precise measures of cellular components and activation profiles representing important functions in biology. Variation of biochemical functions in complex cell populations can be used to extract unique insights into the underlying cellular signaling relationships(159). Flow cytometry is a powerful tool that provides multi-parametric single-cell data of a heterogeneous population of cells(160). This single-cell data allows for quantification of cellular heterogeneity(161, 162), identification of rare cells(87, 163), and analysis and correlation of single-cell features with clinical pathologies(164, 165). Analysis using flow cytometry has becoming increasingly complex, as rapid development of new markers and measurements have grown beyond the ability of conventional manual gating analysis(166, 167). Currently, single-cell flow cytometers provide measurements of up to 12 fluorescent parameters, with the ability to include up to 17 protein parameters(160). In order to adequately analyze this multi-faceted data, it is necessary to have a well-thought out panel, proper controls, and a well-supported gating strategy. With the development of new techniques, such as mass cytometry and new techniques in flow cytometry, more parameters can be tested for than ever before. In fact, mass cytometry allows for the collection of 30-38 antibodies worth of information, providing both intracellular and extracellular information(168).

A major challenge when collecting so much information is deciphering methods to analyze the data. This involves the challenge of elucidating the contribution of each cell to the overall network of information, while minimizing noise and contamination. Importantly, analyzing flow data is subject to quite a bit of bias, and require detailed knowledge of underlying cellular phenotypes. In particular, “gating” of cell populations

is where the researcher selects subsets of cells defined in a biaxial plot of two measurements to calculate a desired phenotype(166). Clustering algorithms have been developed to deal with such data, using unsupervised learning techniques to identify rare cell populations and characterize cell populations across samples(169). Automatic gating algorithms capture abundant cell types at the expense of rare cell types, who are either lost or absorbed into nearby clusters. Due to the high-dimensional nature of multi-color data, novel data analysis tools have been developed to deal with the complex nature of the information obtained, such as SPADE(162) and tSNE(170). These tools derive low-dimensional (2D or 3D) visualizations of that preserve the high-dimensional structure of the dataset.

Spanning-tree Progression Analysis of Density-normalized Events (SPADE) is a computational technique that was developed to create a 2D visualization of multiple populations of cells in a branched "tree"(171). This tree is constructed without much needed oversight from the user. SPADE separates acquired data from flow cytometry and mass cytometry into hierarchically organized clusters that reflect all of the dimensionality in the data(162). Biaxial plots on software such as FlowJo requires the drawing of gates, from which cellular phenotypes can be determined. Instead, SPADE uses topological methods to create geometrical shapes from which clouds of cells are clustered.

SPADE works in four steps(171). First, data is down sampled in a density-dependent manner to normalize the of cellular data. Each cell is identified as a point with multi-dimensions (i.e. the number of cellular markers). Since denser regions represent abundant cell phenotypes, this allows for rare cell types to be equally weighted as abundant cell types. The second step is agglomerative clustering to separate down

sampled data into cell clusters, so that they associate with cells with similar marker makeup. Agglomerative clustering is a bottom-up technique for which each point of data is in 2D space. Each point is a singleton cluster that goes through many iterations to find a pair of clusters that is closest. Clustering iterations continue until the number of clusters reaches an amount specified by the user. The output is a dendrogram, a hierarchical structure, or tree, of clusters. In order to simplify the data, the distance threshold can be set such that every node becomes associated into a cluster. This number of clusters, or nodes, can be modified by techniques such as X-Shift, which uses relative densities to generate centroids(172). The remaining data sets are connected to centroids forming clusters. This algorithm can calculate the number of clusters that can be specified on SPADE in order to obtain unique density-separated populations(173).

Next, SPADE performs minimum spanning tree construction for extraction and creating a summary of the geometry of the cloud(162). This is done by using an algorithm to that links the cell clusters. Lastly, SPADE upsamples the data to map each cell in the dataset to the most similar cluster. Each cell cluster is one node of the tree, and the color of the nodes represents the median intensities of protein markers. This allows for a 2D visualization of how the markers interact, and a thorough analysis of heterogeneity of the diverse cell population. SPADE deals with high-dimensional datasets by using Fruchterman and Reingold algorithms for construction of the tree(174). This means that the creation of the SPADE tree aligns nodes along the longest path of the tree, followed by gradually appending the rest of the nodes to the main arch.

There are many benefits to using SPADE to analyze large datasets. First, an objectively derived topology allows for less subjectivity than gating strategies on FlowJo.

Instead of viewing data in a 2D biaxial plot, SPADE allows for a multidimensional view of cellular phenotypes and expression profiles. In addition, this multidimensional dataset can be uniquely used to identify changes in dimensionality, including differentiation or subtle changes in marker expression as cells transition between phenotypes(163, 165, 171).

There exist some drawbacks to methods like SPADE, however. For example, if many experiments were performed that used different fluorophore-tagged antibodies, it becomes challenging to organize and make conclusions based on the data. In addition, identifying phenotypes when there are multiple markers required can be difficult, especially in cases where cells may be in a transition period or marker expression is changing. To solve this problem, using unsupervised hierarchical clustering methods, such as the creation of heatmaps, can allow for the visualization of marker expression in each node as determined by SPADE at one time. The utilization of a heatmap can be a faster and easier way to organize the median marker expression to quickly identify cell phenotypes of nodes.

SPADE allows for the exploration of high-dimensional datasets in an objective manner. Importantly, SPADE allows for the identification of trends in cellular heterogeneity, as well as the elucidation of rare cell events that may not have been even considered by manual gating. Here, we use SPADE to characterize the immune response to immunomodulatory biomaterials in the context of wound healing and in the gastrointestinal system. These studies highlight the role of dimensionality reduction techniques in painting a full picture of cellular trends in immunomodulation.

CHAPTER 3. DUAL DELIVERY OF IL-10 AND AT-RVD1 FROM RGD-FUNCTIONALIZED PEG HYDROGELS POLARIZE IMMUNE CELLS TOWARDS PRO-REGENERATIVE PHENOTYPES

3.1 Introduction

The immune response to injury is a complex process that involves the orchestration of many different cell populations in coordination to restore tissue homeostasis. In healthy individuals, tissue regeneration can occur without much intervention. However, in the case of disease states, or in wound healing following surgical procedures, the immune response to healing can become dysregulated, and prevent restoration of normal tissue(1, 175, 176). Identification of the key factors required to achieve tissue regeneration has remained elusive, especially in the context of large wounds or transplanted tissues. This can lead to wound closure failure, or a chronic inflammatory state. The involvement of immune cells is required for aspects of development beyond initial inflammation. It has been shown that the specific immune response and the profile of immune cells recruited to the site of injury can determine wound repair quality(177).

Immediately following injury is a cascade of inflammatory signaling that recruits local and blood-derived leukocytes to the wound or transplant site(178). Innate immune cells, cytokines, and lipid mediators have classically been shown to play an early role in directing repair and influencing the immune microenvironment. For example, resolvins are a class of bioactive small molecule lipids that come from the omega-3 polyunsaturated fatty acids eicosapentaenoic acid (EPA) and docosahexaenoic acid (DHA)(179). These lipid mediators act to drive the resolution of inflammation. The “D-series” of resolvins act as endogenous agonists of GPR/32 and ALX/FPR2,

which are expressed broadly throughout immune cells, including lymphocytes, and specialized epithelial cells. AT-RvD1 is part of a class of "specialized proresolving mediators" (SPMs) capable of redirecting the immune response towards resolution and healing. This signaling as a response to injury next effects endothelial cells, which respond to and amplify the signals(180). We have previously utilized Aspirin-Triggered Resolvin D1 (AT-RvD1) to increase the recruitment of anti-inflammatory monocytes and M2 macrophages to an injury site(181).

Macrophages are innate immune cells that play an important role in organ development, host defense, tissue homeostasis, inflammation, and remodeling(182). Their ability to sense and respond to a number of stimuli, combat foreign pathogens, and maintain tissue integrity depicts the unique, yet complex, role they play in immunity. Macrophages are thought to take on a spectrum of roles, spanning from pro-inflammatory to anti-inflammatory. These fates span from naïve (Mo), to classically activated (M1) macrophages containing pro-inflammatory processes, to alternatively activated macrophages (M2), which have anti-inflammatory activity(183).

M1 macrophages are induced by intracellular pathogens and inflammatory cytokines, including IFN- γ and TNF-α, and are characterized by pro-inflammatory cytokine production, such as IL-1B, IL-6, and IL-12(3). The primary function of this subtype is to remove foreign pathogens and tumor cells. M2 anti-inflammatory macrophages are identified by expression of the CD206 mannose receptor in addition to MerTK and CD64(78). M2 macrophages have enhanced phagocytosis abilities, can produce extracellular matrix (ECM) and angiogenic factors, and secrete interleukin 10 (IL-10), a cytokine that plays a critical role in the dampening of immune responses following inflammation.(184) These qualities of IL-10 make it an attractive agent for the promotion of wound healing due to its ability to direct anti-inflammatory effector functions immune cell subsets. Both subsets of macrophages are critical for proper wound healing(185). M1 macrophages remove debris, damaged matrix, and dead cells. Further, they secrete factors such as fibroblast growth factor (FGF) and VEGF that recruit immune cells. The development of new tissue cues the transition from macrophages into the anti-inflammatory state,

which can then secrete anti-inflammatory cytokines, promoting ECM formation and tissue contraction, and initiating the resolution of inflammation and peripheral tolerance(5, 78).

Peripheral tolerance is the process that prevents immune cells from initiating dangerous responses against the body's own tissues. In the context of large injuries or organ transplant, failure of this process can result in dysregulated healing and transplant rejection. This careful balance is mediated by cells from the innate and adaptive immune system, which ensure that the proper signals dictate a pro-inflammatory or anti-inflammatory state(186). Early pro-inflammatory signals and innate cell responses are critical factors in establishing the inflammatory microenvironment. Immature dendritic cells (DCs) express a number of chemokines that are associated with inflammation. Notably, DCs are responsible for detecting and capturing foreign antigen and presenting those antigens to T lymphocytes to induce their actions(187). DCs are also involved in the balance in stimulating the adaptive immune response. In particular, tolerogenic DCs (tolDCs) are involved in communicating the switch to anti-inflammatory phenotypes, and the induction of T-cell polarization towards T-regulatory cells (Treg) via the secretion of cytokines, such as IL-10(188). Interleukin 10 (IL-10) is a cytokine that is expressed by both innate and adaptive immune cells, and plays a critical role in the control of immune response(189). IL-10-producing DCs can induce functional Tregs, which has been shown to reduce the Th17 inflammatory response. Moreover, IL-10 plays an essential role in regulating scar formation during wound healing, reducing scar formation after injury(190). This balance is facilitated by the local micro-environment and the presence of pro- or anti-inflammatory cytokines. Tolerogenic DCs promote resolution of ongoing immune responses and prevention of autoimmunity by generating Tregs and limiting effector T cell differentiation(191, 192). DCs that induce Tregs are characterized by cytokines such as TGF-β and IL-10. Common surface molecules and cytokines used as markers for Tregs are CD25 and IL-10(193). Currently, the balance of effector/regulatory T-cell and M1/M2 macrophages is thought to determine the degree of inflammation or repair(194).

In order to achieve this balance and modulate infiltrating immune cell populations to stimulate repair, we developed a "pro-regenerative" hydrogel via the delivery of AT-RvD1 and IL-10 to specifically recruit and polarize immune cells with anti-inflammatory properties. We have previously shown the utility of AT-RvD1 using a degradable biomaterial to increase the recruitment of anti-inflammatory monocytes and M2 macrophages. AT-RvD1 is part of a class of "specialized proresolving mediators" (SPMs) capable of redirecting the immune response towards resolution and healing. There is thus a important role for AT-RvD1 delivery for the enhancement of wound healing(181). By delivering AT-RvD1 with IL-10, we hypothesize that we can manipulate immune cells to polarize towards anti-inflammatory fates, resulting in recruitment of M2 macrophages, IL-10 expressing DCs, and Tregs. In this study, we show that two bioactive factors, AT-RvD1 and IL-10, are capable of eliciting a synergistic healing response. Using the murine dorsal skinfold window chamber as a test bed to measure the response to immunomodulatory hydrogels, we demonstrate that not only is the recruitment of anti-inflammatory myeloid cells enhanced by AT-RvD1 delivery, but combination IL-10+ATRvD1 treatment is able to concurrently increase populations of macrophages, dendritic cells, and T cells involved in wound healing. These results indicate that dual delivery of IL-10 and AT-RvD1 has broad effects on the recruitment of pro-regenerative, anti-inflammatory innate and adaptive immune cells and can result in the modulation of the immune response after injury to promote tissue regeneration and healing.

3.2 Results

3.2.1 Engineering immunomodulatory hydrogels to promote resolution and immune polarization

A strategy for the promotion of resolution is to modulate the immune profile involved in the inflammatory cascade. In order to modulate the immune response, we identified two factors that play different roles in the inflammatory response, AT-RvD1 and IL-10. AT-RvD1 is

involved in the resolution phase of inflammation, and IL-10 is involved in the polarization phase, influencing the polarization of pro-inflammatory cells to anti-inflammatory cells. In order to increase the half-life of both factors at the site of injury, both were packaged individually or combined into hydrogels for delivery. Here, we used gels formulated by poly(ethylene glycol) (PEG) hydrogels using 10kDa 4-arm PEG macromers containing terminal maleimide groups (PEG-MAL). The cysteine-flanked peptide GCRDVPMSMRGGDRCG (VPM) that contains a protease cleavage site was used to crosslink the PEG-MAL macromers. We expected that protease cleavage of the gels would cause burst release of AT-RvD1, which would promote wound resolution, followed by slow-release of IL-10, which would cause the recruitment and polarization of anti-inflammatory cell subtypes (Figure 1A,B).

We first loaded fluorescently-tagged human IL-10 into a hydrogel and measured its release. Within the first 30 minutes, 58.24±0.67 ng was released, followed by 175±1.34ng after 2 hours, and 209.62±1.73ng after 6 hours. At 24 hours, the gel released 227.40±1.71ng of the loaded IL-10, which was over 90% of the initial dose. By day 5, 235±1.73ng total IL-10 was released, and only 22.39±4.85ng **(**Figure 1C**)** was recovered from the digested gel. To test whether we could achieve gradual release of IL-10, we then attempted to functionalize the IL-10 with free cysteines to allow for interaction with the PEG-MAL macromer. The macromers containing terminal maleimide groups on PEG gels are able to react with free cysteines on peptides or full-length proteins. Since human IL-10 does not have a free cysteine in its structure, and we used Traut's reagent (2-iminothiolane) to thiolate the IL-10. This reagent reacts with primary amines to form sulfhydryl groups. This resulted in about 3 free cysteine groups per IL-10 molecule. In contrast to the unmodified IL-10, thiolated IL-10 releases 7.67 ± 2.76 ng after 30 minutes, 26.91 ± 2.91 ng at 2 hours, 32.39 ± 2.67ng at 6 hours, and 42.03 ± 2.45ng by 24 hours. The thiolated IL-10 released gradually with a measured release of 73.28 ± 3.55ng at 5 days, with 176.72 ± 5.42 ng remaining IL-10 that recovered from the gel after digestion. These data suggest

that thiolation of IL-10 greatly affects release kinetics and allows a more gradual release of therapeutic payload.

We also measured the release of AT-RvD1 and observed that it was released in a manner similar to unmodified IL-10, with 87.66±1.29ng released by 24 hours. By day 5, only an additional 4ng had been released, with total release around 91.24 ±1.11ng (Figure 1D). When the release was measured from dual-loaded gels, there was no effect on the release kinetics of either therapeutic (not shown).

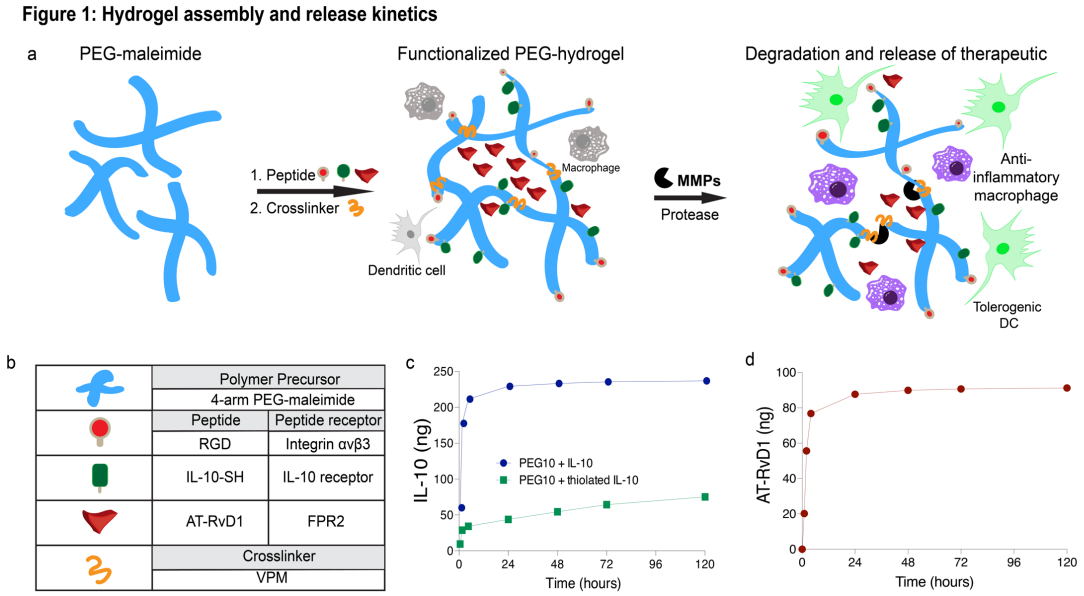

Figure 1. Hydrogel synthesis.

(A) Schematic of hydrogel formulation containing IL-10 and AT-RvD1 (B) Composition of the hydrogel. (C) Release of unthiolated and thiolated IL-10 from 10kDA PEG-MAL hydrogels over the course of 5 days. (D) Release of AT-RvD1 from 10kDA PEG-MAL hydrogels over the course of 5 days.

3.2.2 Anti-inflammatory macrophages and dendritic cells accumulate after local immunomodulatory hydrogel delivery

After profiling the recruitment of circulating immune cell subsets in response to immunomodulatory hydrogels, we extended our analysis to specific macrophage subpopulations. We examined dynamic changes in macrophages at days 1, 3, and 7 after tissue injury and implantation of PEG-MAL hydrogels. Expansion of macrophage populations is a hallmark of the resolution of inflammation and is necessary for tissue regeneration and wound healing (195). We then used flow cytometry to identify specific macrophage subpopulations present in the tissues over time. Macrophages are identifiable with flow cytometry by their surface receptor expression of MerTK and CD64(196).

Macrophages were subclassified into M1 and M2 phenotypes as previously described (197). M1 "classically activated" macrophages were characterized by their expression of the costimulatory molecule CD86 and did not express the mannose receptor CD206. Temporally, we observed an increase in the M1 population at day 3 when they comprised on average 15% of the total macrophage population. The M1 population decreased by day 7 and was significantly decreased after AT-RvD1 or combination IL-10+AT-RvD1 treatment compared to control (Figure 2A). Conversely, M2 alternatively activated macrophages were characterized as CD86-CD206+. At day 1, these macrophages made up a higher proportion of the total macrophage population, possibly due to pre-existing populations of tissue resident macrophages that express CD206(198). We observed significant increases in the M2 macrophage population at 24 hours in the AT-RvD1-treated and IL-10+AT-RvD1 treated animals compared to internal control. At days 3 and 7 the average proportion of M2 macrophages had increased compared to the previous timepoint but did not change between IL-10 treated tissue and internal control. We saw significant increases in the M2 population after AT-RvD1 and dual delivery of IL-10 and AT-RvD1 compared to control at days 3 and 7 (Figure 2B). This accumulation of M2 macrophages

occurred at a faster rate with dual delivery hydrogels, as the population of M2 macrophages was significantly increased in IL-10+AT-RvD1 treated animals compared to AT-RvD1-only delivery at day 3, indicating a modulation in recruitment or differentiation kinetics driven by co-delivery of these two factors.

Given the increasing knowledge of the roles immune system and plays in promoting wound healing and tissue regeneration, we quantified the temporal response of dendritic cells to immunomodulatory PEG-MAL hydrogels. Dendritic cells have been shown to play previously unknown roles in the wound healing cascade, and specifically the CD11c+ IL-10+ tolerogenic or regulatory subset has been shown to enhance left ventricle function and remodeling following acute myocardial infarction and is able to stimulate the proliferation of Tregs(199, 200). Like monocytes and macrophages, dendritic cells are able to carry out pro- and anti-inflammatory effector functions, and pathologic dendritic cell activation leading to increased inflammatory cytokine production and stimulation of the adaptive immune system has been associated with chronic inflammatory disorders such as systemic lupus erythematosus and rheumatoid arthritis (201). In our mouse model, we observed recruitment of IL-10+ dendritic cells after one week across all groups and found that IL-10+DCs were significantly increased in combination IL-10+AT-RvD1 treatment compared to IL-10 only and AT-RvD1 only treatments (Figure 2C). Consistent with our hypothesis that IL-10 and AT-RvD1 delivery are able to reduce the activation of pro-inflammatory pathways, we observe decreased intracellular TNF-α expression in CD11c+ dendritic cells at day 3 in the IL-10 and IL-10+AT-RvD1 hydrogel treatment groups, and reduced TNF-α expression across all groups at day 7 (Figure 2D).

A M1 Macrophages

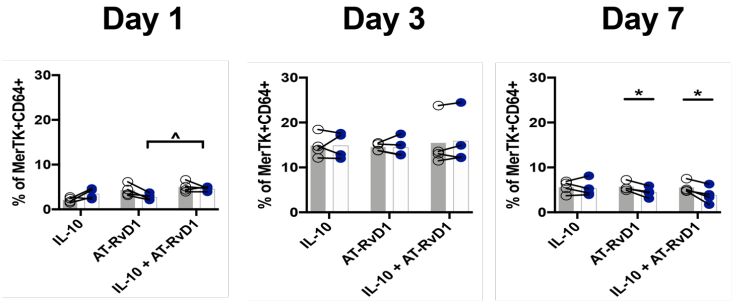

B M2 Macrophages

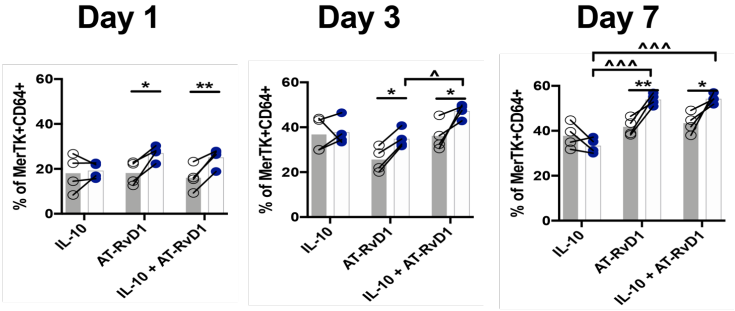

C IL-10+ DCs

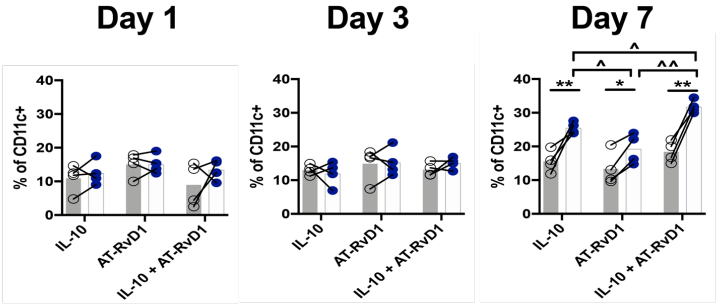

D DC TNF-α expression

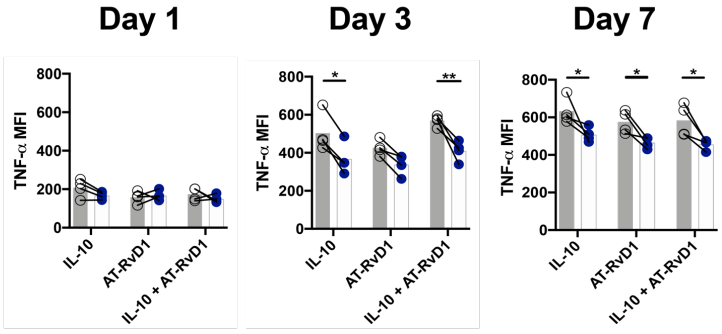

Figure 2. Anti-inflammatory macrophages and dendritic cells accumulate after local immunomodulatory hydrogel delivery.

Flow cytometric analysis of macrophages, (A) CD86+ M1 macrophage and (B) CD206+, and dendritic cell IL-10 (C) and TNF (D) expression in the dorsal skinfold window chamber following treatment with immunomodulatory PEG-MAL hydrogels. Open circles correspond to unloaded internal control; closed circles are treated tissue. Statistical analysis was performed using two-way repeated measures ANOVA with Tukey's or Bonferroni post-hoc test. Data presented as internal control and treatment with connecting lines. *$p<0.05$, **$p<0.01$ compared to internal control, ^$p<0.05$, ^^$p<0.01$, ^^^$p<0.001$ compared to other treatment group, n=4.

3.2.3 Dimensionality reduction analysis reveals trends in innate immune cell heterogeneity by day 7

Flow cytometry and IMARIS imaging (not shown) identified increased populations of pro-regenerative innate immune cells, such as M2 macrophages and IL-10+ DCs. Thus, we created an array of SPADE dendrograms to elucidate trends in cellular heterogeneity by day 7. We created SPADE representations using CD11b+ cells as indicative of myeloid cells, and then used MerTK+ CD64+ markers to create a "base" SPADE dendrogram representative of macrophages that express those markers (Figure 3A). By overlaying individual immune cell markers, such as CD86 or CD206, onto this base SPADE dendrogram, we were able to identify nodes that were specific for CD86+ cells, which indicated an M1 phenotype **(**Figure 3B), or CD206+, indicating an M2 phenotype (Figure 3D). We only identified 3 M1 nodes by day 7, but were able to identify 21 M2 nodes, indicating the prevalence of pro-regenerative phenotypes one week after treatment. We then created tornado plots to indicate the pseudotime trajectory of cell frequencies in each node. This analysis shows that, in IL-10, when comparing the treatment group against the control, there does not seem to be a shift in M1 macrophage cellular heterogeneity (Figure 3C). However, in the AT-RvD1 treatment, group, there is a shift in control cells towards an M1 phenotype in the remaining nodes by day 7. Additionally, in the dual IL-10+AT-RvD1 group, the M1 macrophages skew strongly towards the control group over treatment.

In M2 macrophage dominated nodes, in IL-10 alone and AT-RvD1 alone, there was no clear trend when comparing control nodes against treatment nodes. However, in the dual hydrogel group, there is a robust shift in multiple nodes towards treatment, indicating the immune microenvironment transitioning towards a pro-regenerative phenotype by day 7 (Figure 3E).

3.2.4 Characterization of Dendritic Cell Recruitment Dynamics using SPADE

Given the increasing knowledge of DCS and tolDCs in wound healing and tissue regeneration, we wanted to validate the observed temporal response of DCs to IL-10+AT-RvD1 hydrogels in the dorsal skinfold window chamber model. Flow cytometry revealed decreased intracellular TNF expression in CD11c+ DCs at day 3 in IL-10 alone and IL-10+AT-RvD1 groups, and reduced TNF in all groups compared to control in day 7. In addition, significant increase in IL-10 expression was observed by day 7 in all groups compared to internal control. Notably, IL-10+ alone and IL-10+AT-RvD1 had the highest increases in IL-10+ DCs.

We thus decided to investigate the trends in DC IL-10 expression via SPADE. Thus, we developed a CD11c+ "base" tree to incorporate all positive cells. (

Figure 4A). Next, we isolated the nodes that were positive for IL-10 to create a CD11c+ IL-10+ tree (

Figure 4B). This resulted in the identification of 22 IL-10+ CD11c+ nodes. However, when we created tornado plots to identify cell frequency differences in IL-10+ DCs, we do not see clear

trends in either IL-10 alone or dual hydrogel groups. However, we did observe a clear shift in the AT-RvD1 treatment group compared to internal control (

Figure 4C).

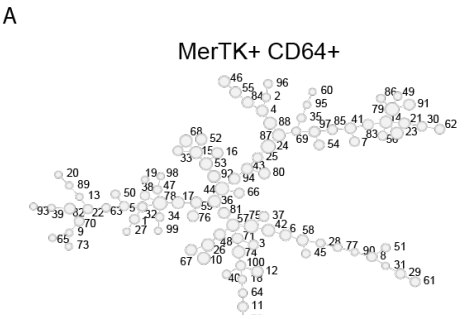

Figure 3. Trends in macrophage heterogeneity in response to immunomodulatory hydrogels.

SPADE trees were developed to identify trends in macrophage heterogeneity. A base macrophage tree was created after gating for CD11b+ MerTK+ CD64+ cells (A). SPADE analysis indicates nodes positive for CD86+ M1 macrophages (B) and CD206+ M2 macrophages (D). Tornado plots were used to identify shifts in cell frequency after IL-10 alone, AT-RvD1 alone, and dual delivery compared to internal control (C, E). Difference in cell frequency was calculated by subtracting control from treatment.

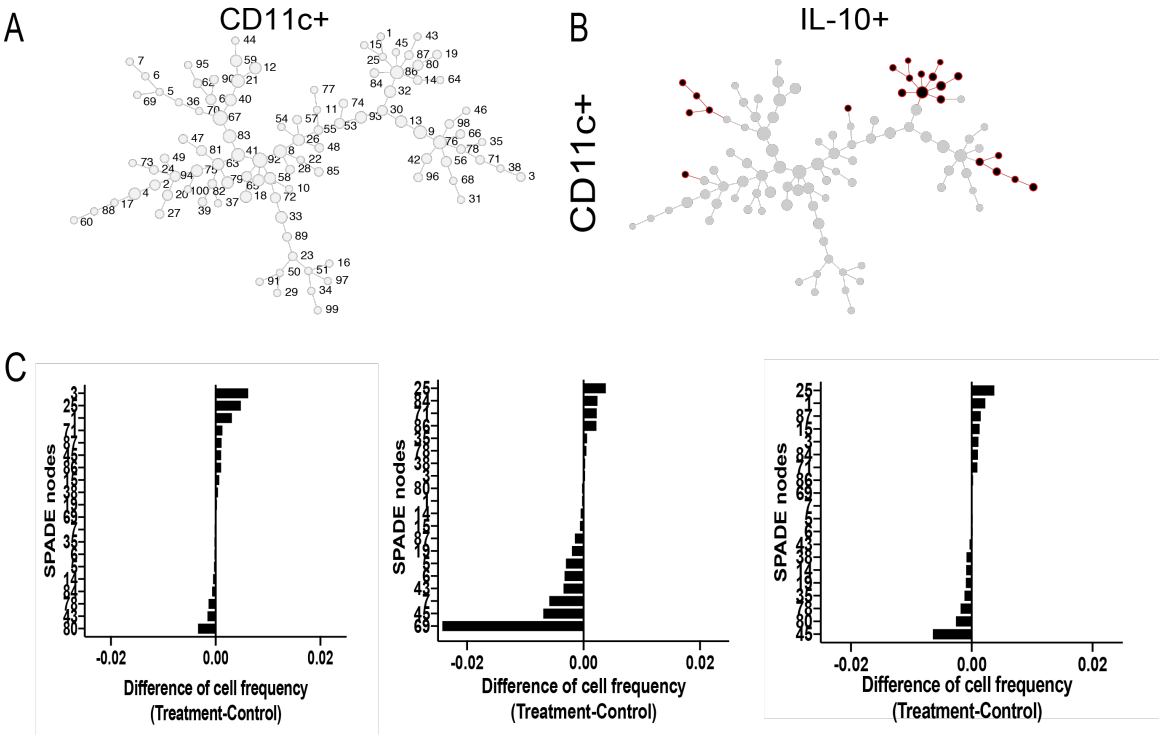

Figure 4 Trends in dendritic cell heterogeneity in response to immunomodulatory hydrogels.

SPADE trees were developed to identify trends in intracellular expression of IL-10 in dendritic cells. (A) A base dendritic cell tree was created after gating for CD11c+ cells. (B) SPADE analysis indicates nodes positive for IL-10 expression (C). Tornado plots were used to identify shifts in cell frequency after IL-10 alone, AT-RvD1 alone, and dual delivery compared to internal control. Difference in cell frequency was calculated by subtracting control from treatment.

3.2.5 T-cell recruitment dynamics in the dorsal tissue

Flow cytometry and imaging studies (not shown) identified increased populations of CD206+ macrophages and IL-10 co-expressing dendritic cells (DCs), with reduction in pro-inflammatory macrophages subtypes. Thus, we hypothesized that the immunomodulatory effects of our hydrogel treatment would likely modulate the adaptive immune system. DCs, for example, have become recognized for their regulation of both innate and adaptive immunity. In particular, DCs have recently been shown to ensure "immunological peace"(192). As tissue-resident DCs mature, they acquire T-cell stimulatory capacity and are able to convert conventional naïve T cells to a Treg phenotype or promote Treg function(202). These "repair" Tregs can be either CD4+ or CD8+, and have been suggested to promote wound healing and repair in multiple tissues(203).

Thus, we performed flow cytometry on isolated tissue from the window chamber, adding CD3+, CD4+, CD25+, and CD8+ markers for adaptive immunity. Because of the increase in IL-10+ dendritic cells, we aimed to identify adaptive immune populations from a base CD3+ SPADE dendrogram (Figure 5A). We first identified CD4+ CD25+ T-regulatory cells using SPADE by creating a CD3+ CD4+ tree (Figure 5B), and then a CD3+ CD4+ CD25+ tree (Figure 5C). From this, we were able to identify 30 nodes that were positive for both CD4 and CD25. We then plotted the difference in cell frequency in the treatment from control samples to identify shifts in cellular heterogeneity (Figure 5D). In accordance with the trends in CD11c+ IL-10+ SPADE nodes, the AT-RvD1 alone group was the only treatment group that showed a slight trend towards treatment in CD4+ CD25+ cells over control. However, we did not observe other trends in either the IL-10+ or dual IL-10+AT-RvD1 groups.

3.2.6 SPADE analysis reveals trends towards unexpected pro-regenerative adaptive immune cell population at day 7 following dual treatment with IL-10+AT-RvD1

For a thorough investigation into the involvement of the adaptive immune system, we also developed SPADE trees for CD8+ T-cells. Following the creation of a CD3+ base SPADE tree (Figure 6A), we then identified CD8+ cells using SPADE by creating a CD3+ CD8+ tree (Figure 6B). Interestingly, while creating the tree, we noticed a subpopulation of nodes that had concurrent IL-10 expression. We thus created a third tree with CD3+ CD8+ IL-10+ nodes (Figure 6C). We then plotted the difference in cell frequency in the treatment from control samples to identify shifts in cellular heterogeneity (Figure 6D). This analysis revealed the presence of a CD8+ IL-10+ subpopulation of cells that were unexpected. This CD8+ IL-10+ co-expressing cell only seems to be robustly increased in the treatment group in the dual IL-10+AT-RvD1 group, suggesting a potential interplay between the delivered therapeutics that caused the recruitment of this rare immune cell population. These data suggest a unique role for the adaptive immune system in response to biomaterials at the injury site. Moreover, these data show the importance of using advanced computational methods to elucidate multidimensional cellular data that we had not even planned to look for using conventional flow cytometry methods.

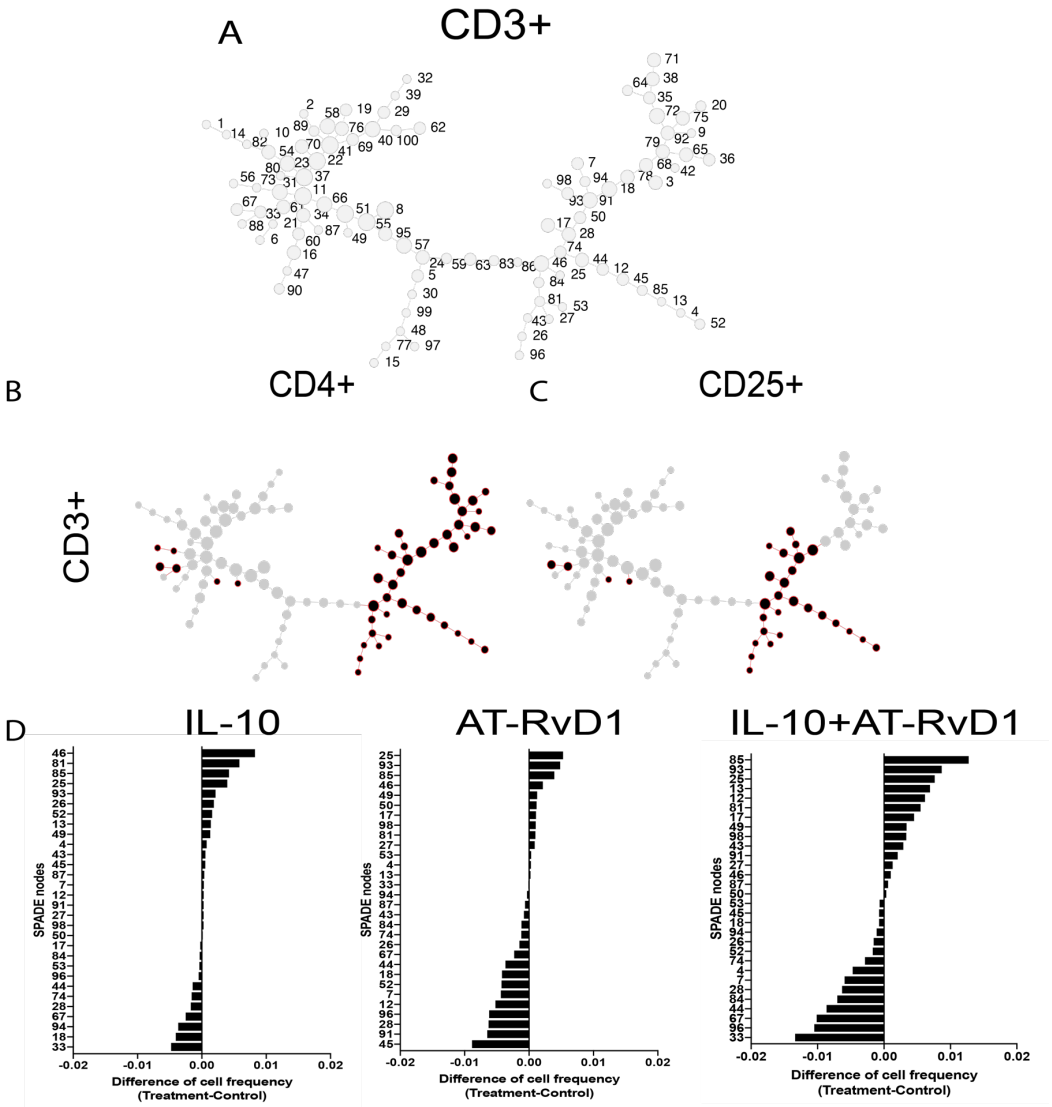

Figure 5. Adaptive immune response to immunomodulatory hydrogels.

SPADE trees were developed following flow cytometric analysis to identify adaptive immune cell subsets. (A) CD3+ base trees were developed after gating for CD3+ cells. SPADE analysis indicates nodes positive for CD4+ cells (B) and CD25+ (C) cells. Tornado plots were utilized to identify trends in cell frequency after IL-10 alone, AT-RvD1 alone, and dual delivery (D).

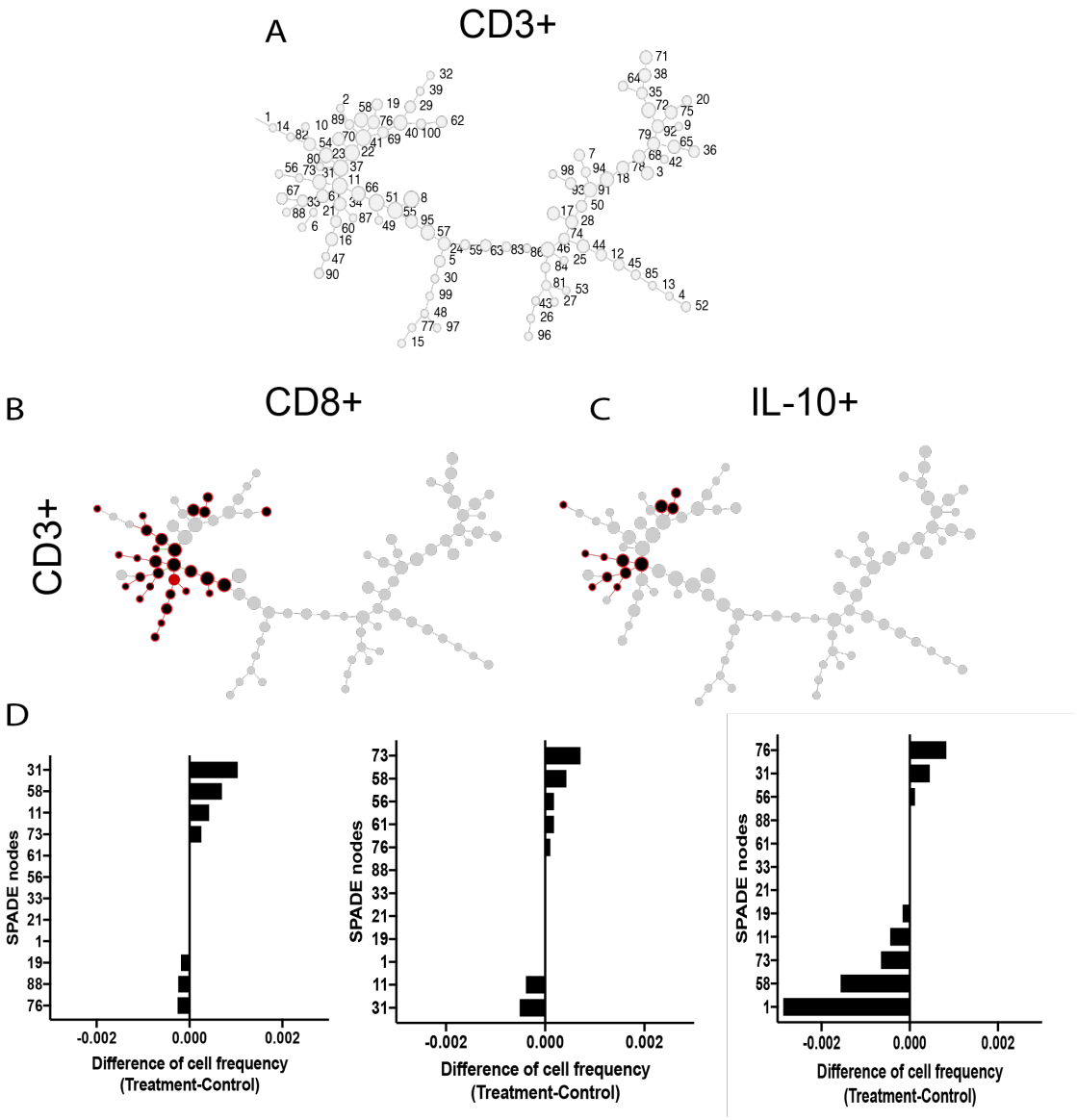

Figure 6 SPADE trees were developed following flow cytometric analysis to identify rare cell subsets.

(A) CD3+ base trees were developed after gating for CD3+ cells. SPADE analysis indicates nodes positive for CD8+ cells (B) and IL-10+ (C) expression. Tornado plots were utilized to identify trends in cell frequency after IL-10 alone, AT-RvD1 alone, and dual delivery (D).

3.3 Discussion

The use of biomaterial implants to deliver cells or bioactive molecules capable of directing the host immune response after injury can modulate processes critical to the restoration of tissue homeostasis, such as cellular cytokine release, vascular remodeling, or deposition of extracellular matrix(175). It is becoming increasingly apparent that these processes are regulated not only by cells of the innate immune system, such as monocytes and macrophages, but that cells of the adaptive immune system play active and important roles. It is our goal to develop a material that can enrich the wound microenvironment with anti-inflammatory cells of both the innate and adaptive immune system to enhance the regenerative response.

To attain a higher level of control over both innate and adaptive immune cell recruitment, we have developed a PEG-4MAL RGD hydrogel-based system capable of the dual delivery of two factors crucial for the recruitment and activation of pro-regenerative cells of both the myeloid and lymphoid lineages. Integrin signaling appears to play different roles in leukocyte migration, depending on the environment in which the cell is migrating. For example, monocytes utilize the integrin LFA-1 to crawl along the endothelium and extravasate into the tissue (204, 205). Conversely, leukocyte migration through interstitial space is not integrin-dependent and instead involves amoeboid-like flowing and squeezing motions (205). The critical parameter appears to be whether the cell comes in contact with a 2D barrier, such as the endothelium. Biomaterials provide a unique context to migrating cells, where the surface serves as a 2D barrier, but materials that are porous or have topographical features may be interpreted by cells as an analogous environment to interstitial space. These hydrogels were engineered with RGD to achieve *in vivo* recruitment of cells to the gel, following which degradation of the gel would result in AT-RvD1 and IL-10 release. In fact, we observed recruitment of macrophages, DCs, and adaptive immune cell populations.

Macrophages are identifiable with flow cytometry by their surface receptor expression of MerTK and CD64(196). Expansion of macrophage populations is a hallmark of the resolution of inflammation and is necessary for tissue regeneration and wound healing (195). We used flow cytometry to identify specific macrophage subpopulations present in the tissues over time. Macrophages were subclassified into M1 and M2 phenotypes as previously described (197). M1 classically activated macrophages were characterized by their expression of the costimulatory molecule CD86 and did not express the mannose receptor CD206. Temporally, we observed an increase in the M1 population at day 3, followed by a decrease by day 7, particularly after AT-RvD1 or combination IL-10+AT-RvD1 treatment compared to control. Conversely, M2 alternatively activated macrophages were characterized as CD86-CD206+. At day 1, these macrophages made up a higher proportion of the total macrophage population, possibly due to pre-existing populations of tissue resident macrophages that express CD206(198). We saw significant increases in the M2 population after AT-RvD1 and dual delivery of IL-10 and AT-RvD1 compared to control at days 3 and 7. This accumulation of M2 macrophages occurred at a faster rate with dual delivery hydrogels, as the population of M2 macrophages was significantly increased in IL-10+AT-RvD1 treated animals compared to AT-RvD1-only delivery at day 3, indicating a modulation in recruitment or differentiation kinetics driven by co-delivery of these two factors.

Because we used 10 different markers to elucidate the roles of 6-7 cell types, we decided to use dimensionality reduction techniques to confirm our flow cytometry findings. Thus, we used SPADE to highlight novel aspects of immune alterations developed after immunomodulatory hydrogel treatment. SPADE is a dimensionality reduction technique that hierarchically clusters phenotypically similar cells into “nodes”. These nodes and their relationships are organized into a minimum spanning tree, or “SPADE tree”. To test this, we created SPADE trees of the individual macrophage populations of which we were interested. In accordance with the results from flow cytometry and intravital imaging (not shown), we observed

a shift in cellular heterogeneity towards the M2 anti-inflammatory macrophage phenotypes, and away from the M1 pro-inflammatory macrophage subtype, particularly in the dual hydrogel group when compared to internal control.

Given the increasing roles of the immune system in promoting wound healing and tissue regeneration, we also quantified the temporal response of dendritic cells to immunomodulatory PEG-MAL hydrogels. Dendritic cells have been shown to play previously unknown roles in the wound healing cascade, and specifically the CD11c+ IL-10+ tolerogenic or regulatory subset has been shown to enhance left ventricle function and remodeling following acute myocardial infarction and is able to stimulate the proliferation of Tregs(27, 28). Like monocytes and macrophages, dendritic cells are able to carry out pro- and anti-inflammatory effector functions, and pathologic dendritic cell activation leading to increased inflammatory cytokine production and stimulation of the adaptive immune system has been associated with chronic inflammatory disorders such as systemic lupus erythematosus and rheumatoid arthritis (29). DCs have become recognized for their regulation of both innate and adaptive immunity. In particular, DCs have recently been shown to ensure “immunological peace”(192). On flow cytometry, we observed increased in IL-10+ tolDCs in in all groups, and reductions in TNF intracellular expression by day 7. Interestingly, however, we did not observe the same trends after creating CD11c+ IL-10+ SPADE trees. The SPADE trees revealed an increase in IL-10+ DCs only in AT-RvD1 alone. If we look at the IL-10+ expression on the CD11c+ SPADE tree, it can be noticed that the nodes separate into 5 separate clusters. Thus, it may be possible that each cluster may be originating from a very heterogeneous DC population, and by simply gating out IL-10+ cells in flow cytometry analysis, we are not appreciating small differences in the changing DC population. Performing a more comprehensive flow cytometry DC panel may be helpful in parsing out the differences in cellular heterogeneity.

As tissue-resident DCs mature, they acquire T-cell stimulatory capacity and are able to convert conventional naïve T cells to a Treg phenotype or promote Treg function(202). These

"repair" Tregs can be either CD4+ or CD8+, and have been suggested to promote wound healing and repair in multiple tissues(203). The increase in anti-inflammatory subtypes of innate immune cells made us interested in the trends in adaptive immunity by day 7 of treatment. SPADE analysis of CD4+ CD25+ Tregs did not show any trends in heterogeneity in response to treatment. Interestingly, however, SPADE revealed the surprising finding of CD8+ IL-10+ T-cell involvement. After developing a base CD3+ tree, we noticed a small subset of CD8+ cells that co-expressed IL-10. Tornado plot analysis indicated a trend towards treatment group in the dual hydrogel group. CD8+ Tregs have been shown to be a heterogeneous population, thus making them difficult to study using conventional methods, and as a result, are often poorly characterized(206). In fact, CD8+ Tregs have been reported in humans, and have strong immunosuppressive properties *in vitro(207).* CD8+ Tregs have also been shown to play a role in human autoimmune disease, including IBD(208).

This data suggests a synergistic interplay between AT-RvD1 and IL-10 that allows for increased control of the recruitment of cells from the innate and adaptive immune system compared to either treatment on its own. Moreover, this data implicates an interesting role for CD8+ Tregs in the process of wound healing. This dual-delivery system has the potential to improve therapeutic wound healing outcomes following trauma or tissue transplantation via synergy of cellular recruitment and polarization processes to promote anti-inflammatory cell recruitment and activity.

3.4 Materials and Methods

3.4.1 Thiolation of IL-10

Carrier-free recombinant human IL-10 was purchased from BioLegend. IL-10 was thiolated using 30 molar excess of Traut's reagent (Sigma) for one hour in PBS containing 0.1uL EDTA per uL buffer to chelate free metals. The thiolation reaction was shaken at RT for one hour. Thiolated IL-10 was separated from unreacted Traut's reagent using a Zeba desalting column according to manufacturer's instructions. Thiolation was detected using a Measure-IT™ Thiol Assay Kit (Invitrogen) according to kit instructions. Number of thiol groups per IL-10 was calculated using the concentration of detected thiols and the known concentration of IL-10 in each measured sample.

3.4.2 Hydrogel Fabrication

Four-arm poly(ethylene glycol) (PEG, 10 kDA molecular weight) end-functionalized with maleimide (>95% purity, Laysan Bio) at 4.5% weight/volume was used for all hydrogel formulations. PEG macromers were functionalized with RGD peptide (GRGDSPC), crosslinked with the cysteine-flanked peptide VPM (GCRDVPMSMRGGDRCG) (AAPPTec) in 0.5M MES buffer, pH 5.5. The final concentration of RGD was 1.0mM. Gels were also loaded with 50ug/mL IL-10, and 4ug/mL AT-RvD1 (Cayman Chemical). The crosslinker concentration was based on the concentration of non-reacted maleimide groups remaining on PEG macromers. For hydrogels used in animal studies, all components were filtered through a spin column after pH measurements and kept under sterile conditions until injection into the animals. To generate pre-formed hydrogels for release studies, the hydrogel was formed on a sterilized petri dish. After crossslinking, hydrogels were incubated at 37˚C for 15 minutes and then swelled in PBS for at least 30 minutes. Release of thiolated and unthiolated IL-10 was measured over time in 1% BSA solution using IL-10 tagged Alexa Fluor 405 NHS Ester (Life Technologies) according to the

manufacturer's recommendation and quantified using a standard curve of known fluorescent IL-10 concentrations. Release of AT-RvD1 was measured with a Shimadzu UFLC High Performance Liquid Chromatograph (Columbia, MD, USA) equipped with a Shimadzu Premier C18, 5μm (250x4.6mm) column. AT-RvD1 elution was measured at 8.6 minutes using a wavelength of 301nm. Known quantities of AT-RvD1 were used to generate a standard curve relating AT-RvD1 mass to total peak area. Using serial dilutions, we determined that the limit of detection was below 0.5pg/μL. The total amount of AT-RvD1 in each release sample was calculated using the standard curve.

3.4.3 Tissue Harvest and Flow Cytometry

To collect samples for flow cytometry analysis, mice were euthanized via CO2 asphyxiation. The dorsal tissue was excised and digested with collagenase type 1-A (1mg/ml, Sigma) at 37°C for 30 minutes and further separated with a cell strainer to create a single cell suspension. Single cell suspensions of dorsal tissue were stained for flow cytometry analysis using standard methods and analyzed on a FACS-AriaIIIu flow cytometer (BD Biosciences). Dead cells were excluded through staining using Zombie Red fixable viability stain (BioLegend). The antibodies used for identifying cell populations of interest were: PE conjugated MerTK (Biolegend), PE-Cy7 conjugated MHC-II (BioLegend), BV605 conjugated CD206 (BioLegend), BV510 conjugated Ly6C (BioLegend), APC-Cy7 conjugated Ly6G (BioLegend), BV711 conjugated CD64 (BioLegend), BV785 conjugated CD19 (BioLegend), APC conjugated Cd11b (BioLegend), BV421 conjugated CD11c (Biolegend, FITC conjugated CD86 (BioLegend), PerCP-Cy5.5 conjugated CD3 (Biolegend), BV785 conjugated CD8 (BioLegend), BV605 conjugated CD4 (BioLegend), and BV711 conjugated CD25 (BioLegend). Staining using BV dyes was performed in the presence of Brilliant Stain Buffer (BD Biosciences). Cells were stained for intracellular cytokines using PE conjugated IL-10 (BioLegend) and PE-Cy7 conjugated TNF- α (eBiosciences). Positivity was determined by gating on fluorescence minus one controls.

Absolute quantification of cell numbers was performed by adding 25μL of AccuCheck counting beads to flow cytometry samples (Thermo Fisher Scientific).

3.4.4 SPADE analysis of flow cytometry data

Dimensionality reduction analysis was performed using MATLAB-based Spanning-tree Progression Analysis of Density-normalized Events (SPADE). SPADE is a computational technique that performs density-dependent down-sampling, agglomerative clustering, linking clusters using minimum spanning-tree algorithm, and finally, up-samples based on user input. The SPADE trees generated here were generated by exporting compensated pre-gated single cells, CD11b+ myeloid cells, MerTK+ CD64+ cells; single cells, CD3-, CD11c+ cells; or pre-gated single cells, CD3+ cells. The markers used to build the SPADE tree were SSC, FSC, CD11b, Ly6G, CD11c, CD64, CD86, CD206, CD8, CD4, CD25, Ly6C, IL-10, TNF-a. The following SPADE parameters were used: Apply compenstation matrix in FCS header, Arcsinh transformation with cofactor 150, neighborhood size 5, local density approximation factor 1.5, max allowable cells in pooled downsampled data 50000, target density 20000 cells remaining, and number of desired clusters 100.

3.4.5 Statistical Analysis

All statistical analyses were performed using Graphpad Prism version 6.0 (La Jolla, CA). Results are presented as mean ± standard error of the mean (SEM). For grouped analyses, one-way ANOVA with Tukey's post-test was used for multiple comparisons. For internally controlled experiments, two-way ANOVA was used. Tukey's post-hoc test was utilized when comparing paired samples, and Bonferroni's post hoc test was used when comparing between treatment groups. Unless otherwise noted, $p<0.05$ was considered statistically significant.

CHAPTER 4. INVESTIGATING THE LOCAL AND SYSTEMIC EFFECTS ON THE IMMUNE RESPONSE FOLLOWING ORAL GAVAGE OF IMMUNOMODULATORY MICROPARTICLE TREATMENT

4.1 Introduction

Salmonella typhimurium is a Gram-negative pathogen that is acquired as a foodborne illness(209). Infection is limited to the intestinal mucosa, causing acute neutrophilic inflammation without epithelial destruction. After ingestion, *Salmonella* reaches the small intestine lumen, where it invades the epithelium of intestinal villi, or translocates across the epithelium to gain access to the Peyer's patches or gastrointestinal lymphoid tissue (GALT), the overlaying mucosal lymphoid aggregates that are the immune sensors of the intestine(94). Another mechanism of pathogenesis may include infection of the dendritic cells (DCs) that extend processes across epithelial tight junctions to sample the contents of the lumen(210, 211). Thus, the pathogen affects innate immunity, infecting either DCs, neutrophils, or macrophages. Ultimately, the early immune response to *Salmonella* involves the accumulation of neutrophils and the development of a systemic inflammatory syndrome(212).

Bacterial pathogens have been shown to prevent and reduce the immune response after initial infection and establishment within host cells(213). Some pathogens secrete proteins into the host via a "type III secretion apparatus" which allows for invasion and intracellular carriage(9). This may include mechanisms by which recruitment of phagocytic leukocytes is suppressed, and apoptosis of inflammatory cells is initiated to allow for bacterial proliferation and

dissemination. Notably, these proteins have been shown to exhibit these inhibitory actions against MAPK or NF- κB signaling pathways(214). Examples of these immunosuppressive factors are AvrA, from *Salmonella,* a member of the family of acetyltransferases that is expressed in several pathogens(215), YopJ/P from *Yersinia pseudotuberculosis(216),* and VopP from *Vibrio parahemalyticus(217).*

Salmonella AvrA has been shown to cause innate immune signaling blockade without causing cell death that is typically seen during host inflammatory inhibition. While cells infected with *Salmonella* can initiate apoptosis and activate pro-inflammatory processes, AvrA has been shown to dampen both host responses for the establishment of infection and avoidance of an adaptive immune response(218). Notably, loss of AvrA increased host cell apoptosis, and increased microbial burden beyond local inflammation to systemic lymphoid tissues, suggesting AvrA may play a role in limiting pathogenesis to a local infection(218). Previous reports show that AvrA exhibits these actions by acting as an acetyltransferase, blocking the actions of target MKK4/7(9). As a result, AvrA indirectly inhibits activation of downstream JNK signaling. In addition, although traditional bacterial pathogens, such as *Shigella* or enterohemorrhagic *E. coli*, initiate apoptosis of infected cells, AvrA inhibits apoptosis pathways, preventing the elimination of host cells(9).

The combined properties of AvrA to inhibit the inflammatory response while preventing cell death suggests that AvrA may be a potent and local therapeutic for the treatment of inflammatory disease. Inflammatory bowel disease (IBD) affects 3.1 million people in the United States, and its incidence appears to be on the rise(219, 220). Crohn's disease (CD) and ulcerative colitis (UC), two major forms of IBD, and are chronic inflammatory disorders of the gastrointestinal tract. Current therapeutics include small molecules, systemic corticosteroids, monoclonal antibodies, and, in the case of UC, surgical removal of the entire colon(221). These therapeutics are typically effective for some time, but have extensive side effects and, ultimately, patients become unresponsive and must be switched to new medication. Recent literature has

suggested that AvrA, with its dual anti-inflammatory and anti-apoptotic functions, may be a potential agent to ameliorate inflammation in IBD(222). In order to utilize the unique aspects of AvrA, it was necessary to deliver it to the gastrointestinal tract for it to come into contact with the intestinal epithelium and local immune cells.

Efficient drug delivery system must meet several requirements to serve as an ideal delivery vehicle of an active therapeutic. Such requirements include improved stability, reduced dosage and frequency of administration, reduced side effects, minimum toxicity, and the ability to deliver the required amount to the target location for a long time(223). Techniques in nanotechnology have led to the development of different types of carriers for controlled release and targeted delivery. Previous IBD studies have attempted to deliver therapeutics in the form of biodegradable polymeric nano- and microparticles (144, 224). However, among nanoparticle technologies, the ability to be synthesized from naturally occurring or engineered proteins provide a promising method for drug delivery application. Protein-based carriers are nontoxic, biodegradable, and can be degraded by physiological changes or by enzymes present in the body(225). Protein NPs also increase cellular internalization and have high protein loading capacities. Further, protein NPs can passively target enflamed tissue(226). Thus, we previously developed AvrA nanoparticles for the therapeutic targeting of IBD(227). However, delivery to the gastrointestinal tract proves difficult due to the harsh environment in the stomach. The gastric system possesses low pH and a number of digestive enzymes whose goals are to break down and digest proteins. For effective and convenient administration of drugs, pH- and ion-responsive polymers have been employed for site-specific drug release(228). For example, anionic polymers have been used for delivery to the colon due to their responsiveness to high intestinal pH preventing gastric degradation of the drug(228).

In order to effectively deliver AvrA NPs to the small intestine, we developed an approach to deliver therapeutic proteins encapsulated within gastro-protecting alginate and chitosan microparticles (MPs). Alginate and chitosan are naturally derived biocompatible polymers that

have been extensively applied for controlled drug release(229, 230). Alginate is commonly used for the encapsulation of therapeutic agents(231), and is the most studied material for encapsulating live cells(232). Chitosan is a cationic polysaccharide, and has numerous favorable biological properties, such as non-toxicity and mucoadhesive properties(52, 233). Alginate can form hydrogels in the presence of divalent cations that interact with carboxylic groups in the alginate backbone(234). Chitosan was chosen to coat the alginate particles to prevent drug leakage. The complementary electrostatic properties of anionic alginate and cationic chitosan create interpolymeric associations that are strengthened by the protonation of chitosan at low pH(235). However, at intestinal pH, which is more basic, alginate gels swell, and the chitosan charge becomes negative. This allows for the release of AvrA specifically in the more basic environment of the intestine.

The absorptive environment of the GI tract suggests that the released AvrA nanoparticles may be taken up directly by either the absorptive epithelium/intraepithelial lymphocytes (IELs), or in the Peyer's patches(236). It has been shown that early infection is established within macrophages, then rapidly spreads to phagocytic cells of the splenic reticuloendothelial system. Thus, we aimed to identify whether the regulation of inflammation by orally delivered AvrA would follow a similar mechanism of immune suppression. Moreover, we hypothesized that local delivery of AvrA microparticles would inhibit the immune response in the Peyer's patches, but due to the lack of extensive infectious machinery of *Salmonella*, it would not lead to a systemic immune suppression.

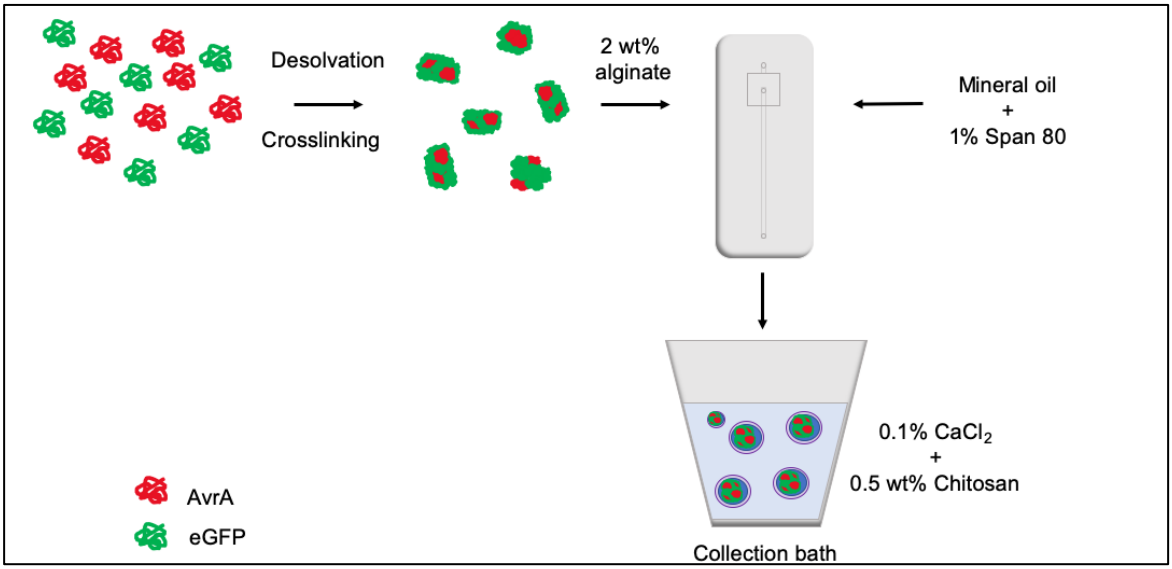

Figure 7. AvrA microparticle synthesis.

Schematic representation of AvrA NP loading into alginate droplets via flow focusing microfluidic device, and MP crosslinking and coating with calcium and chitosan.

4.2 Results

4.2.1 AvrA MPs reduce local innate immunity in the gastrointestinal system

AvrA protein NPs were manufactured by desolvation of eGFP and AvrA with ethanol under constant stirring, followed by crosslinking with 3,3'-dithiobis-(sulfoccinimidylpropionate) (DTSSP) for stabilization(237). AvrA NPs were then mixed with alginate and droplets were formed using a flow focused microfluidic device. The droplets were directed into a bath containing chitosan and $CaCl_2$ (

Figure 7). To study the role of AvrA on intestinal infection *in vivo*, we treated mice with either AvrA MPS or control by oral gavage for 5 days. Three groups of female mice were then administered either *E. coli* lipopolysaccharide (LPS) or PBS for 24 hours. After sacrifice, we digested Peyer's patches from the small intestine, following which we isolated epithelial cells and intraepithelial lymphocytes from the small intestine lamina propria for flow cytometry (Figure 8A). In typical *Salmonella* infection, neutrophils migrate across the epithelial barrier to the apical membrane(238). This suggests that in response to infection, neutrophils are the first responders and may influence intestinal epithelial functions and the subsequent immune response(239). Thus, we hypothesized that treatment with AvrA would reduce neutrophil infiltration into the epithelium, and particularly into the Peyer's patches.

In order to test this, after treatment with AvrA and LPS, we sacrificed the animals and quantified neutrophils by identifying CD11b+ Ly6G+ and activation levels of intracellular

epithelial (E-cadherin+) TNF. We also quantified macrophages using CD11b+ F4/80+ cells, as previous research has shown that macrophages transduced with AvrA expressing adenovirus were protected from apoptosis induced by exogenous stimuli, indicating that macrophages are a potential target for the immune suppression caused by AvrA(240). We particularly focused on cell populations from the intraepithelial/intraepithelial lymphocytes (EC), small intestine lamina propria (SI), and Peyer's patches (PP).

Interestingly, we observed a reduction of intracellular TNF in the EC (Figure 8B). Moreover, we observed a local reduction of neutrophils in the PP, but not in the intraepithelial lymphocytes or SI (Figure 8D).This early response at 24 hours following infection suggests an immediate inhibition of neutrophil transmigration across the intestinal epithelium in the PP(240). The inhibition of neutrophil migration and the additional reduction of TNF in epithelial cells potentially suggests that migrating neutrophils may signal to the epithelium. However, we did not notice changes in macrophage numbers following stimulation with LPS or following treatment with AvrA (Figure 8C).

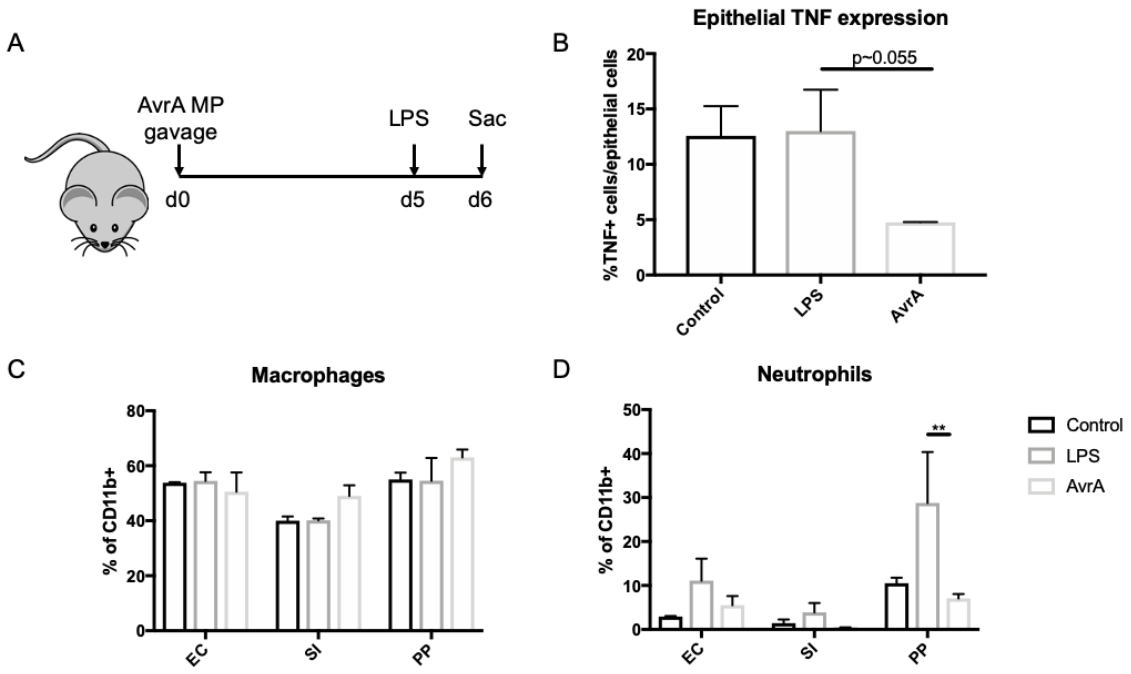

Figure 8 Treatment with AvrA influences the innate immune system following *E. coli* LPS stimulation.

(A) C57bl/6 mice were treated with either AvrA or control (PBS) for 5 days. LPS or vehicle was administered, and mice were sacrificed after 24 hours. Mouse small intestine was isolated and processed to separate intraepithelial lymphocytes (EC) from small intestine lamina propria (SI). (B) Intracellular expression of TNF in epithelial cells was determined by flow cytometry. (C) F4/80+ CD11b+ macrophages were quantified for each treatment group: PBS+intraperitoneal PBS, control PBS+LPS, or AvrA microparticles+LPS. (D) No significant changes in neutrophils in EC or SI were observed; however, a significant reduction of neutrophil infiltration in the Peyer's patches was observed between control PBS+LPS versus AvrA microparticle+LPS groups. Data

presented as mean ± SEM. Statistical analysis was performed using two-way repeated measures ANOVA with Tukey's post-hoc test. *$p<0.05$, **$p<0.01$, n=3.

4.2.2 AvrA reduces local adaptive immunity in the gastrointestinal system

We then wanted to investigate whether the modulation of innate immunity had effects on the adaptive immune system. In the same animals that were treated with AvrA or control, we identified CD3+ T-cells to further elucidate the roles of individual subpopulations (Figure 9A). Out of CD3+ T-cells we identified T-helper cells, also known as CD4+ T-cells, and cytotoxic T-cells, or CD8+ T-cells, in samples isolated from the IELs, small intestine lamina propria, and Peyer's patches.

Interestingly, we found a reduction in CD4+ T-cells in the Peyer's patches and no changes in the IELs or small intestine (Figure 9B). In contrast, we noticed a reduced CD8+ population in the IELs, but no significant changes in either small intestine or Peyer's patches (Figure 9C). This suggests potential interesting role for CD4+ and CD8+ T-cells in the epithelium and Peyer's patches that should be further elucidated in future work.

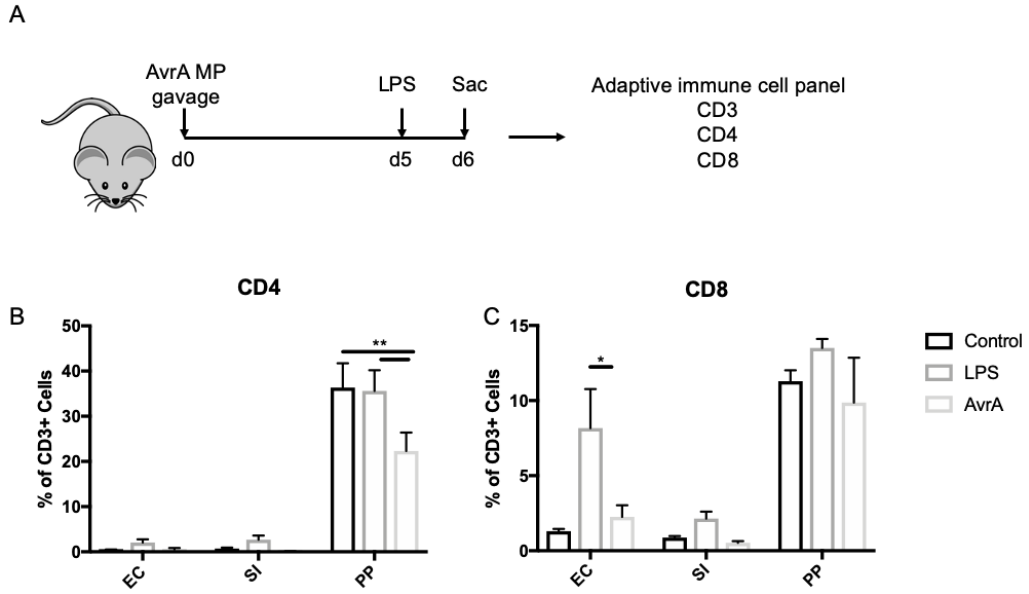

Figure 9 Treatment with AvrA influences adaptive immunity.

(A) C57bl/6 mice were treated with either AvrA or control (PBS) for 5 days. LPS or vehicle was administered, and mice were sacrificed after 24 hours. Mouse small intestine was isolated and processed to separate intraepithelial lymphocytes (EC) from small intestine lamina propria (SI). (B) Flow cytometric analysis reveals a reduction in CD4+ T-cells in Peyer's patches, but no differences in EC or SI. (C) CD8+ T-cells were reduced in EC cells that were treated with AvrA microparticles when compared to control PBS+LPS, but no changes were observed in SI or Peyer's patches. Data presented as mean ± SEM. Statistical analysis was performed using two-way repeated measures ANOVA with Tukey's post-hoc test. *$p<0.05$, **$p<0.01$, n=3.

4.2.3 Local delivery of oral AvrA microparticles likely do not acutely affect systemic immunity

In typical *Salmonella* infection, the infection rapidly disseminates to cells within the splenic reticuloendothelial system(212). Thus, we were interested to investigate whether local

delivery of AvrA microparticles would result in only a local immune modulation or whether its signalling effects would influence systemic immunity as well. Thus, we isolated and prepared spleens for flow cytometry from wild-type mice that had been pre-gavaged with AvrA microparticles or controls for 5 days, and then administered intraperitoneal LPS or intraperitoneal PBS (**Error! Reference source not found.**A).

We stained for innate immune cells, including neutrophils (CD11b+ Ly6G+), macrophages (CD11b+, F4/80+), and T-cells, including CD3+ CD4+ and CD3+ CD8+ T-cells. Although neutrophil and T-cell infiltration was reduced in the local GI tract, there were no changes observed in either innate (**Error! Reference source not found.**B) or adaptive immune cells (**Error! Reference source not found.**C) in AvrA treated or LPS treated animals.

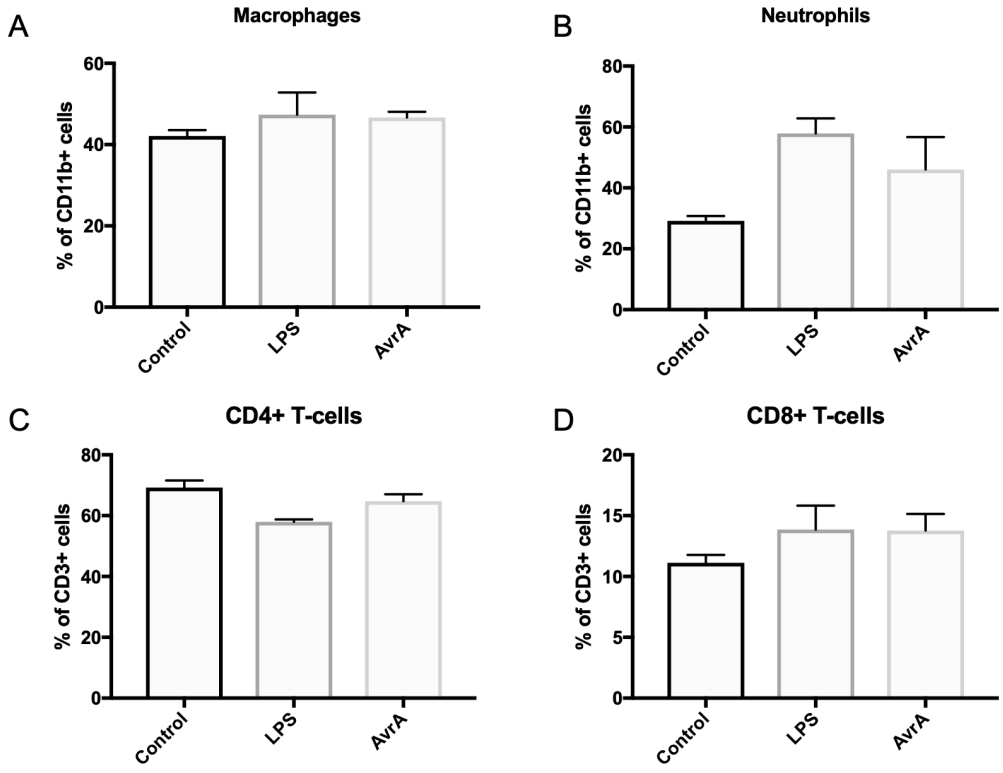

Figure 10. Effects of orally administered AvrA likely do not result in systemic immunosuppression.

C57bl/6 mice were treated with either AvrA or control (PBS) for 5 days. LPS or vehicle was administered, and mice were sacrificed after 24 hours. Mouse spleens were isolated for staining. Flow cytometric analysis shows no changes in neutrophils (A) or macrophages (B) in mice treated with PBS control + PBS vehicle (black), PBS control+LPS (light gray), or AvrA microparticles+LPS (dark gray). This analysis did not show any changes in CD4+ (C) or CD8+ (D) cell populations in either PBS or AvrA microparticle treatment. Statistical analysis was performed using two-way repeated measures ANOVA with Tukey's post-hoc test. *$p<0.05$, **$p<0.01$, ***$p<0.001$, n=3.

4.2.4 Marker expression heatmaps allow for phenotype interpretation

Observing the amelioration of innate immune cell recruitment from both GALT and IELs suggested a more extensive picture of the spatial dynamics of the innate and adaptive immune systems. Thus, we sought to organize the multidimensional dataset observed in response to LPS and AvrA microparticle treatment. In order to conduct a non-biased, unsupervised analysis of phenotypic differences between treatment groups, we used Spanning-tree Progression Analysis of Density-normalized Events (SPADE) to identify populations of cells. SPADE is an invaluable tool to analyze multidimensional flow cytometry data. The SPADE algorithm clusters similar populations into nodes and projects them into a tree**.** Each node contains cells with similar marker expression across all parameters, and the size indicates the number of cells within a population. To more clearly visualize our dataset, the marker expression per node was then hierarchically clustered using R Studio to make conclusions about cell phenotypes at each time point The identified cell populations included CD11b+ Ly6G+ (neutrophils), dendritic cells (CD11b- CD11c+), T-cells (CD11b-, CD3+), and CD4+ T-Cells (CD11b-, CD3+, CD4+). Interestingly, we observed a third population of T-cells that stained for Ly6C+, CD3+, AND CD8+ in 5 nodes (Figure 11).

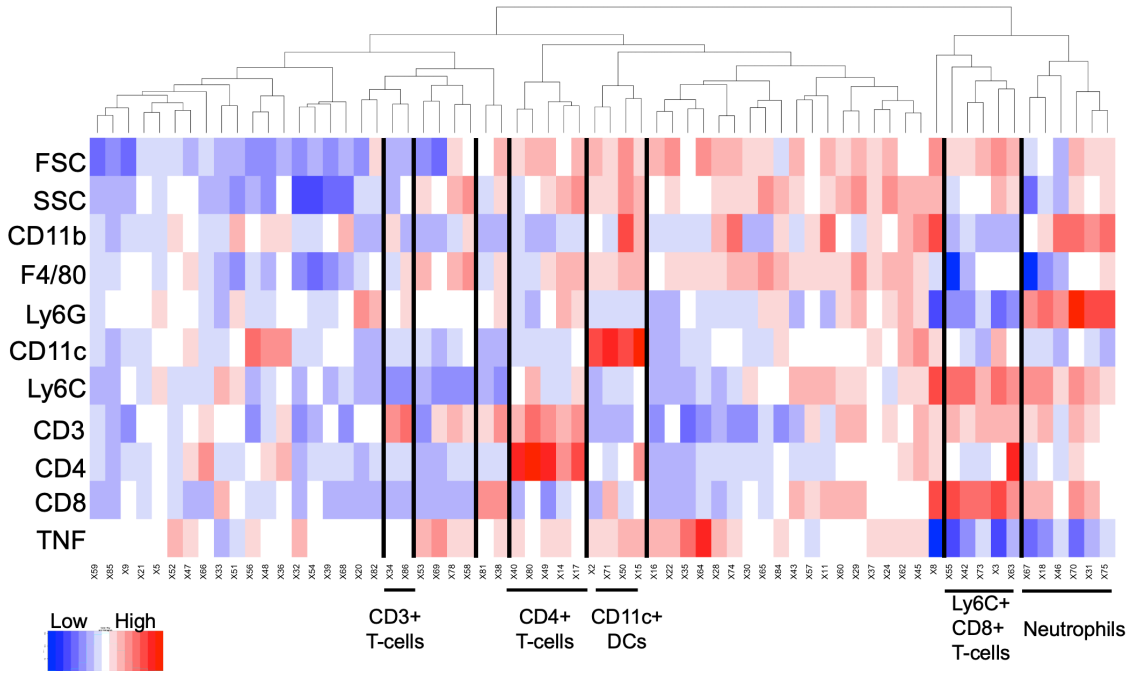

Figure 11. Expression of phenotypic markers used for node characterization.

Median expression for each marker was averaged for all 100 nodes. Results are shown on heatmap following unsupervised hierarchical clustering. Color intensity indicates expression level. Combined expression of different markers was used to identify traditional immune populations, as well as rare cell subsets.

4.2.5 Node distribution shows different proportions in AvrA Peyer's patches compared to controls

Identification of the unique population of CD8+ T-cells led us to compare proportions of adaptive immune cells between control and AvrA treated mice. We developed a base SPADE tree for CD3+ T-cells (Figure 12A) and identified CD4+ cells (Figure 12B) in epithelial/intraepithelial lymphocytes (EC), small intestine lamina propria (SI), and Peyer's patches (PP) populations. We identified six nodes that were CD3+ CD4+. In those nodes, we exported the cell frequencies in the control+LPS group and the AvrA+LPS group. To determine the difference in cell frequencies in the six nodes, we subtracted control from treatment and created tornado plots in order to highlight SPADE nodes with important variations in cell proportions. Nodes were ranked in descending order according to their subtracted proportions between control (n=3) and treatment (n=3). A difference under 0 reflected an abundance of CD4+ cells in treatment groups, whereas a positive difference suggested an increased node proportion in the control+LPS group. The differences in cell frequencies were then plotted (Figure 12C) and compared to the results obtained from flow cytometry (Figure 12D). The trends in cellular heterogeneity reflect the abundance of CD4+ T-cells in control samples with no nodes occupied by CD4+ T-cells in the AvrA treatment group.

Since the SPADE trends validated the shift of cells towards LPS-treated controls in accordance with the raw flow cytometry data, we aimed to elucidate the role of the novel CD8+ Ly6C+ cells in control versus treatment groups. Thus, we created SPADE trees for CD3+ CD8+ T-cells (Figure 13A). Interestingly, from the heatmap, we noticed some nodes had overlapping expression of CD8+ and Ly6C+ cells. Thus, we then created a SPADE tree for CD3+ CD8+ Ly6C+ nodes to elucidate this unexpected cell population (Figure 13B). Potentially increased or decreased nodes' frequencies were plotted for control, control+LPS, and treatment+LPS groups with individual values based on the four nodes that were identified from the CD3+ base tree. We

analyzed node frequencies across these four nodes and found reduced CD8+ Ly6C+ cells in three of the four nodes, #45, #64, and #89, with a statistically significant reduction in cell proportion in AvrA treated groups in node #89 (Figure 13C). However, when analyzing the raw flow cytometry data, though the AvrA group trended towards reduced CD8+ Ly6C+ cell populations, we did not observe the shift in cellular heterogeneity from the raw flow data (Figure 13D). CD8+ T-cells were originally added to the panel for completion, and we did not initially expect to see any changes in this subpopulation of cells. These data suggest a shift in pseudotime, indicating that LPS stimulation increases CD8+ Ly6C+ cells, which are reduced in treated groups.

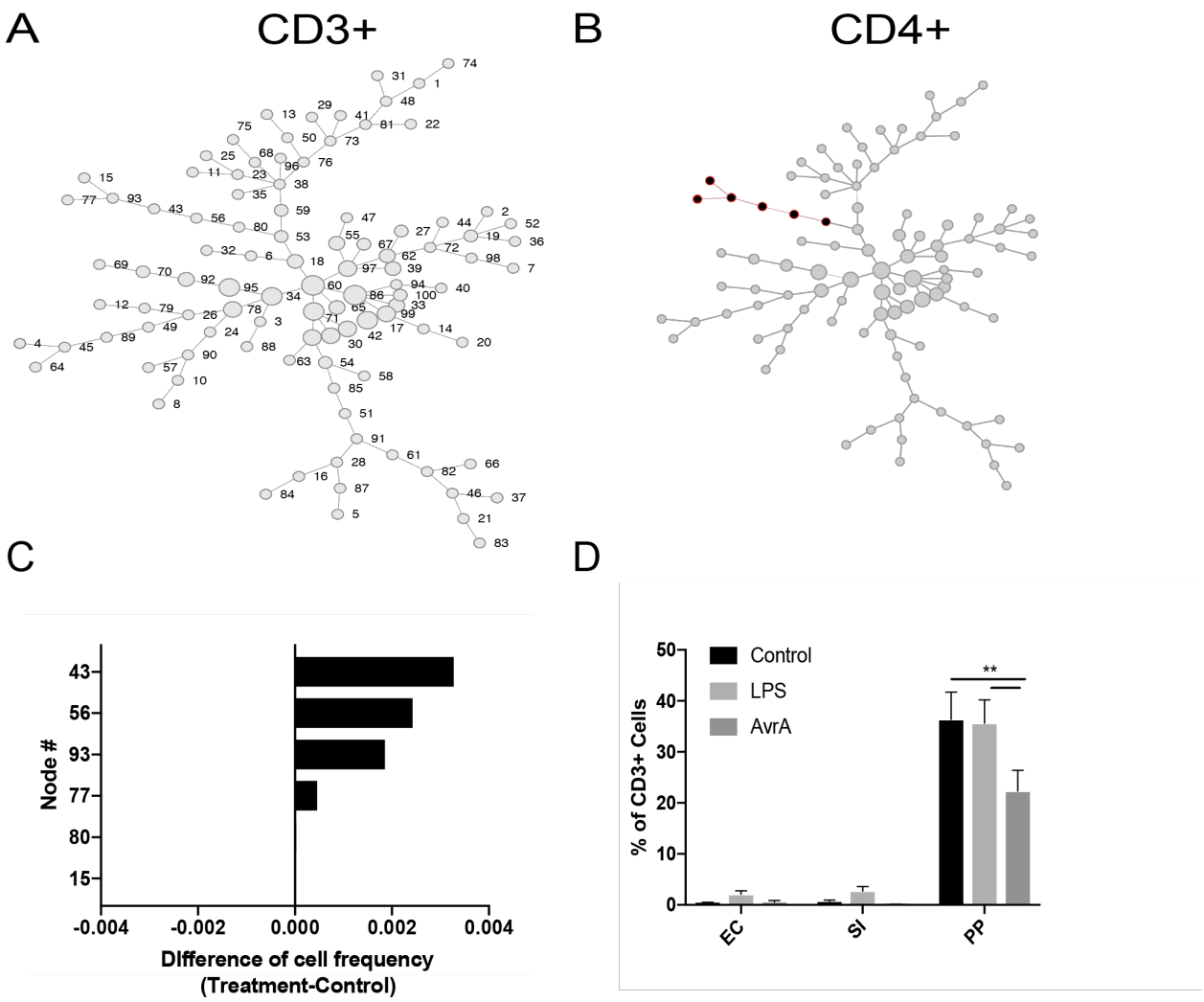

Figure 12 SPADE allows for the identification of characteristic immune populations.

A) A CD3+ base tree was developed after gating for CD3+ T-cells. (B) SPADE analysis indicates nodes positive for CD4+ cells. (C) Cell frequency within each identified node was exported and the difference in cell frequency was plotted on a tornado plot by subtracting control+LPS from the AvrA treatment group. (D) Flow cytometric analysis of CD4+ cells were plotted for comparison. Data presented as mean ± SEM. Statistical analysis was performed using two-way repeated measures ANOVA with Tukey's post-hoc test. *$p<0.05$, **$p<0.01$, n=3.

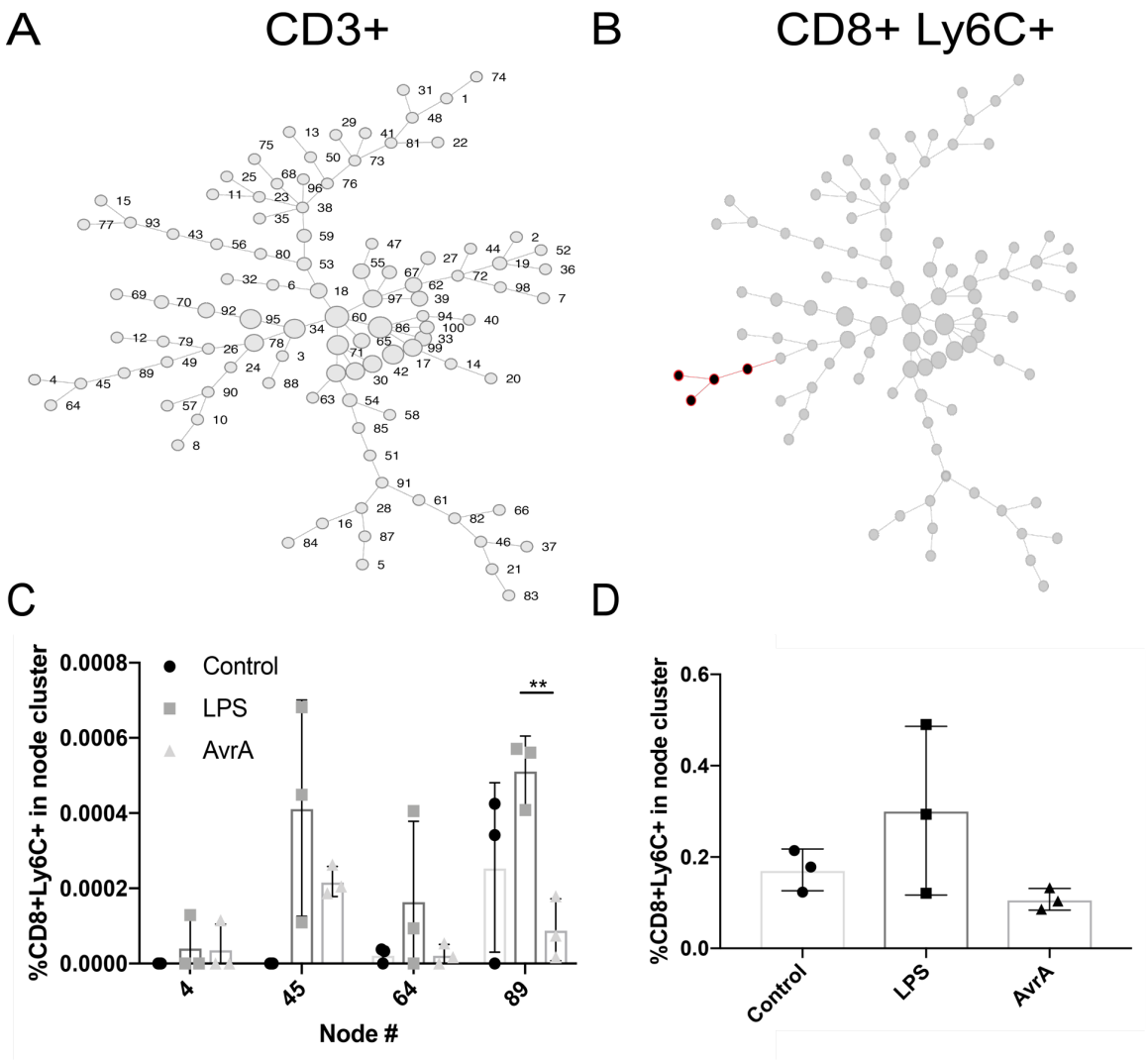

Figure 13 SPADE allows for the quantification of known and rare immune cell subsets.

(A) A CD3+ base tree was developed after gating for CD3+ T-cells. (B) CD8+ Ly6C+ nodes were also identified from the CD3+ base tree. (C) Cell frequencies within each of the four nodes was exported and plotted on a graph to compare control, control+LPS, and AvrA+LPS. (D) CD8+ Ly6C+ cell populations were analyzed from raw flow cytometry data. Data presented as mean ± SEM. Statistical analysis was performed using two-way repeated measures ANOVA with Tukey's post-hoc test. *$p<0.05$, **$p<0.01$,

4.2.6 Salmonella LPS induces both systemic and gastrointestinal inflammation

Unfortunately, *E. coli* LPS stimulation did not produce as robust of an immune response as was expected, particularly in the gastrointestinal tract. In order to validate our findings of the CD8+ Ly6C+ subpopulation of T-cells, we needed to establish a more robust model of acute inflammation. Because immune stimulation is necessary to identify the local and systemic effects of AvrA, we aimed to identify a strain of LPS that would induce inflammation both locally and systemically. LPS are complex amphiphilic molecules that are released from the bacterial cell wall by shedding or through lysis, and are found in the outer membrane of Gram-negative bacteria (241, 242). Thus, we decided to compare LPS isolated from *Salmonella Typhimurium* to that from *E. coli*. *S. Typhimurium* causes self-limiting gastroenteritis in humans and severe inflammation of the intestinal mucosal epithelial, and can also cause systemic infection(243). Thus, LPS from *S. Typhimurium* would likely allow us to investigate the influence of LPS locally versus systemically.

To test this, we treated wild-type mice with both strains of LPS for 24 hours, following which we isolated terminal ileum and spleen for RT-PCR analysis. In the terminal ileum, *E. coli* LPS did not show a change IL-1β or TNF, two inflammatory cytokines (Figure 14A), whereas LPS from *S. Typhimurium* showed a significant increase in both cytokines (Figure 14C). In the spleen, both strains showed a robust increase in TNF following LPS, with increases in IL-1β only observed in the *E. coli* strain (Figure 14B, D).

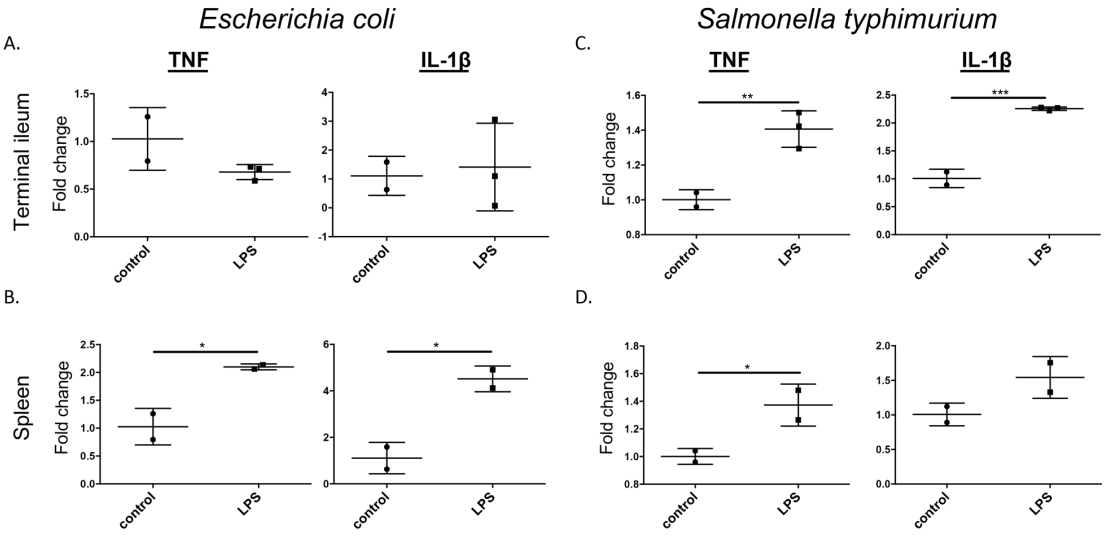

Figure 14. In vivo inflammatory response to E. coli and S. typhimurium.

C57bl/6 mice were given LPS intraperitoneally isolated from E. coli or S. typhimurium. Inflammatory cytokines were measured 24 hours after infection using RT-PCR. TNF and IL-1β were measured in E. coli infected terminal ileum (A) and spleen (B), as well as in S. typhimurium infected terminal ileum (C) and spleen (D). Statistical analyses were conducted using a one-tailed t-test. *$p<0.05$, **$p<0.01$, ***$p<0.001$, across 2-3 animals per group.

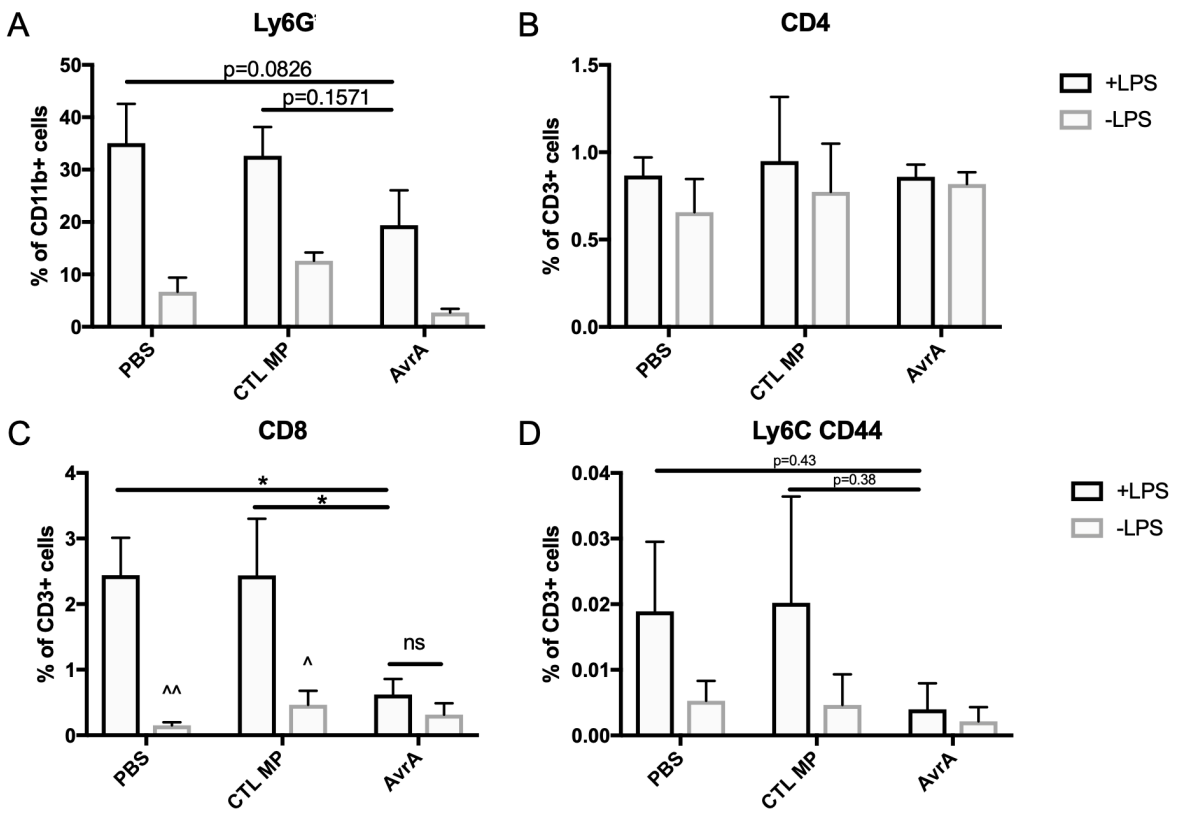

Figure 15. Increased inflammatory cell recruitment induced by *Salmonella* LPS in the IELs is reduced by AvrA MP treatment.

C57bl/6 mice were treated with either PBS alone, PBS+LPS, empty microparticle (CTL MP) alone, CTL MP+LPS, AvrA MP alone (AvrA), or AvrA+LPS, and were sacrificed after 24 hours. Flow cytometric analysis was performed for neutrophils (Ly6G+) (A), CD4+ T-cells (B), CD8+ T-cells (C), and CD8+ Ly6C+ CD44+ T-cells (D). Statistical analysis was performed using two-way repeated measures ANOVA with Tukey's post-hoc test. *$p<0.05$, **$p<0.01$, ***$p<0.001$, $n=4$.

4.2.7 LPS derived from S. Typhimurium *induces gastrointestinal and systemic inflammation*

To study the role of AvrA in a robust model of acute inflammation, we organized treatment groups into PBS alone, PBS+LPS, empty microparticles (CTL MP), CTL MP+LPS, AvrA alone, and AvrA+LPS. Empty microparticles were manufactured by mixing alginate with PBS before loading into the microfluidic device. We pre-treated mice with each treatment group for 5 days, after which we administered intraperitoneal LPS for 1 day. After sacrifice, we isolated epithelial cells and intraepithelial lymphocytes from the small intestine lamina propria for flow cytometry, and identified CD11b+ Ly6G+ (Figure 15A), CD4+ T-cells (Figure 15B), CD8+ T-cells (Figure 15C), as well as the CD8+ Ly6C+ population of cells that was identified by SPADE. We also included CD44+, which is a marker of T-cell activation. We noticed a more robust inflammatory response following intraperitoneal injection of this strain of LPS. Moreover, we observed a reduction of Ly6G+ neutrophils in AvrA treated groups when compared to treatment groups. We also observed a significant reduction in CD8+ T-cells in AvrA compared to both PBS and CTL MPs. Lastly, we also noticed a reduction in CD8+ Ly6C+ CD44+ cells after AvrA treatment compared to both controls. We did not observe significant changes in the CD4+ T-cell population. Lastly, we also did not notice changes in macrophage numbers following stimulation with LPS or following treatment with AvrA (not shown).

Importantly, we did observe a robust increase in splenic immune cell populations, including neutrophils (Figure 16A), macrophages (Figure 16B), and CD8+ T-cells (Figure 16D). There were no differences observed between any of the treatment groups in any of the immune cell subsets. Additionally, CD4+ T-cells (Figure 16C) and CD8+ Ly6C+ CD44+ (Figure 16E) T-cells were unaffected by LPS stimulation.

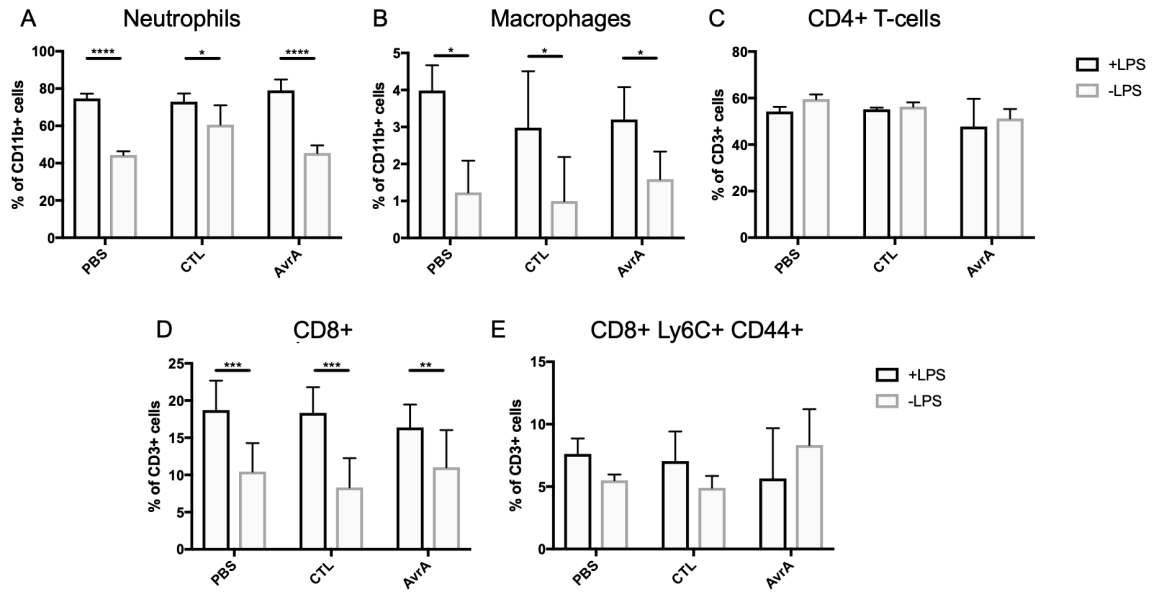

Figure 16. LPS from S. Typhimurium induces a robust systemic immune response

C57bl/6 mice were treated with either PBS alone, PBS+LPS, empty microparticle (CTL) alone, CTL MP+LPS, AvrA MP alone (AvrA), or AvrA+LPS, and were sacrificed after 24 hours. Each spleen was homogenized and processed for flow cytometry. Cell subsets analyzed included neutrophils (CD11b+ Ly6G+) (A), macrophages (CD11b+ F4/80+), CD4+ T-cells (C), CD8+ T-cells (D), and CD8+ Ly6C+ CD44+ T-cells (E). Statistical analysis was performed using two-way repeated measures ANOVA with Tukey's post-hoc test. *$p<0.05$, **$p<0.01$, ***$p<0.001$, ****$p<0.0001$, n=4.

4.3 Discussion

AvrA is an enzyme derived from *Salmonella* that is able to modulate the immune system and influence apoptotic cellular pathways. We have previously shown that AvrA nanoparticles are a clinically viable method of reducing inflammation in the gastrointestinal tract(227). In order to deliver AvrA orally, we previously developed gastro-protective alginate/chitosan MPs that have site-specific effects in the small intestine and colon(8). Here, we wanted to elucidate the spatial distribution of the immune response to AvrA microparticles. The intestinal mucosal immune system is made up of three major areas: the small intestine lamina propria (LP), the intraepithelial lymphocytes (IEL), and Peyer's patches (PP). These different immune centers create a complex network to adequately mount an immune response in the intestine. IELs contain large numbers of T-cells with CD8+ T-cells predominating, whereas the LP is made up of 60% T-cells and 40% B-cells(244, 245). The LP and IELs contain diffusely distributed lymphocytes and contain mostly effector populations. Notably, the IEL populations exhibit minimal recirculation, indicating their functions are limited particularly to the GI tissue(246).

PPs are aggregated lymphoid follicles that collectively make up the GALT(247). This lymphoid tissue is separated into three main areas: the follicular area, interfollicular area, and follicle-associated epithelium (FAE). The follicular and interfollicular areas contain a germinal center (GC), which is made up of proliferative B-lymphocytes, follicular dendritic cells (FDCs), and macrophages. Outside of this area is the corona, made up of B-cells, T-cells, macrophages, and DCs(94). The FAE contains both epithelial cells and M-cells, specialized cells involved in the transcytosis of luminal material. In the mouse, PPs contain 60% B-cells (B220+); 25% T-cells (CD3+), with 45% CD4+ cells, 35% CD8+, and 20% CD4-/CD8- cells; 10% DCs (CD11c+); and around 5% macrophages (F4/80+) or neutrophils (Ly6G+)(248). There also exists a CD11c+ CD8a+ CD11b- DC population within the interfollicular region(249, 250). Targeting cells in the PP has become a strategy for oral therapeutics because of its important role in the mucosal

immune system and due to its constant sampling of the intestinal lumen(251, 252). The PP also have been shown to uptake of nanoparticles through the lymphatic system(253).

Here, we show that AvrA MPs influence local innate and adaptive immunity at several layers of GI immunity. First, we demonstrate that AvrA MPs influenced innate immunity in the PPs and epithelium. Notably, we observed a reduction in intracellular TNF in the intestinal epithelium. Epithelial cells (ECs) play an important role in maintaining integrity of the mucosal barrier, and is an important mediator in signaling to the surrounding immune microenvironment(254). In addition, we observed a reduction in neutrophil populations in mice treated with AvrA microparticles in the local PPs when compared to controls as well as a reduction in CD4+ T-cells. Lastly, we found a significant decrease of CD8+ T-cells in the IELs after AvrA microparticle treatment.

In order to confirm reliability of our data, we validated our work using non-supervised dimensionality reduction approach. Thus, we used SPADE to highlight novel aspects of immune alterations developed after immunomodulatory hydrogel treatment. SPADE is a dimensionality reduction technique that hierarchically clusters phenotypically similar cells into “nodes”. These nodes and their relationships are organized into a minimum spanning tree, or “SPADE tree”. We then created a heatmap to create a 2D visualization representing marker expression of each node for all the markers used. Using SPADE analysis, we were able to confirm that AvrA treatment results reduced CD4+ T-cells in the PPs. However, on our heatmap, we also noticed 4-5 nodes that were positive for Ly6C+ and CD8+ T-cells. When we explored this on our SPADE tree, we confirmed a population of CD8+ T-cells that co-expressed Ly6C+. Ly6C is an activation marker of CD8+ T-cells, potentially indicating that, in a more robust model of inflammation, AvrA is inhibiting the activation status of this subset of T-cells(255). Previous studies also suggest that Ly6C+ expression on naïve CD8+ T-cells may be involved in the effector fate of this subset of T-cells(256).

In order to elucidate the effects of CD8+ Ly6C+ T-cells, we aimed to identify a more robust method to induce acute inflammation. After testing strains of LPS isolated from *Salmonella typhimurium* and *E. coli*, we established that *S. tymphimurium* infection causes both systemic and GI inflammation. We then separated mice into a control PBS group, a control empty alginate/chitosan microparticle group (CTL MPs), and an AvrA treatment group, and mice were treated for 5 days prior to LPS stimulation. Half of each group (n=4) received *S. typhimurium* LPS administration intraperitoneally, while the other half (n=4) received intraperitoneal administration of vehicle(257). Interestingly, when we attempted to isolate PPs for flow cytometry, we were unable to find any in the AvrA+LPS treated groups, and thus decided to focus on IELs and spleen. Within the IEL immune population, we found that AvrA MP treatment caused a reduction in Ly6G+ neutrophils, and a significant reduction in CD8+ T-cells. CD4+ T-cells were not affected by either LPS or AvrA treatment. Within our adaptive immune cell panel, we included CD44+ as a marker for T-cells, as CD44 is an activation-associated surface marker on T-cells in order to confirm the presence of CD8+ Ly6C+ effector T-cells. As a result, we noticed a reduction in CD8+ Ly6C+ CD44+ cells. However, 24 hours is too short of a time frame to truly visualize the effects on T-lymphocytes. In order to get a full appreciation of the effects on this adaptive immune cell population, it would be necessary to sacrifice animals around 72 hours following LPS stimulation. These data suggest that AvrA results in an amelioration of the innate immune response at several levels of the GI immune system. More interestingly, however, AvrA seems to modulate the activation of CD8+ T-cells, potentially playing an immunosuppressive role on the adaptive immune system. Lastly, the usage of SPADE analysis allowed discrimination of rare cell subsets, highlighting new features of the immune response to explore while developing immunomodulatory therapeutics.

4.4 Methods

4.4.1 Synthesis of AvrA nanoparticles

eGFP and AvrA nanoparticles were prepared as previously described(8). In brief, eGFP was expressed in BL21 *Escherichia coli* with chloramphenicol (VWR) in 2XYT media. eGFP was purified on Ni-NTA agarose (Qiagen) following imidazole purification. AvrA was contained in a plasmid (GE Lifesciences) and expressed in AFIQ Escherichia coli with chloramphenicol and ampicillin in 2XYT media. AvrA bacterial cultures were grown to o.d. 0.7 at 37ºC and induced with 0.4 mM isopropyl B-D-thiogalactoside (IPTG) at 25ºC for 4 hours. AvrA was purified with glutathione sepharose 4B (GE Healthcare), then repurified on Ni-NTA agarose following manufacturer's native imidazole purification. Purified proteins were concentrated using 10k MWCO centrifugal ultrafiltration devices (Milipore) using eGFP concenrations of ~12mg/ml and 1mg/ml AvrA in elution buffer.

4.4.2 AvrA and eGFP Nanoparticle Synthesis

Protein nanoparticles were prepared by desolvation as previously described(258). 50 µl of eGFP and 50 µl of AvrA were combined in a glass vial. The combined solution was desolvated via continuous, drop-by-drop addition of 400 µl ethanol at an addition rate of 1 ml/min. After desolvation, particles were crosslinked with 5 mg/ml Dithiobis(sulfosuccinimidyl-propionate) (DTSSP; Pierce) at a 1:2.2 ratio. After stirring for 90 minutes, cross-linking was stopped by centrifugation at 500 g for 5 min. Particles were re-suspended in PBS and sonicated on ice (1s on, 3s off, 50% amplitude, 1 minute).

4.4.3 Nanoparticle characterization

Average particle size was calculated as the mean of 2 batches of particles. NP concentration was determined using a BCA assay (Pierce) following manufacturer's protocol. Gel electrophoresis

was used to determine NP composition. Briefly, 50 µg of NP were heated in sodium dodecyl sulfate-polyacrylamide gel electrophoresis (SDS-PAGE) loading buffer (50 mM Tris-Cl, pH 6.8, 2% SDS, 100 mM DTT, 0.1% bromophenol blue, 10% glycerol), for 5 minutes. Proteins were transferred to nitrocellulose membrane and labelled with an Alexa-Fluor 488 conjugated penta-his antibody (Qiagen) for imaging.

4.4.4 Microfluidic device preparation

A silicon master wafer was fabricated using multi-layer soft lithography and was generously gifted from Emily Jackson-Holmes and Professor Hang Lu. Polydimethylsiloxane (PDMS) devices (Sylgard 184, Dow Corning) were prepared at a 10:1 base to crosslinker ratio. The mixture was degassed for 1 hour at 70ºC. PDMS was poured onto the master wafer and cured overnight. PDMS was then cut from the master wafer molds, and inlet and outlet channels were created using 18-gauge needles. Each device was plasma treated (PDC-32G plasma cleaner) and bonded onto glass slides. PDMS devices were stored at room temperature until needed.

4.4.5 Microparticle fabrication

Low viscosity alginate (4% w/v) Protanal LF 200FTS, FMC Biopolymers) was dissolved in deionized water (DI) overnight. Protein NPs or PBS (empty microparticles, Sigma) were comined with alginate solution to a final alginate concentration of 2% w/v. The alginate/NP/PBS mixture was loaded into a 10 ml syringe with a 20-gauge needle (dispersed phase). 1% Span 80 (TCI America) in mineral oil (VWR) was loaded into a 60-ml syringe with a 20-gauge needle (continuous phase). The syringes were loaded on two syringe pumps and the needles were connected to the microfluidic device. The flow rate of the dispersed phase was loaded as 10 µl/min, and the flow rate of the oil phase was 50 µl/min.

The outflow of the microfluidic device was dropped into a solution of 0.5% chitosan (85% deacetylated, Alfa Aesar) and 0.1% $CaCl_2$ (VWR) at a final pH of 5.5. The device was

allowed to run overnight at constant stirring. Alginate/chitosan MPs were collected the following morning and washed at 500g, and resuspended in DI water until no more oil was observed. 200 µL of chitosan-coated alginate MPs were imaged on bright-field microscopy to measure MP diameter.

4.4.6 LPS stimulation of C57bl/6 mice

Care of experimental animals was performed in accordance with Emory University IACUC guidelines. C57BL/6 mice were fasted overnight and treatment groups (n=4) were administered with 4 mg empty MPs, 4 mg AvrA NPs in MPs, or PBS via oral gavage. Total volume of gavage was 200 µl. Mice were gavaged once a day at the same time for 5 days prior to LPS stimulation. LPS was prepared using a stock from either Escherichia coli 0111:B4 under sterile conditions to a working concentration of 0.2 µg/µl. Female mice were weighed and 10 µl/g body weight of LPS was administered intraperitoneally. Mice were monitored for 24 hours, including observing fur appearance, activity, level of consciousness, and respiration rate. After 24 hours, spleen, Peyer's patches, and small intestine were isolated and processed for RT-PCR or flow cytometry.

4.4.7 RT-PCR

For transcriptional analysis, spleen and small intestine (terminal ileum) were dissected and processed. Terminal ileum was identified as the tissue about 1.5 cm proximal to the cecum. Tissue was mechanically disrupted in Trizol using a MagnaLyser with MagnaLyser beads. RNA was prepared according to manufacturer's instructions. RT-PCR was performed using SybrGreen Supermix (Bio-Red) using the following primers:

Table 1 RT-PCR Primers for Inflammatory Cytokines

Name	**Forward Primer**	**Reverse Primer**
Actin	CGGTTCCGATGCCCTGAGGCTCTT	CGTCACACTTCATGATGGAATTGA
IL-1b	AATCTGTACCTGTCCTGCGTGTT	TGGGTAATTTTTGGGATCTACACTCT
TNF	TCTTCTCGAACCCCGAGTGA	CCTCTGATGGCACCACCAG

Data was normalized to Actin. In addition, data was analysed using 2^{ddCt} method.

4.4.8 Tissue Harvest and Flow Cytometry

To collect samples for flow cytometry analysis, mice were euthanized via CO_2 asphyxiation and digested according to previously described protocol(259). Briefly, Peyer's patches and spleen were identified and isolated using scissors. Tissue from both PPs and spleen was separated with a 100 μm cell strainer to create a single cell suspension. Small intestine was isolated and flushed with cold PBS. Tissue segments were placed in extraction media (Hank's Buffered Salt Solution, Millipore Sigma, 5 mM EDTA, 10 mM HEPES) and incubated for 15 minutes while shaking at 37ºC.

After incubation, the supernatant containing epithelial cell and intraepithelial lymphocytes was isolated using a 100 μm cell strainer. The remaining small intestinal tissue was placed into 6 ml of digestion media (RPMI, Millipore Sigma, 1 mg/ml collagenase V) and vigorously shaken at 37ºC. The digested tissue was filtered through a 100 μm strainer and rinsed with RPMI containing 10% FBS. The four solutions, containing epithelial cells, small intestine,

spleen, and Peyer's patches, were centrifuged at 800 x g for 5 minutes at 4ºC. The cell pellet was resuspended in 1 ml RPMI containing 2% FBS. Single cell suspensions were stained for flow cytometry analysis using standard methods and analysed on a BD LSRFortessa (BD Biosciences).

Dead cells were excluded through staining using Zombie UV fixable viability stain (BioLegend). The antibodies used for identifying cell populations were: PerCP conjugated CD3 (BioLegend), BV605 conjugated CD4 (BioLegend), BV785 conjugated CD8, APC-Cy7-conjugated Ly6G (BioLegend), BV510-conjugated CD11b (BioLegend), BV711-conjugated Ly6C (BioLegend), BV421 conjugated CD11c (BioLegend), PE-Cy7 conjugated E-Cadherin (BioLegend), APC conjugated F4/80 (BioLegend), PE conjugated TNF (BioLegend), and Alexa Fluor 488 conjugated CD44 (BioLegend). Staining using BV dyes was performed using Brilliant Stain Buffer (BD Biosciences). Cells were stained for intracellular cytokines using a Fixation/Permeabilization Solution Kit (BD Biosciences). Absolute quantification of cell numbers was performed by adding 30 µl of CountBright Absolute Counting Beads (Thermo Fisher Scientific) to flow cytometry samples.

4.4.9 SPADE analysis

Dimensionality reduction analysis was performed using MATLAB-based Spanning-tree Progression Analysis of Density-normalized Events (SPADE). SPADE is a computational technique that performs density-dependent down-sampling, agglomerative clustering, linking clusters using minimum spanning-tree algorithm, and finally, up-samples based on user input. The SPADE trees generated here were generated by exporting compensated pre-gated single cells. The markers used to build the SPADE tree were SSC, FSC, CD11b, Ly6G, CD11c, CD8, CD4, E-Cadherin, Ly6C, CD44, and TNF-a. The following SPADE parameters were used: Apply compensation matrix in FCS header, Arcsinh transformation with cofactor 150, neighborhood size 5, local density approximation factor 1.5, max allowable cells in pooled downsampled data 50000, target density 20000 cells remaining, and number of desired clusters 100.

4.4.10 Statistical analysis

All statistical analyses were performed using Graphpad Prism version 7.0d (La Jolla, CA). Results are reported as mean ± standard error of the mean (SEM). For grouped analyses, one-way ANOVA with Tukey's post-test was used for multiple comparisons. Tukey's test was used when comparing paired samples. $p<0.05$ was considered statistically significant.

CHAPTER 5. DEVELOPMENT OF NANO-PARTICLE BASED IMMUNE MODIFIERS FOR THE TREATMENT OF TH2-MEDIATED DISEASE

5.1 Introduction

Each immune process is the result of a single initial signal, such as recognition of a foreign antigen by an immune cell(260). The first line of defense is the innate immune system. Upon antigen recognition, macrophages and neutrophils mount an immune response, which results in the production of signaling cytokines and chemokines to signal to the local microenvironment(261). The second line of defense is the adaptive immune system. Naïve CD4+ T cells undergo clonal expansion and differentiation into distinct helper T (Th) cell subtypes, including Th1, Th2, and Th17 cells. Each subtype directs immune responses by producing specific cytokines to manage the immune response to pathogens(262). Upon contact with antigen, differentiated cells migrate to inflammatory sites and produce large quantities of effector cytokines.

The imbalance of T-cell subtypes is associated with the pathogenesis of autoimmune and allergic diseases.(263) Th1 and Th17 cell dysregulation is implicated in autoinflammation, whereas Th2 cells can drive allergic inflammation(10). Th2 cells express GATA-binding protein 3 (GATA3), and secrete IL-4, IL-5, and IL-13. GATA3 is expressed in early T cell precursors and plays important roles throughout T cell development and maturation(264). Deletion of GATA3 in CD4+ T cells prevents their differentiation into Th2 cells, forcing a Th1 phenotype(265). Introducing GATA3 into differentiating Th1 cells induces the production and release of Th2 cytokines(266). Thus, GATA3 acts as a master transcription factor for Th2 cell differentiation

and inhibition of the Th1 phenotype. Elevated GATA3 expression has been reported in a number of other chronic inflammatory disorders, including atopy and allergic asthma, and ulcerative colitis(267). Therefore, efforts have been focused on modulating the expression of GATA3(221).

Asthma is a chronic respiratory illness that affects millions of Americans each year, resulting in billions of dollars of healthcare costs. Viral upper respiratory tract infections, allergens, and stress often trigger asthma symptoms and worsen inflammation (268). The current backbone of asthma therapy is maintenance and control of symptoms. If symptoms are not well controlled, additional asthma medications are added in a step-wise approach (269). Corticosteroids have long been used to manage asthma because they inhibit synthesis of key factors that cause and augment inflammation. Currently, inhaled corticosteroids are first line treatment for mild and moderate asthma, but severe asthma often requires oral corticosteroids to manage the disease. Oral corticosteroids have numerous side effects including hyperglycemia, weight gain, psychosis, and osteoporosis (270). Therefore, directed therapies to regulate these inflammatory signals without causing side effects are imperative for disease management.

The most prevalent type of asthma (50% of patients) displays a Th2 endotype, which is characterized by an overabundance of Th2 cells that overexpress GATA3, causing a cascade in production and release of inflammatory cytokines such as IL-4, IL-5, and IL-13(271). Moreover, GATA3 has been found to be upregulated in biopsies and serum from patients with severe asthma, even while on oral corticosteroids (13), and has been shown to be expressed in resident lung cell types, such as mast cells (272), eosinophils (273), and airway epithelial cells (274). GATA3 blockade is a promising therapeutic strategy for the Th2 asthma endotype (275). Inhibiting GATA3 production by gene knockdown has been shown to suppress expression of cytokines and prevent the induction of airway hyperresponsiveness amongst other asthma symptoms (276). A recent phase I clinical trial demonstrated that administering GATA3-based inhibitors by inhalation can reduce the impact of an allergen challenge on FEV1 (forced expiratory volume in one second) in mild asthmatics (277). This study found that after treatment,

both the early and late asthmatic responses were attenuated, improving overall airway function(278). This emphasized the importance of GATA3 in regulating the asthmatic response.

GATA3 has also been implicated in IBD, an autoimmune disease with similar pathogenic features of immune dysregulation. Inflammatory bowel disease (IBD) is comprised of 2 major disorders: ulcerative colitis (UC)(279) and Crohn's disease (CD)(280). The exact etiology of IBD remains unknown, although studies have shown contributions from both the adaptive and innate immune systems. Several studies suggest the important roles of GATA3 in inducing and activating Th2 cytokine production. A recent study found increased expression of GATA3 in patients with active UC(267), and tested the efficacy of the same GATA3 based inhibitor in patients with UC. After rectal administration, this GATA3 inhibitor ameliorated colitis activity and led to suppression of Th2 cytokines(267). This work indicates the potential for GATA3 blockade in colitis.

Current therapies for UC, however, mainly focus on anti-TNF-α and alleviation of the acute phase immune response. Infliximab and Adalimumab, two of the most popular medications, are TNF-inhibiting antibodies(281). New developments in the treatment of inflammatory disorders include monoclonal antibodies, such as omalizumab and mepolizumab (282), that have specific inflammatory targets. While these drugs specifically bind IgE and IL-5 respectively, they present a risk of anaphylaxis, a potentially life threatening condition (283). Recently, nucleic acid-based therapeutics have gained significant interest for their sequence-specific gene modulation. Six oligonucleotide-based drugs have been approved by the US Food and Drug Administration. Current oligonucleotides therapies have been approved for cytomegaloviral retinitis, familial hypercholesterolemia, Duchenne muscular dystrophy, and spinal muscular atrophy (SMA)(284, 285).

Three gene regulation strategies are commonly utilized with oligonucleotide therapies, where the goal is to modulate disease intracellularly at the most upstream transcriptional level. These strategies are antisense oligonucleotides (ASO), which inhibit gene expression by binding

mRNA via Watson-Crick base pairing(286), catalytically active DNA enzymes (DNAzymes, Dz), which bind and cleave complementary RNA, and small interfering RNA (siRNA), which recruit the RISC complex to degrade RNA(287). However, major disadvantages to ASO delivery *in vivo* include nonspecific binding to proteins like fibroblast growth factor, and the upregulation of pro-inflammatory factors(285). RNA interference (RNAi), such as small interfering RNA (siRNA) and microRNA (miRNA), requires the RNA-induced silencing complex (RISC) to induce mRNA degradation depending on sequence complementarity(288). While this technique exhibits higher efficiency compared to ASO, controlling intracellular bioavailability has proven difficult. Further, RNAi delivery and maintenance is difficult due to anatomical barriers, immunoreactivity, delivery challenges, and drug stability (289).

Alternatively, Dzs represent a novel class of antisense molecules with several important properties that make them a strong candidate for gene regulation therapy. A well-known and widely studied Dz is the ’10-23’ Dz, described by Santoro and Joyce in 1997(290). It is an RNA-cleaving DNA molecule consisting of a catalytic domain and 2 substrate binding arms. The binding arms hybridize to RNA sequences of interest, allowing the ’10-23’ Dz to accurately identify the RNA target in the cytoplasm, and the 15 base catalytic core cleaves at preferred purine-pyrimidine junctions. Though the exact mechanism of cleavage by the ’10-23’ Dz remains elusive, Liu et al. recently postulated that the ‘8-17’ Dz, a structurally similar Dz, likely adopts a V-shape fold consisting of a twisted DNA pseudoknot, forcing the RNA to bend and form a kink at the site of cleavage. This suggests a general acid-base mechanism of RNA catalysis(291).

In 2008, Sel et al. manually scanned the GATA3 mRNA code and identified 70 potential Dzs *in vitro*, selecting specifically around purine-uracil junctions(292). The authors hoped to identify a Dz for targeting allergic and inflammatory disorders and identified a Dz, denoted as SB010. This therapy was an intracellular approach to regulate Th2 cell differentiation and control of subsequent cytokine transcription. Beyond the targeting capabilities of Th2 cells, GATA3 was recently shown to be expressed in epithelial cells, mast cells, basophils, and eosinophils(293).

This suggests that GATA3 signaling may contribute to progression and perpetuation of the inflammatory response. Thus, intracellular disruption of GATA3 signaling is promising in reducing long-term inflammatory signals that damage the integrity of tissues. The authors validated each sequence using *in vitro* cleavage assays and verifying activity in acute and chronic allergic airway mouse models of asthma. Moreover, they compared the Dz to alternative antisense strategies, such as traditional antisense and siRNA, showing no differences in efficacy between the three. Notably, the Dz approach had the most potent effect on eosinophils.

The authors note two important challenges in this technology. The first is off-target effects. The authors note that off-target effects are unfortunately common as a result of the interaction of foreign oligonucleotides with pattern recognition receptors, including toll-like receptors (TLRs), that respond to single- or double-stranded DNA, RNA, or CpG-motif-containing DNA molecules(294, 295). Introducing a foreign piece of DNA is likely to stimulate the host's innate immune system, resulting in an increased Th1 inflammatory component. This was observed using the traditional ASO approach in the study, which seemed to stimulate proinflammatory signals.

The second challenge is efficacy of delivery, a challenge that has long plagued the antisense field with regards to *in vivo* applications. Oligonucleotide movement across the plasma membrane is challenging. Accordingly, clinical trials require 2 mg doses of oligonucleotides per patient per day, only showing moderate efficacy(296). In principle, improving the stability and delivery of Dzs will transform this new class of therapy.

To overcome the challenges of delivering Dzs as gene regulation agents, we have developed and tested Dz-coated gold nanoparticles (DzNP) for gene regulation. This approach is based on the recent discovery by Mirkin and colleagues that showed that high density DNA arranged spherically around a ~10 nm nanoparticle leads to rapid recognition and uptake by over 50 different cell types(297). These conjugates have passed phase 1 clinical trials for the treatment of inflammation in psoriasis (See Exicure press release http://www.exicuretx.com/). Importantly,

Mirkin and colleagues have shown that internalization is driven by caveolae-mediated endocytosis through binding of the scavenger receptor A (SRA) on the cell surface(298). The primary role of this receptor is the internalization of negatively charged oxidized LDL particles (that are ~20 nanometer in size). Building on this work, our lab demonstrated that 100 copies of Dz molecules immobilized onto a 14 nm gold nanoparticle through the 3' terminus (but not the 5' terminus) are highly active for mRNA knock down (299). We recently showed that DzNP can be used to knockdown TNF-α in a rat model of myocardial infarction(300). These DzNPs showed significant improvement in heart function following treatment with the active nanoparticle. In addition, DzNPs evade nuclease activity, as the conjugation to the gold nanoparticle creates a shell protecting the Dz. DzNPs showed minimal off-target effects and did not require the use of any transfection agents (300). Therefore, DzNPs offer an attractive approach for delivering functional nucleic acids.

One concern with the DzNP strategy is the accumulation of gold metal within the cell. This is unlikely to be an issue because gold is one of the most biocompatible and least reactive metals known (301). Animal studies and human trials (rheumatoid arthritis (302, 303) and psoriasis) with DNA-modified gold particles have been successful both in our lab and others. Further, it does not elicit an immune response from the surrounding environment when injected, making it non-immunogenic and an ideal carrier for functionalized oligonucleotides (304). This proposal will focus on developing DzNPs to target two inflammatory diseases, asthma and IBD. We will investigate optimal methods of GATA3 DzNP delivery to the lung, and its efficacy on reducing inflammation in asthma. In addition, we develop a combined method of treating inflammatory colitis using our improved GATA3 DzNP in combination with an anti-TNF-α DzNP. This technology has broad applications, as this work opens the door to targeting additional signals within the immune system and provides enhanced insight to the role of key players in inflammatory disease.

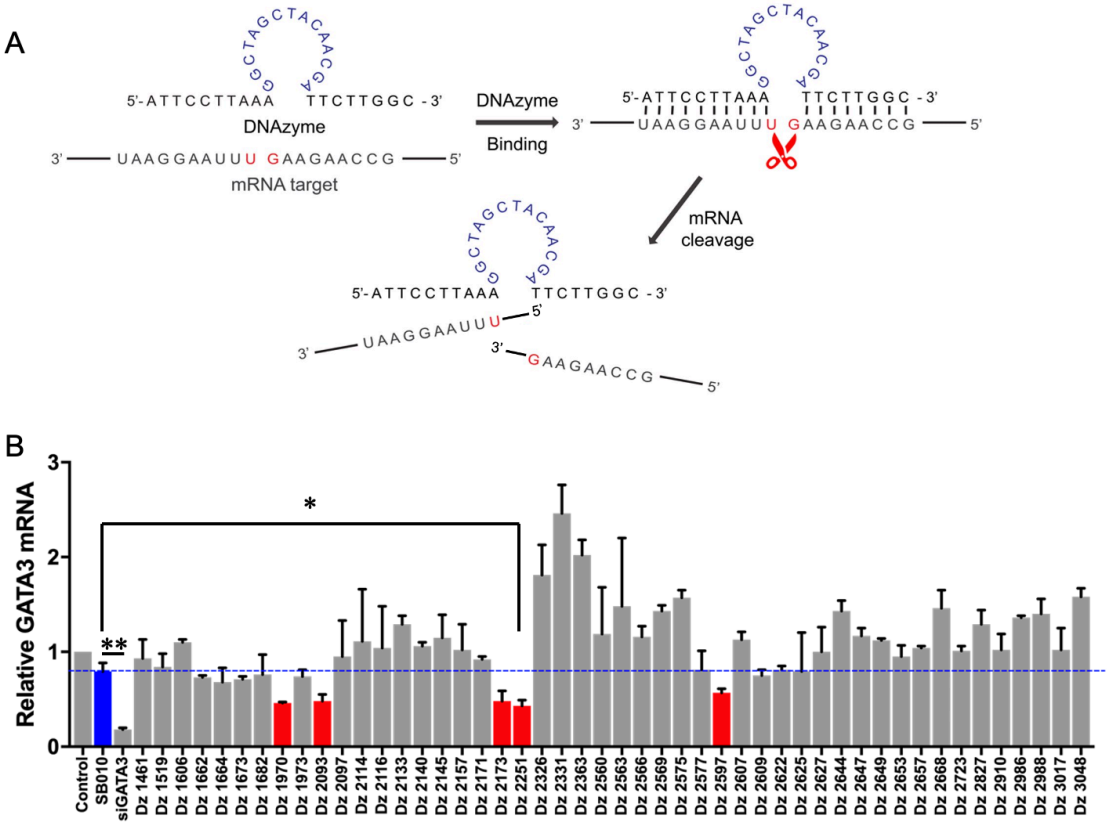

Figure 17. *In silico* Dz screen reveals 48 possible sequences.

(A) Schematic illustration of the 10-23 Dz. Catalytic motifs are shown in blue. (B). Screening of a library of of 48 Dz sequences determined by *in silico* analysis for optimal GATA3 targetic sequence. Knockdown of GATA3 in a T47D breast cancer cell line was determined by RT-PCR. Red dotted line indicates level of SB010, a previously published GATA3 Dz. 18S was used as a housekeeping gene. Data is represented as mean + SEM. Statistical analysis was performed using one-way repeated measures ANOVA with Tukey's post-hoc test. *$p<0.05$, **$p<0.01$

5.2 Results

5.2.1 In silico GATA3 DNAzyme screen

The '10-23' Dz, described by Santoro and Joyce, is composed of a 15 deoxyribonucleotide catalytic core flanked by two substrate recognition arms(290). In the presence of Mg^{2+}, it will cleave any RNA substrate between an unpaired purine (A, G) and a paired pyrimidine (U, C) (Figure 17A). Its catalytic efficiency is determined by the rate of association between Dz and RNA substrate, and has been shown to have excellent catalytic efficiency(305). Because this heteroduplex formation determines the rate of catalysis, it is necessary to select an accessible cleavage site within the secondary structure of mRNA. Moreover, Dzs display strong substrate specificity and are thus sensitive to base-pairing mismatches in the recognition arm(306).

We developed an algorithm for determining the optimal Dz sequence for any RNA sequence of interest. The RNA sequence of interest is scanned from 5' to 3' for AU or GU junctions. The free energy of hybridization is calculated for each binding arm to achieve optimal thermodynamic parameters for the DNA-RNA duplex. The algorithm then matches human with mouse gene variants and ranks each sequence by the free energy of the most stable secondary structure. Each sequence is then converted to a Dz sequence and the sequences are ranked based on human and mouse gene target base locations, left and right arm lengths, and secondary structure.

Because the authors of the previously published GATA3 Dz only tested the first 70 hits around purine-uracil junctions, we anticipated that our algorithm would be able to identify their sequence, but likely also predict more optimal sequences. We performed this analysis for a GATA3 specific Dz, which resulted in a library of 48 possible additional hits. To validate these results, we tested each sequence by transfecting them *in vitro*, using a model breast cancer cell

line known to overexpress GATA3 (Figure 17B). RT-PCR analysis allowed for the isolation of three hits, 2093, 2251, and 2597, that had the highest level of knockdown over SB010, verifying that our algorithm can identify potent Dz sequences. These hits were selected for further analysis due to their increased potency of GATA3 knockdown.

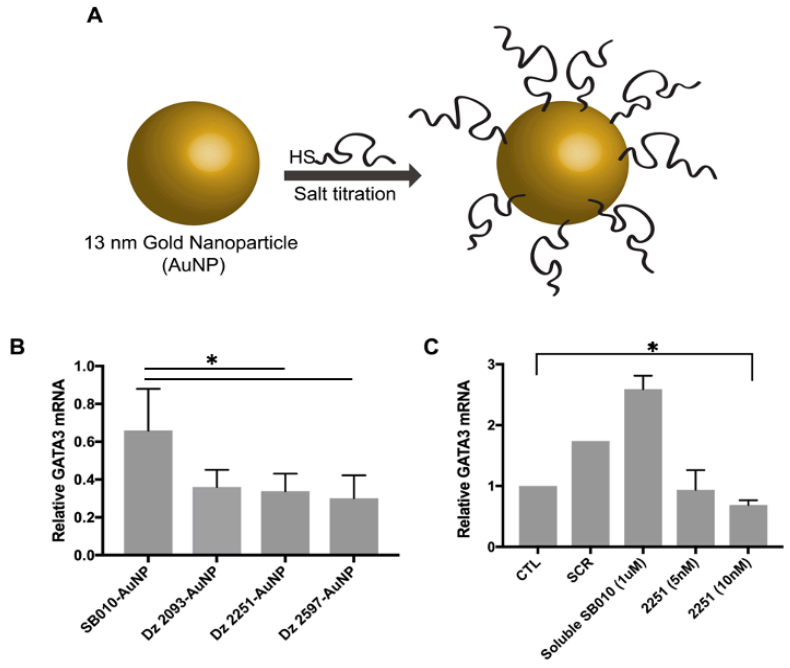

Figure 18 DzNP synthesis and catalytic efficiency.

(A) Schematic showing synthesis of Dz-modified gold nanoparticles (AuNP). Thiolated DNA was mixed with 13 nm AuNP with gradual increase in salt concentration. (B) Dzs SB010, 2093, 2251, and 2597 were conjugated on AuNP (DzNP). T47D cells were treated with 5 nM of each DzNP construct and RNA was isolated after 48 hours. RT-PCR analysis for GATA3 implicated sequence 2251 with the highest potency. (C) 2251-AuNP was tested against soluble SB010 in T47D cells at 5 nM and 10 nM concentrations and GATA3 expression was quantified. GATA3 mRNA was significantly reduced at 10nM in just 24 hours. Statistical analysis was performed using one-way repeated measures ANOVA with Tukey post-hoc test. *$p<0.05$, **$p<0.01$, n=3.

5.2.2 DzNPs regulation of GATA3 gene

Dz sequences 2093, 2251, and 2597 showed improved efficacy over SB010 when tested *in vitro* following Lipofectamine transfection. To validate our DzNP technology, we tested the efficacy of each of the three sequences, 2093, 2251, and 2597, against SB010 when functionalized on gold nanoparticles (DzNPs). To achieve this, we purchased a 3'thiol modified 2093, 2251, and 2597 and conjugated it to AuNPs. Approximately 100 copies of this Dz were functionalized onto a 14-nm gold via the salt-aging method previously published by Hill et al (307) (Figure 18A). A model breast cancer cell line, T47D, was used due to its overexpression of GATA3.

Cells were incubated with 5 nM of each DzNP for 48 hours, and RT-PCR was performed to assess GATA3 expression. These data showed DzNPs 2251 and 2597 reducing GATA3 mRNA expression, with 2251 consistently exhibiting the most potent knockdown of GATA3 (Figure 18B). DzNP-2251 was compared to soluble SB010 without Lipofectamine to demonstrate the effects of DzNP against soluble Dz. This showed that the DzNP significantly enhanced potency of GATA3 knockdown *in vitro* (Figure 18C)**.** These data suggest that DzNP-2251 is a viable GATA3 therapeutic for inflammatory disease.

5.2.3 Investigate DzNP-mediated delivery to the lungs of an animal model

The airways are characterized into two vital regions: the conducting, or upper, airways and the lower respiratory region. The respiratory airway consists of respiratory bronchioles, alveolar ducts, and alveolar sacs. The lung encounters a number of foreign particles on a daily basis, which are either captured at the level of the upper airway on the mucocilliary surface or interact with the immune cells in the lower airway(308). At the level of the alveoli are a number

of immune cells, including alveolar macrophages, eosinophils, T-cells, and mast cells. Asthma is a common disease that is characterized by difficulty breathing and wheezing. Allergic asthma is a Th2-mediated disease, and a number of Th2-animal models of asthma have been established for the development of therapeutics(309).

Delivering DzNPs to the lung poses several challenges. Directly targeting lung tissue by administering drug dropwise intranasally (IN) may lead to loss in the anatomical dead space, mainly in conducting airways. Nebulization (neb) may be a possible alternative, though it would require much higher volumes of drug to account for loss through the aerosolization process. Oropharyngeal (OP) administration has been proposed as an easy alternative to deliver different materials to the lungs. This method involves administering material to the trachea through the mouth (310). A recent study using silica particles showed less variability among animals and results in high uniformity of pulmonary distribution(311). Another study validated the use of OP induction over IN approaches, finding it to be as effective but without the disadvantages of administering the drug IN.(310) Further, a third study found that OP administration achieved similar dosing to that seen after IT administration.(312)

To test this technique against the IN approach, we treated animals IN with 50 µl of 100 nM Cy7-tagged AuNP (Figure 19C)**.** Our collaborators administered the same Cy7-AuNP using their expertise in OP aspiration, experimentally dosing 100 µl at 5, 25, and 50 nM (Figure 19A). After 24 h, mice were sacrificed, and lungs were isolated for IVIS imaging analysis. Regions of interest were drawn around each lung, from which background was subtracted. Fluorescence intensity was calculated over the area of each lung to calculate integrated intensity and was plotted for OP (Figure 19B) and IN approaches (Figure 19D). Administration of AuNP at 25 nM ($2.7x10^7$p/s) and 50 nM ($3.1x10^7$p/s) exhibit higher integrated intensities via the oropharyngeal approach than IN administration of 50 µl of 100 nM (~$2.3x10^7$p/s). Moreover, OP administration resulted in more homogeneous distribution at lower concentrations of DzNP.

However, for ease of administration, the work presented in this thesis will be using the IN approach.

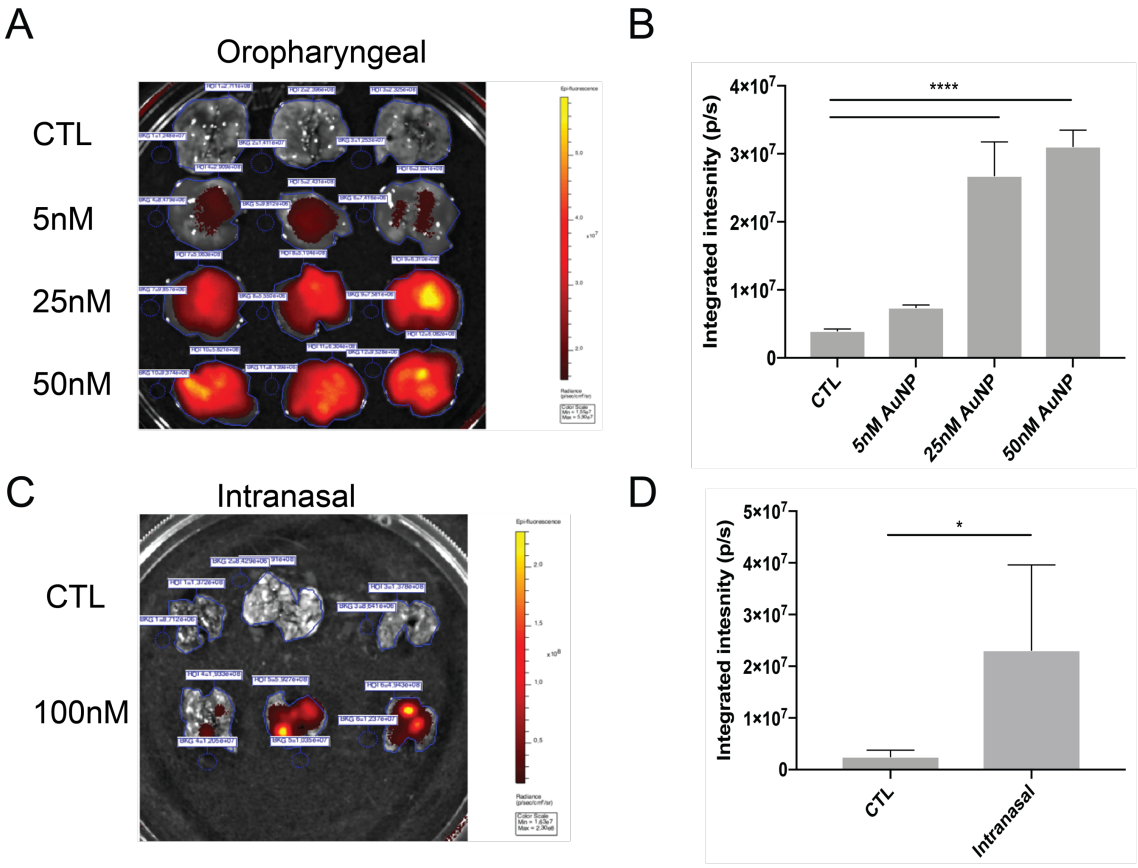

Figure 19. Intranasal (IN) versus oropharyngeal (OP) administration of AuNP.

(A) Cy7-AuNP was administered to C57bl/6 mice via OP technique. (A) Control mice were dosed with saline. Experimental animals were dosed at 55nM, 25nM, and 50nM. After 24h, lungs were isolated and fluorescence was visualized using IVIS. (B) Uptake was quantified by fluroescence intensity integrated over lung area. (C) 50ul of 100 nM was administered into C57bl/6 mice and lungs were isolated after 24 hours for fluorescence visualization using IVIS. Control mice were dosed with 50ul of saline. (D) AuNP uptake was quantified by fluorescence intensity integrated over lung area. Data presented as mean ± SEM statistical analyses was performed using one-way ANOVA with Tukey's post-hoc test, *p<0.05, **p<0.01, ***p<0.001, ****p<0.0001, n=3.

5.2.4 Determine biodistribution of fluorescently tagged DzNP versus soluble Dz to elucidate the pattern of uptake in immune cells and resident lung cells.

Potential biomedical application of NPs has been shown to be possible to the lungs via inhalation(84) or aspiration. (313) Because of the large epithelial surface area of both systems, the respiratory and GI tracts are some of the most promising for therapeutic nanoparticle technology. In the case of the lung, airborne particles deposit in different regions of the respiratory tract in a size dependent manner. Smaller particles, like nanoparticles, preferentially deposit in peripheral lung regions, like the alveoli. Depending on their size and composition, nanoparticles will interact with and become entrapped in pulmonary surfactants, which allows them to come into contact with pulmonary cells(314). Within the lung live a variety of immune cell populations, including phagocytic cells and antigen presenting cells. Thus, specific targeting to lung-resident immune cells by nanoparticles has been of great interest(315).

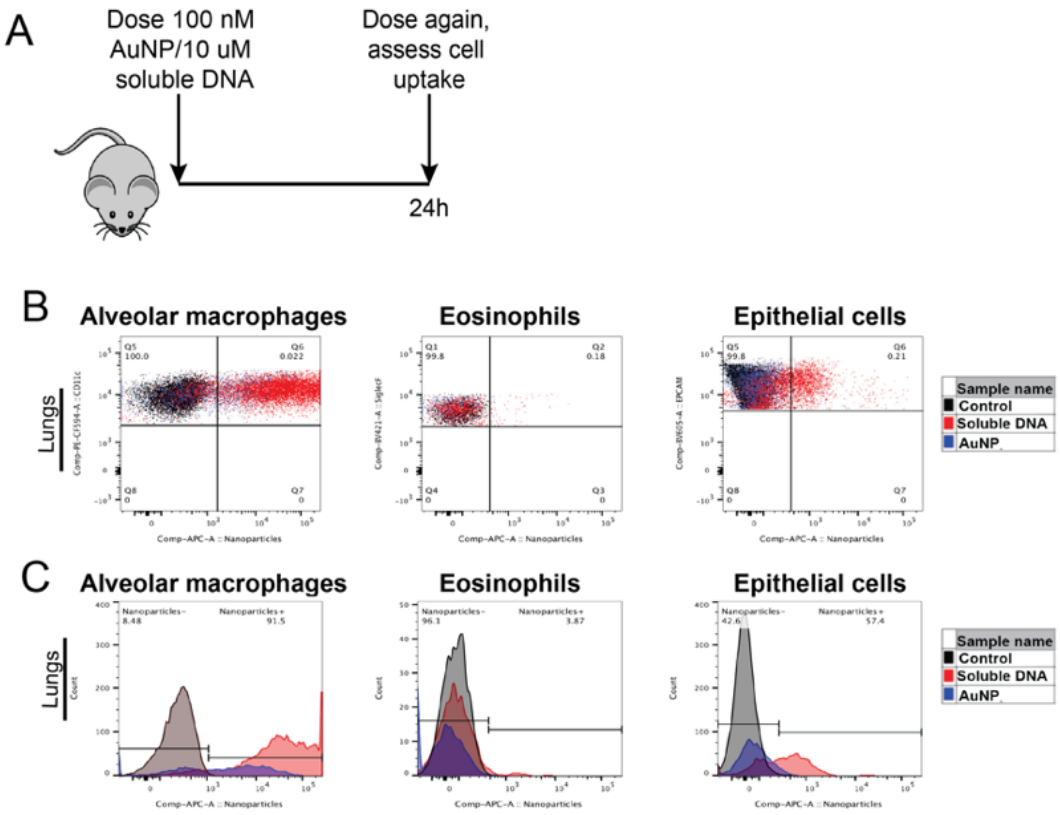

Figure 20. Intranasal administration of ATTO647-AuNP Or ATTO647-soluble DNA results in differential uptake by immune and epithelial cells.

(A) Experimental setup. Animals were dosed with equimolar concentrations of AuNP or soluble DNA. (B) After 24 hours, lungs were isolated and immune cell subtypes from the lung parenchyma were partitioned. Alveolar macrophages, eosinophils, and epithelial cells were gated based on control cells. Control (black), soluble DNA (red), and AuNP (blue). (C) Immune cell uptake of AuNP or soluble DNA represented by histogram.

In order to elucidate the efficacy of DzNP action, it is necessary to understand their biodistribution. GATA3 is traditionally thought to be expressed in the Th2 population of T-cells in the perpetuation of the immune system. However, Th2 inflammation is mediated by a number of other cell types. Moreover, GATA3 is expressed in a number of other cells, including mas cells, eosinophils, and basophils(293). Interestingly, studies have shown that the major site of GATA3 expression in the lower airways is the bronchial epithelium (316). Understanding the cell uptake profile of DzNPs not only confers a potential mechanism of action of GATA3 knockdown, but also provides information for the rational design of future therapeutic targets in inflammation. Thus, due to the expansive surface area covered by epithelial cells, we hypothesize that epithelial cells and macrophages will show the highest uptake of DzNPs. Understanding which cell type is mediating inflammatory regulation will be crucial for future development of therapeutically active DzNPs.

To visualize soluble DNA or tagged AuNPs in specific immune cell populations, we selected ATTO647 as a fluorescent dye in the red spectral region to avoid macrophage autofluorescence in the fluorescein channel. Soluble DNA and AuNP were tagged with ATTO647 and resuspended in phosphate buffered saline (PBS) for delivery to mice. Wild-type C57bl/6 mice were anesthetized using isoflurane and administered either 100 nM AuNP or 10 μM soluble DNA (Figure 20A). Importantly, these concentrations were selected to match the concentration of DNA in each dose. After 24 h, mice were sacrificed, and lungs were digested to stain for flow cytometry. Alveolar macrophages (AMs), eosinophils, and epithelial cells were partitioned and nanoparticle versus soluble DNA uptake was measured (Figure 20B,C). Because these were wild-type mice, eosinophil counts were lower than would be expected in an inflamed model of asthma. Interestingly, we observed high uptake of soluble DNA in alveolar macrophages over AuNP. This was expected, as AMs are the primary phagocytes of the immune system(317). Epithelial cells also take up high levels of soluble DNA but seem to endocytose a

fraction of AuNP as well. This is significant, as in an inflamed lung, the tight junctions between the epithelial cells become leaky, and a larger number of immune cells are recruited.

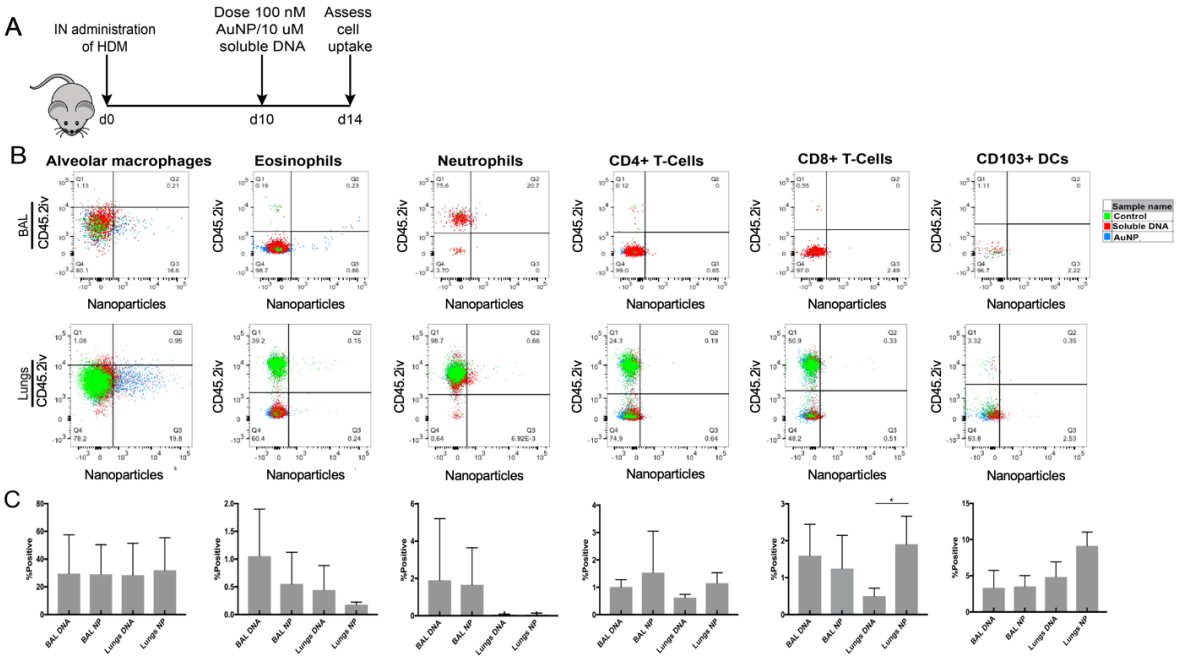

Figure 21. Intranasal administration of ATTO647-AuNP or ATTO647-soluble DNA following HDM sensitization results in differential cell uptake.

(A) HDM-sensitized mice were treated IN with ATTO647-AuNP or ATTO647-soluble DNA d10-14. (B) Partitioning of immune cell subtypes in the bronchoalveolar lavage (BAL) and lung parenchyma of control (green), AuNP (blue), and soluble-DNA (red) treated groups. Intravenous αCD45 Ab staining was used to differentiate between migratory immune cells and resident lung immune cells. (C) Graphed total immune cell uptake of AuNP or soluble DNA between BAL and lung. Data presented as mean ± SEM. Statistical analyses was performed using one-way ANOVA

To investigate the role of inflammation in DzNP uptake, we performed a similar experiment with HDM sensitization. In this case, we treated animals intranasally with 25 μg HDM daily for 3 weeks. During the last week, we co-administered 50 μl of 100 nM ATTO647-AuNP or 50 μl 10 μM soluble DNA (Figure 21A)**.** Mice were sacrificed, and cells were partitioned for flow cytometry, staining for AMs, neutrophils, CD103+ DCs, eosinophils, CD4+ T-cells, and CD8+ T-cells. In order to identify which immune cells were resident to the lung, or if they migrated in as a response to HDM, cells were stained with a CD45.2 antibody. CD45.2+ intravenous staining implies the cells are migratory immune cells. This information allows us to identify whether DzNP is largely taken up by the resident lung cells or by cells recruited to the site of inflammation.

Surprisingly, we observed a statistically significant increase in CD8+ T-cells uptake of fluorescently tagged DzNP in the lungs versus soluble DNA. Similar trends were observed in CD103+ DCs, and CD4+ T-cells (Figure 21B). In this case, AMs actually showed consistent uptake of both soluble DNA and AuNP, conflicting with our observed results in non-HDM sensitized animals (data not shown). Neutrophils and eosinophils did not significantly phagocytose either AuNP or soluble DNA. The difference in uptake between resident lung cells versus migrating cells was also intriguing. Most of the cell uptake was observed in resident cells, suggesting that the mechanism of action of DzNPs may be caused by these cells in particular. Moreover, these data suggest differential DzNP uptake by resident and migratory immune cells (Figure 21C).

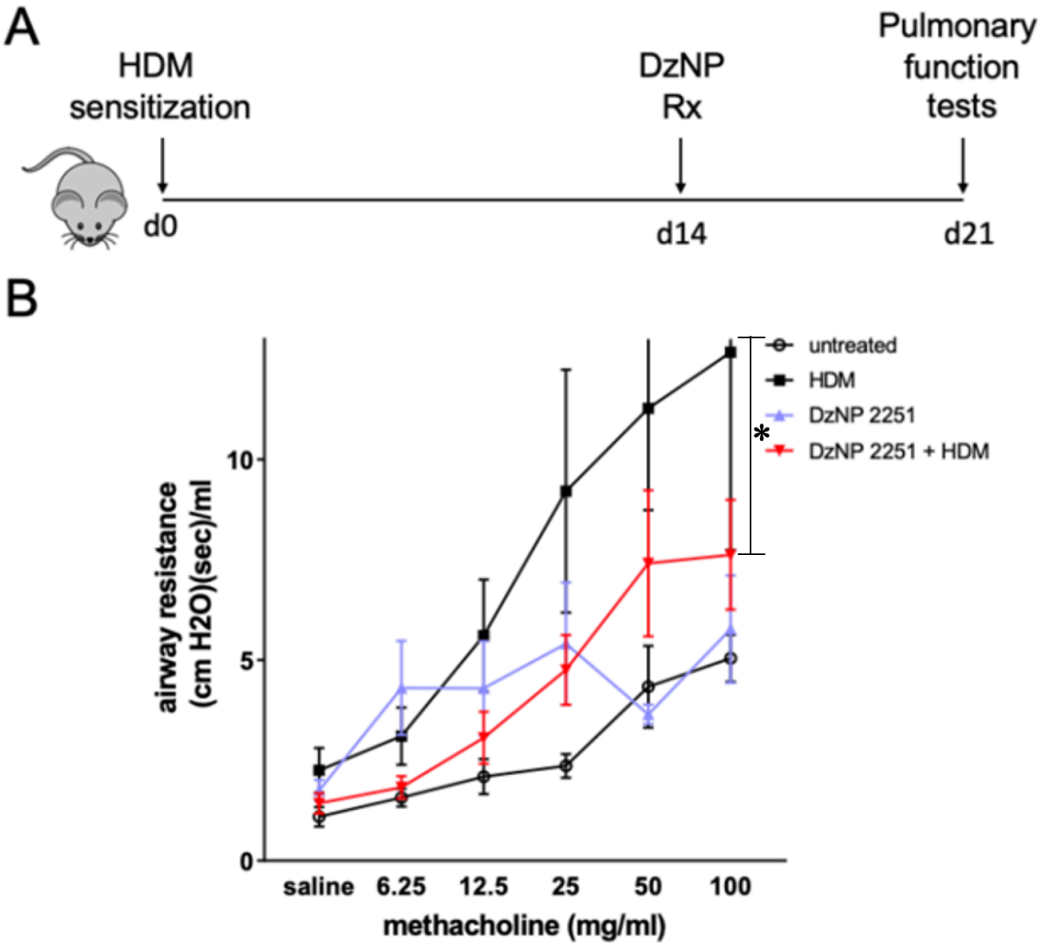

Figure 22. DzNP 2251 reduces airway resistance and Th2-related cytokines in mouse model of asthma.

(A) Two groups were sensitized to HDM for three weeks under isofluorane anesthesia. Two groups were not given HDM. DzNP was administered intranasally to HDM-sensitized and a group of wild-type mice during week 3. (B) After 21 days, animals were anesthetized using ketamine/xylazine and airway resistance was measured using a SCIREQ Flexivent. Data presented as mean ± SEM statistical analyses was performed using two-way ANOVA with Tukey's post-hoc test, *$p<0.05$, n=8.

5.2.5 Determine 2251-DzNP efficacy in a Th2-mouse model

To test the efficacy of our therapy, we prepared 100 nM solutions of DzNP-2251, our GATA3 DzNP, resuspended in PBS for intranasal delivery. Animals were administered either HDM or vehicle for 21 days to emulate chronic asthma. The 2251-DzNP alone was administered in two groups: in an HDM sensitized group and an unsensitized group to determine the effects on asthmatic mice, as well as to determine if 2251-DzNP alone had an immunostimulatory effect (Figure 22A). On day 21, mice were anesthetized using a combination of ketamine and xylazine to simultaneously induce anesthesia, as well as paralyze the diaphragm to accurately measure pulmonary resistance. Each trachea was cannulated, and mice were transferred to the FlexiVent (SCIREQ) system for forced oscillation measurement. Airway resistance was plotted against increasing methacholine concentrations. HDM-sensitized mice experienced the highest airway resistance, while control mice did not have large increases in resistance.

HDM-sensitized mice experienced the highest airway resistance, while control mice did not have large increases in resistance. Control versus HDM mice showed a significant increase of airway resistance. DzNP 2251 alone did not seem to result in augmented levels of airway resistance, though the baseline was mildly higher than control animals. Remarkably, DzNP 2251 significantly reduced airway resistance in HDM treated mice when comparisons were made between HDM and HDM+2251 treated groups.

5.2.6 Determine efficacy of orally delivered DzNP using an alginate hydrogel delivery method.

To test particle release following nanoparticle encapsulation and delivery, we modified AuNP with Cy7-tagged DNA, which permits visualization in the colon using IVIS imaging. C57bl/6 mice were administered 200 nM Cy7-tagged AuNP in a 10 mg/ml alginate solution, followed by a second gavage of $CaCl_2$ to initiate gelation in the stomach, as per a previously published protocol by Laroui et al(316). Levels of fluorescently tagged AuNP were visualized using IVIS imaging. Control mice were given alginate alone followed by $CaCl_2$ double gavage.

Mice were sacrificed after 6, 24, and 48 hours, and the colon was isolated and flushed with PBS to remove any contaminating fecal signal. Cy7-fluorescent signal was visualized using IVIS, and images were taken of colons in duplicate (Figure 23A). Regions of interest were drawn around each colon, and background signal was subtracted. Signal was integrated over the length/area of each colon and normalized to control. Overall integrated intensity was calculated and plotted (Figure 23B) to visualize time points when the highest DzNP release had occurred. These data suggested that the highest levels of DzNP accumulated in the colon around 6 h, with signal still visible around 24 h. These results validated that our method of oral delivery was sufficient to achieve DzNP release in the large intestine.

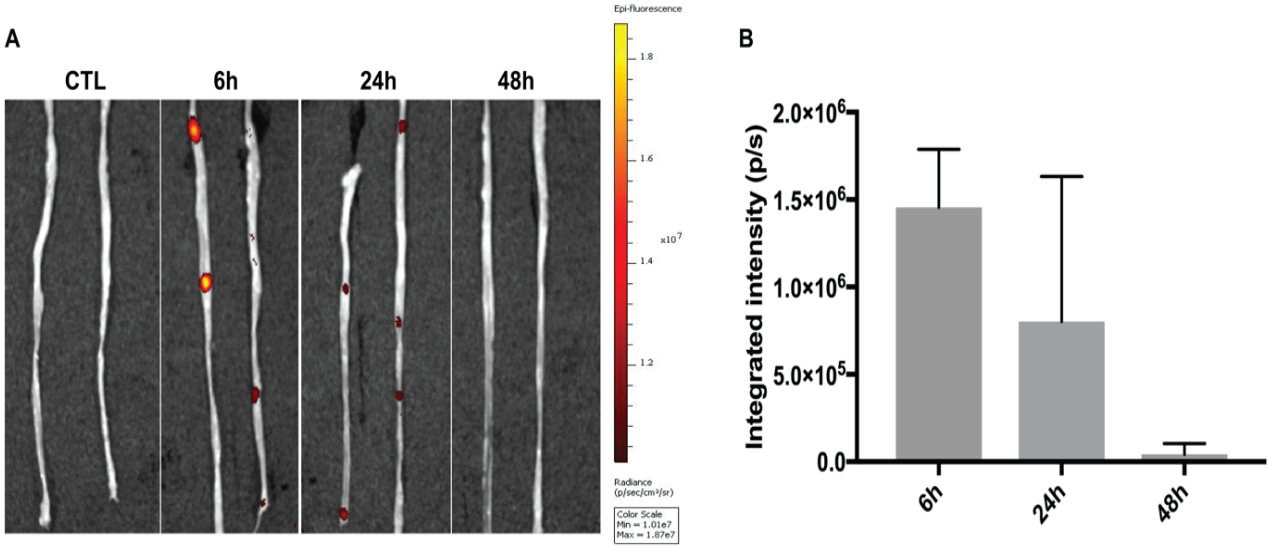

Figure 23. DzNP localization to the colon following oral delivery.

(A) 200 nM Cy7-tagged AuNP in 10mg/ml alginate solution were delivered orally to mice, followed by second gavage of $CaCl_2$. Mice were sacrificed after 48 hours, 24 hours, and 6 hours. The colon was isolated and imaged using IVIS. (B) Regions of interest (ROIs) were drawn around each colon and compared to background. Integrated intensity (p/s) was calculated taking into account fluorescent intensity per area of colon. Each colon was normalized to control (no fluorescent particle). Data presented as mean ± SEM. Statistical analysis was performed using one-way ANOVA with Tukey's post-hoc test, n=2.

5.2.7 Evaluate DzNP distribution within the intestinal villi, characterizing the role of intestinal epithelial cells (IECS), gut-associated lymphoid tissue (GALT), and immune cells in particle uptake.

Because of the absorptive nature of the large intestine, it is necessary to understand the distribution profile of DzNP. We sought to take advantage of the endocytic uptake mechanisms of intestinal epithelial cells (IECs), gut-associated lymphoid tissue (GALT), and immune cells because GATA3 is traditionally thought to be expressed in the Th2 population of T-cells in the perpetuation of the immune system. However, the intestine epithelial cells (IECs) play a significant role in the immune response, and due to their surface area, likely take up a large number of DzNPs. The immune cells in the gastrointestinal tract are also highly active and constantly coming into contact with luminal agents. GALT includes Peyer's patches and mediastinal lymph nodes, which are hubs for T- and B-cell interactions and communication. We hypothesize that DzNP will likely be found in highest concentration in IECs cells.

We first evaluated uptake in a few different immune cell subtypes isolated from intestinal tissue to determine whether immune cells can take up the nanoparticles after encapsulation and release from alginate hydrogels. We tagged AuNP with ATTO647, a fluorescent dye, and mixed the AuNP with alginate solution. Animals were gavaged first with ATTO647-AuNP or vehicle, followed by $CaCl_2$ to induce gelation in the stomach. After 24 hours, they were sacrificed, the

colon tissue was isolated, and immune cells were isolated for flow cytometry. Nanoparticle uptake was tested in CD4+ T-cells, (Figure 24A), CD8+ T-cells (Figure 24B), macrophages (Figure 24AC), and neutrophils (Figure 24D). Gates were set based on vehicle-treated control. Interestingly, all four cell types showed significant signal of fluorescently tagged AuNP when compared to control animals. This indicates that the gastrointestinal immune cells take up much higher levels of AuNP than we observed in the lung. Neutrophils showed the highest uptake of AuNP, followed by macrophages. Remarkably, CD4+ T-cells showed the highest levels of adaptive cell uptake over controls, in contrast to the high levels of CD8+ T-cells that we found to exhibit the highest uptake in the lung.

.

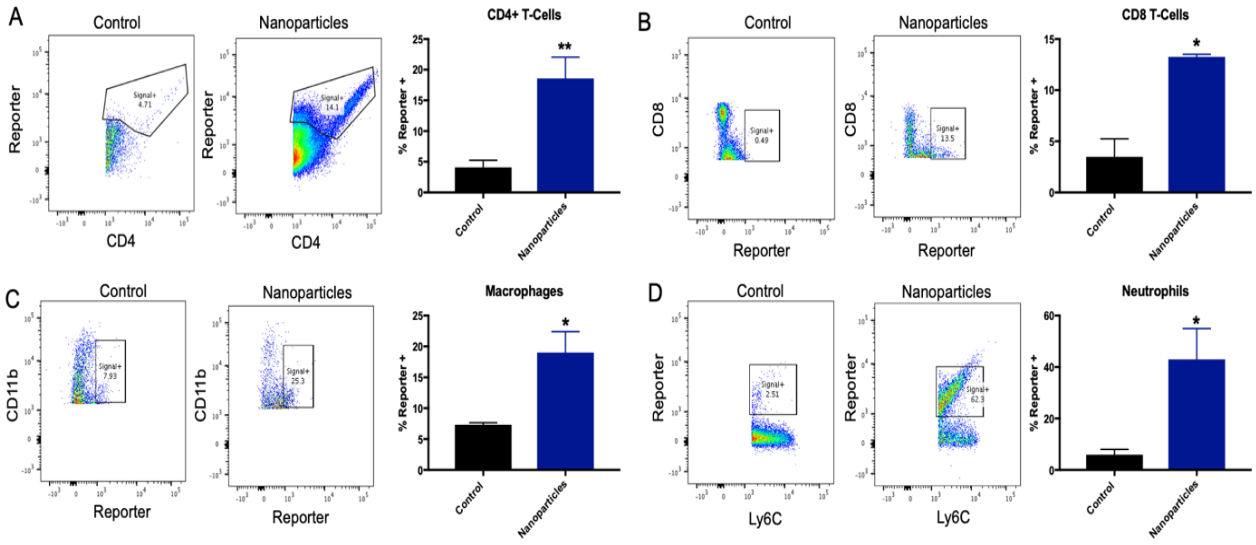

Figure 24. Alginate hydrogel delivery of DzNPs for GI cell uptake

ATTO647-tagged nanoparticles in an alginate hydrogel solution were gavaged, followed by a $CaCl_2$ chelating solution. Mice were sacrificed after 24h and GI cells were isolated and stained for flow cytometry. Cell uptake was assessed by gating against control (untreated) cells in CD4+ T-cells (A), CD8+ T-cells (B), macrophages (C), and neutrophils (D).

5.2.8 Evaluate efficacy of orally delivered GATA3 and TNF-α DzNPs in a mouse model of colitis.

Oral drug delivery is the most attractive pathway for chronic debilitating gastrointestinal diseases, such as UC and Crohn's disease. Conventional approaches have many drawbacks, including inefficacy, ineffective drug release, and limited targeting to inflamed areas. Furthermore, developing a drug that can effectively bypass the acidity of the stomach would be ideal. Current therapeutics for UC include biologics, with anti-TNF-a monoclonal antibodies being the most popular. These are widely used for their ability to alleviate immediate inflammation, but unfortunately, do not exhibit long-term effects. Based on the promise of our GATA3 DzNP and a recent publication highlighting the promise of GATA3 therapy in UC, we tested a combination oral therapy of GATA3 and TNF-α DzNPs.

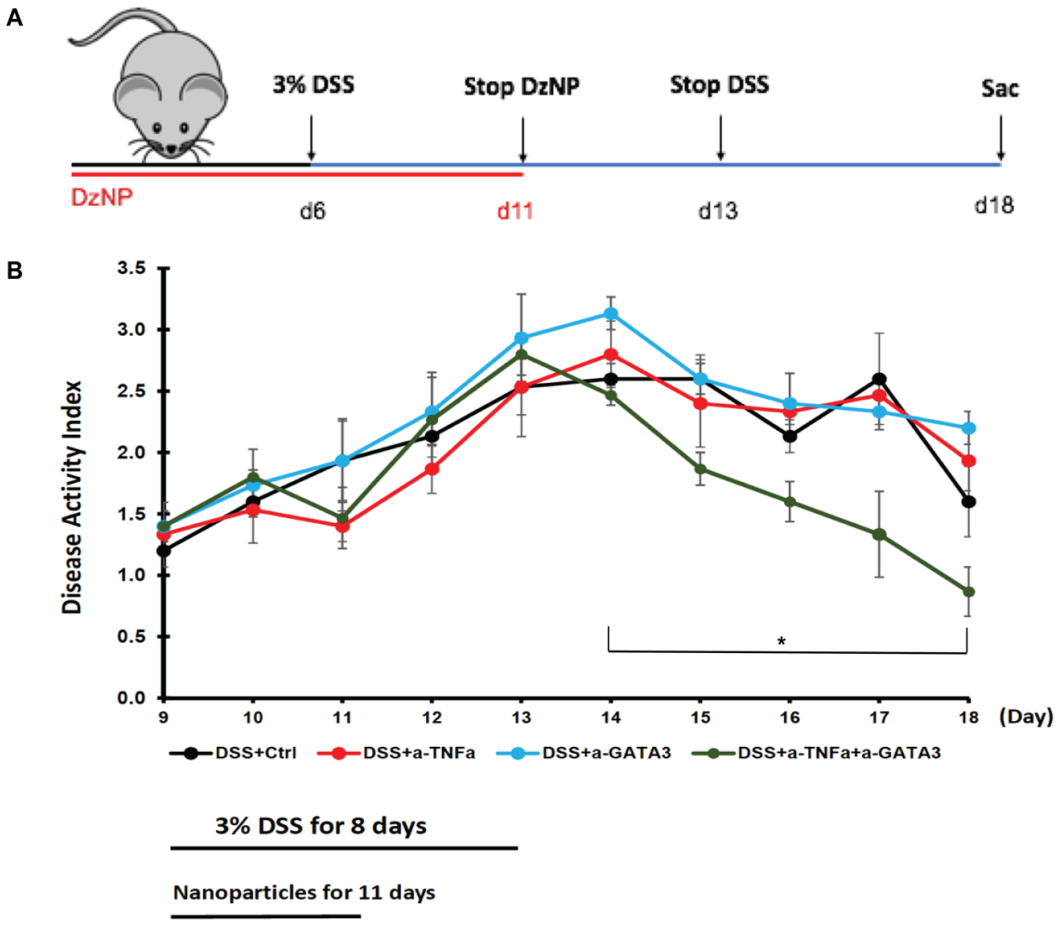

Figure 25. Hydrogel delivery of GATA3 and TNF DzNPs alleviates inflammation in DSS colitis mouse model.

C57bl/6 mice were treated for 11 days with either GATA3 alone, TNF alone, or a combination of the two in a DSS mouse model of colitis. Control mice received a DzNP with a scrambled Dz sequence. (B) Disease activity index (DAI) shows a combined therapeutic of the two DzNPs results in a statistically significant improvement in relative disease. Data presented as

Mice were administered alginate encapsulated DzNP for 5 days before beginning DSS. Animals were either treated with a scrambled DzNP (control), TNF-α DzNP alone, GATA3 DzNP alone, or a combination of TNF-α and GATA3 DzNPs (Figure 25A). On day 5, DSS was added to the water of each group. Hydrogel polymerization was achieved by double gavage, meaning that the alginate-DzNP solution (200 nM DzNP in 10 mg/ml alginate) was gavaged first, followed by a second gavage of $CaCl_2$ chelating solution for hydrogel formation in the stomach.

On day 11, DzNP treatment was stopped while mice continued DSS until day 13. The mice were given 5 days to resolve following cessation of DSS. Weight, stool consistency, and blood in stool were measured every day from day 0 to day 18. These parameters allowed for the calculation of disease activity index (DAI), which is a research tool that defines severity of disease. DAI is the gold standard for assessing disease index in animal models of colitis.(318) DAI analysis indicated that TNF-α and GATA3 DzNPs alone did not cause any major improvements in UC. However, the combination of both DzNPs resulted in a statistically significant improvement of disease (Figure 25B). This was confirmed by histology scoring by a blinded pathologist (Figure 26A) and histological markers of disease (Figure 26B).

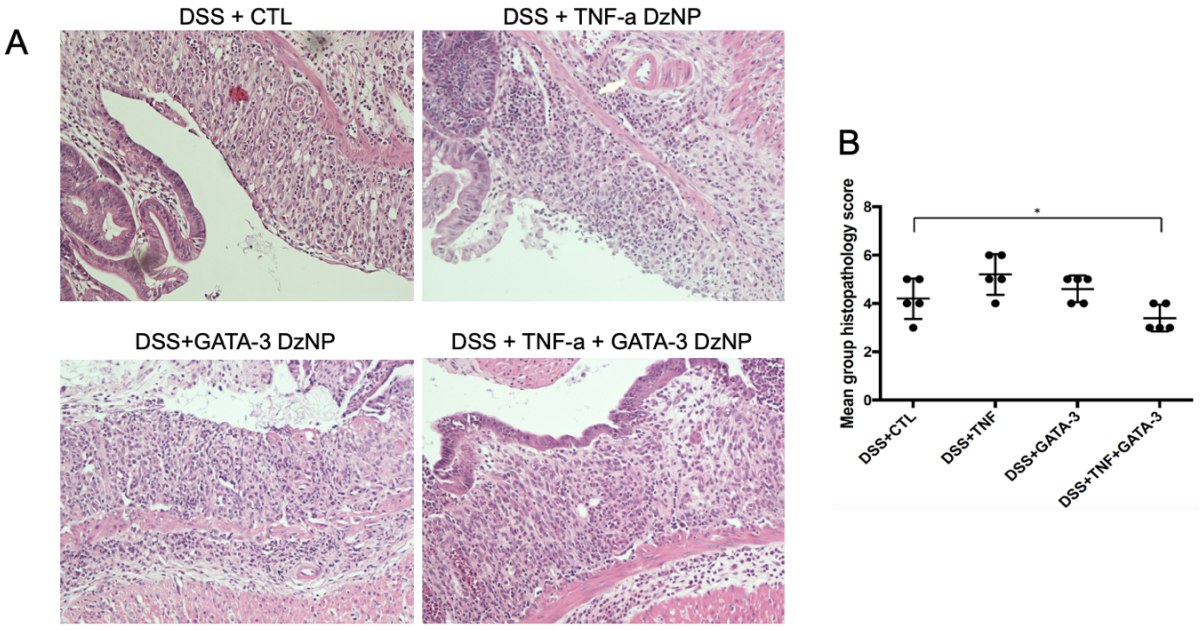

Figure 26. Hydrogel delivery of GATA3 and TNF DzNP alleviates inflammation in a DSS model of colitis.

Hydrogel delivery of GATA3 and TNF DzNP alleviates inflammation in a DSS model of colitis. C57bl/6 mice were treated for 11 days with either GATA3, TNF, or a combination of the two DzNPs. Control mice received a scrambled DzNP. DzNPs were mixed in alginate and delivered via oral gavage, followed by a second $CaCl_2$ solution to form a hydrogel in the stomach. (A) Representative colon gross pathology from mice sacrificed after treatment. (B) Histological scoring by a blinded pathologist. Data presented as individual values ± S.E.M. Statistical analyses were performed using a one-way ANOVA. *$p<0.05$. n=5 samples per group.

5.3 Discussion

We developed a DNAzyme-based therapeutic for the treatment of chronic inflammatory disorders, such as asthma and IBD. We first performed a screen *in vitro* using a model cell line that overexpresses GATA3. After selection of a promising GATA3 Dz sequence, we conjugated it to AuNPs to confirm its efficacy over current GATA3 therapeutics. Next, we hypothesized that the selected DzNP would be an effective method of regulating GATA3 *in vivo*, leading to reduction of Th2-specific measures of disease.

Multiple mouse models of allergic airway inflammation have been established to investigate different questions in a Th2 model of disease.(319) These models include the house dust mite (HDM), ovalbumin, molds and cockroach antigen(320). HDM sensitization is becoming increasingly common and is one of the most clinically-relevant models, reflecting the allergic response and respiratory changes in 85% of asthmatic patients(321). Observations of airway remodeling, such as goblet cell hyperplasia and collagen deposition, are usually observed in chronic HDM models.(322) Airway inflammation and enhanced methacholine responsiveness are observed as a result of this experimental model of asthma. No therapy to date has shown efficacy in reversing airway remodeling, though treatments exist for airway hyperresponsiveness and symptom management. Therefore, any therapeutic for long term therapy should assess their effects on collagen deposition and airway remodeling. Thus, we utilized an HDM-model of asthma with intranasal administration of therapeutic because of its clinical relationship to Th2-mediated asthma. Interestingly, when we analyzed DzNP biodistribution, we observed high uptake of soluble DNA in alveolar macrophages over AuNP. This was expected, as AMs are the primary phagocytes of the immune system(317). Epithelial cells also take up high levels of soluble DNA but seem to endocytose a fraction of AuNP as well. This is important, as in an inflamed lung, the tight junctions between the epithelial cells become leaky, and a larger number of immune cells are recruited. Moreover, when we assessed DzNP overall efficacy using

pulmonary function tests (PFTs), we observed a reduction airway resistance in mice that had been treated with both 2251-DzNP and HDM over HDM alone. This supported our hypothesis that DzNP-treatment would alleviate Th2 disease.

Thus, we aimed to confirm our findings in another Th2 mouse model of inflammation. Inflammatory bowel disease (IBD) is comprised of 2 major disorders: ulcerative colitis (UC)(279) and Crohn's disease (CD)(280). The exact etiology of IBD remains unknown, though studies have shown contributions from both the adaptive and innate immune systems. Inflammatory stimulation from the adaptive immune system includes mucosal inflammation caused by T-cell-derived cytokines. Interestingly, different T-cell subtypes are at play in CD versus colitis. Studies have shown increased levels of Th1 cytokines in CD, such as interferon-g (IFN-g) and tumor necrosis factor (TNF). In UC, however, patients exhibit elevated levels of Th2 cytokines, including IL-4, (323)IL-5 and IL-13(324, 325). Both diseases have been shown to produce increased levels of IL-6(326) and a cytokine more associated with Th17 T-cells, IL-17A.(327)

In the mucosal immune system, several studies suggest the important roles of GATA3, signal transducer and activator of transcription (STAT)-6, c-Maf, and others in inducing and activating Th2 cytokine production. STAT6 induces GATA3 via activation of GATA3 promoters(328). Interestingly, GATA3 itself has been shown to induce its own expression, either directly via autoregulation or indirectly via Dec2, a transcription factor(325, 329). This suggests that GATA3 transcription leads to stabilization in GATA3 expression in immune cells. GATA3 has been shown to inhibit STAT4 and subsequently, IFN-g expression, thus suppressing the Th1 immune response.(330)

In mouse models, conditional knockdown of GATA3 prevented the induction of oxazolone colitis, a murine colitis model(331). Recent clinical work has shown increased expression of GATA3 in pediatric UC. (332) Another study identified increased expression of GATA3 in mucosal T lymphocytes in patients with active UC(267). This study characterized GATA3 expression primarily in gut T-cells and epithelial cells. Further, this group tested the

efficacy of SB010, a GATA3 Dz previously shown to have efficacy in allergic asthma, in patients who had UC. After rectal administration, GATA3 blockade ameliorated colitis activity and led to suppression of Th2 cytokines. This work indicates the potential for GATA3 blockade in colitis.

Current therapies for UC, however, mainly focus on anti-TNF-α and alleviation of the acute phase immune response. Infliximab and Adalimumab, two of the most popular medications, are TNF-inhibiting antibodies. Even in the SB010 trial, the authors deliver their drug intrarectally, which would pose future problems with patient compliance. Procedures such as enemas that are often used to target drugs to the colon are difficult, and can lead to complications locally in the intestine, including bleeding or perforation. Thus, we proposed designing a method of treating colitis using our improved GATA3 DzNP in combination with an anti-TNF-α DzNP. As described above, we previously published successful use of a TNF-α DzNP therapy for myocardial infarction. Local injection of DzNP yielded TNF-α knockdown of 50%, and subsequent reduction of inflammation with improved cardiac function(300). By combining the two DzNP therapies we can therefore target both the acute immune response (TNF-α), and a long-term inflammatory pathway (GATA3).

As an alternative to rectal delivery, we chose to deliver these nanoparticles in an alginate hydrogel formed by giving a double gavage of alginate/DzNP followed by $CaCl_2$ as previously described(333). Oral delivery to the intestine is challenging because of the acidic pH of the stomach, so oral drugs are often given frequently, or in high doses to circumvent degradation, which may lead to an increased number of side effects. By targeting both GATA3 and TNF-α specifically in the colon, we hypothesized that we would see resolution of symptoms of colitis. We utilized flow cytometry to confirm that the double gavage method would deliver DzNPs to the Gi tract. Indeed, we observed intracellular uptake within the colon. Moreover, we confirmed uptake of nanoparticles in both innate and adaptive immune cell populations by flow cytometry.

We next aimed to test dual delivery of GATA3 and TNF in a mouse model of colitis. Because part of our therapeutic aimed to modulate GATA3, a transcription factor, we selected to administer DzNP for 5 days before beginning the DSS colitis model. This would ensure that we were modifying how the T-cells differentiate into their future roles and subsequently recruit more inflammatory cells, while still targeting the acute phase reactors, such as TNF- α. Thus, we delivered GATA3 treatment alone, TNF alone, and dual GATA3 and TNF via double gavage. We did not see any changes in either therapeutic alone, but combined delivery of both factors resulted in significantly lower scores of disease activity than control. These findings were confirmed by histological scoring by a blinded pathologist.

The reduction in severity of colitis symptoms in dual TNF-α and GATA3 treated mice was expected, but we did not expect the degree of disease amelioration observed in these mice. This introduces a number of questions. The mechanism of action of this dual therapy is intriguing, indicating there is potential synergy at play. It is thus necessary to pursue molecular analysis of Th1 and Th2 cytokines to elucidate which pathways are contributing to the response. It is also interesting to note that TNF-α and GATA3 therapies alone did not perform better than control, potentially suggesting that the formation of the alginate hydrogel confers protection of the intestinal epithelium against DSS.

While DSS is a viable model of colitis, it is more of a general model of inflammation in the colon. To further investigate these results, it will be necessary to follow these studies up with another mouse model of colitis, such as the TNBS models of colitis. Since TNBS is a more Th2 skewed model of colitis, it will be interesting to note if the trends are the same or are as pronounced as the DSS model. Further, future directions should examine the levels of Th1 and Th2 cytokines known to be upregulated in colitis, such as IL-4, IL-5, IL-6, KC, to better understand how the DzNPs are ameliorating disease. Ideally, the results from these studies will show a role for synergistically treating UC and other inflammatory disorders by our DzNP therapeutic.

5.4 Methods

5.4.1 In silico screen of DzNP

T47D cells were brought to 80% confluency on 24-well plates and incubated for 48 hours with Lipofectamine RNAiMAX in 50 ul total volume along with fresh OPTI-MEM. siGATA3 (GATA3 siRNAs, ThermoFisher) was used as a positive control. After 48 hours, cells were trypsinized and total RNA was extracted using RNeasy Mini Kit (Qiagen). Purified RNA was eluted into RNAse-free water and stored at -80C until use. RNA concentration and 260/280 ratios were determined using a Nanodrop UV spectrophotometer (Thermo Scientific). Total RNA was reverse transcribed to cDNA using iScript cDNA Synthesis Kit (Bio-Rad) following the manufacturer's protocol. Target gene expression was quantified using GATA3 primer (Mm00484683_m1) and normalized to 18S. cDNA was amplified with TaqMan Universal PCR Master Mix (Applied Biosystems).

5.4.2 IVIS imaging

100 nmoles of amine-T20-SH DNA were functionalized with 300 ug of Cy7 dissolved in DMSO using 0.1 M sodium bicarbonate. The Cy7-T20-DNA was filtered through a P2 bead and added to 23 mls of AuNPs (4 nM) overnight. The Cy7-T20-AuNPs were salted in 20-minute increments up to 0.7 M, then were washed to remove excess salt and DNA, as per previously described protocol. The DzNPs were administered to mice for flow cytometry at 3 concentrations: 5 nM, 25 nM, and 50 nM. Control animals were given intranasal administration of PBS.

Care of experimental animals was performed in accordance with Emory University IACUC guidelines. Mice were anesthetized using isofluorane (3%) for 3 minutes. Mice

were administered Cy7-AuNP either via intranasal or oropharyngeal method. After 24 hours, lungs were isolated and utilized for *ex vivo* IVIS imaging. Radiance emitted from the chest of mice was quantified using Living Image software (Perkin Elmer Inc. Boston, MA, USA). Data were expressed as integrated intensity (ps(over the baseline fluorescence of each mouse.

5.4.3 Biodistribution of AuNP in the lung

100 nmoles of amine-T20-SH DNA were functionalized with 300 ug of ATTO647 dissolved in DMSO using 0.1 M sodium bicarbonate. The ATTO647-T20-DNA was filtered through a P2 bead and added to 23 mls of AuNPs (4 nM) overnight. The ATTO647-T20-AuNPs were salted in 20-minute increments up to 0.7 M, then were washed to remove excess salt and DNA, as per previously described protocol. The remaining DzNPs were administered to mice for flow cytometry. Soluble amine-T20 SH DNA-Cy7 was separately utilized as a control.

Mice were anesthetized using isofluorane (3%) for 3 minutes. Following anesthesia, each mouse was given 50 ul of ATTO647-T20-AuNP dropwise via a pipette. After 24 hours, mice were sacrificed and lungs were isolated and homogenized for flow cytometry, as previously described(334). The following panel was utilized to identify nanoparticle uptake in lung resident cells and circulating immune cells:

Table 2 Lung flow cytometry panel

Marker	Fluorochrome
CD103	PE
CD11c	PE/Daz594
CD64	PerCP/Cy5.5
MHCII	PE-Cy7
Nanoparticles	A647
Ly6C	APC-e780
SiglecF	BV421
Ly6G	BV510
EPCAM	BV605
CD45	BV650
CD4	BV711
CD8a	BV785
CD11b	BUV395
ZUV	BUV496

5.4.4 Th2 animal model of asthma

Care of experimental animals was performed in accordance with Emory University IACUC guidelines. Mice were administered either 2.5mg/ml HDM or vehicle for 21 days to emulate chronic asthma. The 2251-DzNP alone was administered in two groups: in an HDM sensitized group and an unsensitized group to determine the effects on asthmatic mice, as well as to determine if 2251-DzNP alone had an immunostimulatory effect. On day 21, mice were anesthetized using a combination of ketamine and xylazine to simultaneously induce anesthesia, as well as paralyze the diaphragm to accurately measure pulmonary resistance. Each trachea was cannulated, and mice were transferred to the FlexiVent (SCIREQ) system for forced oscillation measurement. Measurements included resistance, compliance, and elastance(335). To measure airway hyperreactivity(336), mice were challenged with increasing concentrations of aerosolized methacholine generated by an in-line nebulizer, starting from saline, 6.25, 12.5, 25, 50, and 100 mg/ml (Figure 22B). Airway resistance was plotted against increasing methacholine concentrations. HDM-sensitized mice experienced the highest airway resistance, while control mice did not have large increases in resistance.

5.4.5 Oral gavage and gastrointestinal flow cytometry

100 nmoles of amine-T20-SH DNA were functionalized with 300 ug of ATTO647N dissolved in DMSO using 0.1 M sodium bicarbonate. The ATTO647-T20-DNA was filtered through a P2 bead and added to 23 mls of AuNPs (4 nM) overnight. The ATTO647-T20-AuNPs were salted in 20-minute increments up to 0.7 M, then were

washed to remove excess salt and DNA. The remaining DzNPs were administered to mice for flow cytometry.

5.4.6 In vivo DSS colitis mouse model

Dextran sodium sulfate colitis (36000-50000 MW; MP Biomedical) was induced by administering 3% w/v in autoclaved water and allowing mice to drink *ad libidum* for 9 days. Treatment groups (n=5) of DSS+control, DSS+TNF, DSS+GATA3, and DSS+TNF+GATA3 were administered via an oral gavage needle. Total volume was 200ul. Mice were fasted overnight, then gavaged once daily for 5 days prior to induction of DSS. After starting DSS, mice were gavaged daily for another 6 days of DSS in the water supply. Disease activity index (DAI) was scored daily. DAI was calculated as the sum of the stool consistency scores (0:hard, 2: soft, 4:diarrhea), fecal occult blood (0:negative, 2:positive, 4:macroscopic), and weight loss (0:<1%, 1:1-5%, 2:5-10%, 3:10-20%, 4:>20%). Fecal occult blood was calculated using Hemoccult Sensa (Beckman Coulter). DzNP treatment and DSS administration, mice were sacrificed, and colons were measured, then harvested and preserved as swiss rolls in paraffin for histology.

5.4.7 Tissue Harvest and Flow Cytometry

To collect samples for flow cytometry analysis, mice were euthanized via CO_2 asphyxiation and digested according to previously described protocol(259). Small intestine was isolated and flushed with cold PBS. Tissue segments were placed in extraction media (Hank's Buffered Salt Solution, Millipore Sigma, 5 mM EDTA, 10 mM HEPES) and incubated for 15 minutes while shaking at 37ºC.

After incubation, the supernatant containing epithelial cell and intraepithelial lymphocytes was isolated using a 100 μm cell strainer. The remaining small intestinal tissue was

placed into 6 ml of digestion media (RPMI, Millipore Sigma, 1 mg/ml collagenase V) and vigorously shaken at 37ºC. The digested tissue was filtered through a 100 µm strainer and rinsed with RPMI containing 10% FBS. The four solutions, containing epithelial cells, small intestine, spleen, and Peyer's patches, were centrifuged at 800 x g for 5 minutes at 4ºC. The cell pellet was resuspended in 1 ml RPMI containing 2% FBS. Single cell suspensions were stained for flow cytometry analysis using standard methods and analysed on a BD LSRII (BD Biosciences).

The antibodies used for identifying cell populations were: PerCP conjugated CD3 (BioLegend), BV605 conjugated CD4 (BioLegend), BV785 conjugated CD8, APC-Cy7-conjugated Ly6G (BioLegend), BV510-conjugated CD11b (BioLegend), BV711-conjugated PE-APC conjugated F4/80 (BioLegend).

5.4.8 Statistical analysis

All statistical analyses were performed using Graphpad Prism version 7.0d (La Jolla, CA). Results are reported as mean ± standard error of the mean (SEM). For grouped analyses, one-way ANOVA with Tukey's post-test was used for multiple comparisons. Tukey's test was used when comparing paired samples, while Bonferroni's test was employed when comparing between treatment groups. $p<0.05$ was considered statistically significant.

CHAPTER 6. CONCLUSIONS AND FUTURE DIRECTIONS

6.1 Overall summary

The work presented in this thesis represents a contribution to the fields of biomaterials and regenerative medicine by demonstrating the use of dimensionality reduction techniques for the elucidation of cellular heterogeneity of the immune response to stimulation and treatment with immunomodulatory hydrogels. In particular, this work explores the role of both innate and adaptive immune systems, and their respective roles in the processes of healing or immune resolution. This work expands the understanding of the relationship between pro-regenerative innate and adaptive immune cells and identifies methods by which we can manipulate these processes and pathways. The enhanced recruitment of anti-inflammatory, and inhibition of pro-inflammatory cellular subsets can be manipulated for the reduction of disease processes, such as in IBD or in acute or chronic wounds.

In Aim 1, we explored the ability to target the recruitment of pro-regenerative cells from both the innate and adaptive immune systems. In particular, we engineered a hydrogel for the release of both anti-inflammatory factors IL-10 and AT-RvD1 *in vivo.* Increased evidence suggests that the promotion of healing actually involves a reduction in pro-inflammatory cell subtypes, such as M1 macrophages, and the recruitment of pro-resolving immune cell subtypes. In fact, dysregulation of the shift between M1 and M2 macrophages is seen in chronic wounds(337-339). Chronic wounds have an increased and prolonged inflammatory stage, with high levels of pro-inflammatory cytokines in wound fluid. (29, 339, 340). By combining IL-10 with AT-RvD1, we aimed to deliver the major cytokine involved in the transition between the inflammatory to proliferative phase of inflammation, IL-10, as well as a lipid mediator previously shown to induce resolution of inflammation (181, 341). Combined delivery of the two factors

allowed for synergy of both factors, by promoting the recruitment of M2 macrophages, IL-10 DCs, and reducing M1 macrophage recruitment. Moreover, because we were interested in a big picture view of immune cell recruitment, the usage of SPADE allowed us to visualize the high dimensional dataset into a 2D "tree" that elucidated the cellular heterogeneity in response to treatment. The trees developed by SPADE not only validated our findings but were instrumental in helping us identify a CD8+ IL-10 expressing cell that only seemed to be present in dual hydrogel samples. Taken together, these results indicate that local immunomodulation using combined delivery of therapeutic factors can influence the immune milieu at the site of injury. Furthermore, using dimensionality reduction techniques such as SPADE allow for the development of a big-picture view of all immune cells involved; crucial data that may have been missed by traditional flow cytometry gating.

In aim 2, we investigated the immune response at the single-cell level to AvrA microparticles. We previously identified AvrA, used by *Salmonella*, as an enzyme with anti-inflammatory and anti-apoptotic effector functions (9, 218). Autoimmune disorders, like IBD, are a potential target for novel therapeutics, particularly because 30% of IBD patients do not respond to the standard-of-care, anti-TNF therapy(342). Moreover, the current therapies for IBD have a range of side effects that lead to poor compliance from patients. Because *Salmonella* utilize a type III secretion system to deliver AvrA, we previously developed a protein nanoparticle encapsulating AvrA for intracellular targeting(227). We have also established alginate and chitosan microparticles for oral delivery of AvrA(8). In this aim, we characterized the effects of the immune response at the single-cell level using flow cytometry. We observed reduced neutrophil infiltration in the Peyer's patches, the small masses of lymphatic tissue within the small intestine. We also found decreased numbers of CD4+ cells in the Peyer's patches, and reduced CD8+ T-cells in the intraepithelial lymphocyte population following AvrA microparticle treatment in LPS stimulated mice. The effects of AvrA only seemed to lead to a local immune modulation, as both innate and adaptive immune cell counts were unchanged in the spleen after

LPS stimulation. Interestingly, macrophage numbers were unaffected in the small intestine. Future directions must focus on further parsing out the macrophage phenotypes, using dimensionality reduction techniques such as SPADE to determine the pseudotime trajectory of macrophage maturation and differentiation. SPADE was instrumental in uncovering the activation status of CD8+ T-cells in this aim. SPADE analysis showed reduced CD8+ Ly6C+ T-cells in AvrA treated groups, which led us to investigate the phenotype of this cell subset. Further investigation elucidated a CD8+ Ly6C+ CD44+ population which was modulated by AvrA therapy. CD44 is an activation-associated surface marker on T-cells, with $CD44^{hi}$ cells having an effector phenotype(343). CD8+ $CD44^{high}$ Ly6C+ cells have also been suggested to have memory-type phenotypes(256). These data suggest local effects on both the innate and adaptive immune system that may be further elucidated with more extensive models of gastrointestinal inflammation.

In aim 3, we developed a DNAzyme-based therapeutic for the treatment of chronic inflammatory disorders, such as asthma and IBD. We hypothesized that the selected DzNP would be an effective method of regulating intracellular GATA3, leading to reduction of Th2-specific cytokines. We observed a reduction in inflammation in both a Th2-mouse model of asthma, as well as in the DSS model of inflammatory colitis. Interestingly, by delivering these nanoparticles in an alginate hydrogel that was formed by giving a second gavage of $CaCl_2$ as previously described(333), we observed intracellular uptake of nanoparticles in both innate and adaptive immune cell populations. Oral gavage of DzNP nanoparticles encapsulated in alginate also reduced histological scores of inflammation.

6.2 Characterization of innate and adaptive immune cell function in inflammatory mouse models

While the studies outlined here utilized well-established models of inflammation to understand and parse out the roles of both innate and adaptive immunity, the field of immunology

continues to evolve. Immune cells are able to take on specific phenotypes. Future studies must focs on determining the biological response to biomaterials and how the individual cell populations are modulated can inform future drug development. Our increased understanding of the spectrum of cellular phenotypes instructs more sophisticated methods that aim to elucidate the origin, activation status, and function of immune cells. Neutrophils, for example, are thought to possess distinct subpopulations, and staining cellular markers for flow cytometry is now more complex than typical CD11b+ Ly6G+ markers.

Similarly, macrophages exhibit remarkable plasticity, and are able to change phenotypes in response to their local microenvironment(344). Macrophage phenotypes adapt based on three functions: host defense, wound healing, and immune regulation. These macrophages are thought to exist on a "spectrum" based on their function. In fact, there may exist more characteristically diverse phenotypes of macrophages that have yet to be identified(345). Thus, elucidation of the roles of macrophages in response to injury, and in response to immunomodulatory biomaterials, is crucial to understanding their function, and to understanding how the innate and adaptive immune systems respond.

Most relevant from this work is the importance of further characterization of lymphoid cell populations. We focused our analysis on CD4+ and CD8+ T-cells, due to their recruitment by macrophages and dendritic cells. Importantly, CD4+ and CD8+ cells have been implicated in healing(28). However, additional subpopulations of Tregs exist in both CD4+ and CD8+ populations, such as Th17, and Gr1+ subpopulations, and we have yet to characterize their recruitment or activity following immunomodulatory biomaterial delivery. Future studies should focus on characterizing a wider range of cell surface and intracellular markers, especially focusing on markers of effector function and activation status. Here, we focused mainly on cell numbers, but understanding the expression level of cytokines such as TNF, IL-10, IL-4, and IL-6 would be useful in establishing how an immune cell is responding to a stimulus, both in the innate and adaptive systems. This can be achieved using novel techniques such as mass cytometry or

single cell qPCR. Mass cytometry, in particular, is a novel technique that utilizes metal antibodies to tag cell surface and intracellular markers. Flow cytometry is limited to 10-15 markers, thus, techniques like mass cytometry would vastly expand our knowledge of the immune microenvironment in response to injury or in disease. Moreover, analysis of such extensive data could be made simple using dimensionality reduction techniques such as SPADE.

6.3 Further characterization of immune modulation using dimensionality reduction techniques

SPADE is an algorithm that was developed to explore high-dimensional data in an objective manner. SPADE helps investigators infer likely cellular progressions and can aid in the identification of unexpected cellular behavior or novel types of cells. Here, we used SPADE to identify trends in cellular heterogeneity in response to PEG-4MAL hydrogels in a chronic injury model, and in response to alginate/chitosan microparticles delivering AvrA to the small intestine. In both cases, SPADE was able to recover a hierarchy that aligned with our previous work and with known biology. In addition, we found trends in cells that we would not have considered to study otherwise.

However, SPADE was originally developed to analyze datasets with a large number of markers. In our work, we studied at most 12 markers in one panel to characterize around 6-7 different cell phenotypes. Future directions should focus on developing panels for the purpose of using SPADE to understand cell phenotypes. In the original SPADE publication, the authors outline a concept called “progression similarity”, where they identified genes that are concordant with hierarchical structure. This allows for the selection of protein markers that support a common cellular phenotype hierarchy(162). This strategy should be used for future studies that aim to gain

an understanding of biological signaling and differentiation processes, and the temporal and spatial development of the immune response.

6.4 Understanding the expansive roles of CD8+ Tregs

It was our overall goal in this work to use immunomodulatory biomaterials to alleviate inflammation in different disease contexts. While we observed the reduction of local immune cell recruitment after hydrogel therapy, ultimately, we identified some unique subsets of CD8+ T-cells that may be useful in better understanding the CD8+ T-cell response to injury, biomaterials, and the innate immune response. CD8+ T-suppressor cells (Tsups or Tregs) are a heterogeneous population, thus making them difficult to study using conventional methods, and as a result, are often poorly characterized(206). CD8+ Tregs are present in low quantities at steady state in both mice and humans. CD8+ Tregs, like CD4+ cells, respond to IL-2 activation, and express markers similar to CD4+ Tregs, such as CD103(346) and CTLA-4(347). In fact, CD8+ Tregs have been reported in humans, and have a strong immunosuppressive properties *in vitro(207).* CD8+ Tregs have also been shown to play a role in human autoimmune disease, including IBD(208).

On the pro-inflammatory side, this work found the involvement of a subset of CD8+ Ly6C+ $CD44^{hi}$ T-cells. Ly6C+ is an activation marker for CD8+ T-cells, and some populations of Ly6C+ T-cells have been shown to change their phenotype and function from naïve to effector cells(255). Using SPADE was instrumental to our discovery of these T-cell subsets responding to our method of delivery. Future analysis of data in response to immunomodulatory biomaterials should utilize a separate T-cell panel to consider potential contributions from the adaptive immune system, focusing on CD8+ T-

cells. Moreover, analysis using techniques like mass cytometry would provide useful information on the activation status of these cells. Lastly, employing SPADE to analyze and elucidate such data would lead to the identification of novel subpopulations of adaptive immune cells involved in processes in which they currently are not thought to play a role.

REFERENCES

1. Guo S, Dipietro LA. Factors affecting wound healing. J Dent Res. 2010;89(3):219-29. Epub 2010/02/09. doi: 10.1177/0022034509359125. PubMed PMID: 20139336; PMCID: PMC2903966.

2. Gonzalez AC, Costa TF, Andrade ZA, Medrado AR. Wound healing - A literature review. An Bras Dermatol. 2016;91(5):614-20. Epub 2016/11/10. doi: 10.1590/abd1806-4841.20164741. PubMed PMID: 27828635; PMCID: PMC5087220.

3. Hesketh M, Sahin KB, West ZE, Murray RZ. Macrophage Phenotypes Regulate Scar Formation and Chronic Wound Healing. Int J Mol Sci. 2017;18(7). Epub 2017/07/18. doi: 10.3390/ijms18071545. PubMed PMID: 28714933; PMCID: PMC5536033.

4. Jimmy B, Jose J. Patient medication adherence: measures in daily practice. Oman Med J. 2011;26(3):155-9. Epub 2011/11/02. doi: 10.5001/omj.2011.38. PubMed PMID: 22043406; PMCID: PMC3191684.

5. Spiller KL, Freytes DO, Vunjak-Novakovic G. Macrophages modulate engineered human tissues for enhanced vascularization and healing. Ann Biomed Eng. 2015;43(3):616-27. Epub 2014/10/22. doi: 10.1007/s10439-014-1156-8. PubMed PMID: 25331098; PMCID: PMC4380684.

6. Mikos AG, Herring SW, Ochareon P, Elisseeff J, Lu HH, Kandel R, Schoen FJ, Toner M, Mooney D, Atala A, Van Dyke ME, Kaplan D, Vunjak-Novakovic G. Engineering complex tissues. Tissue Eng. 2006;12(12):3307-39. Epub 2007/05/24. doi: 10.1089/ten.2006.12.3307. PubMed PMID: 17518671; PMCID: PMC2821210.

7. Ma WT, Gao F, Gu K, Chen DK. The Role of Monocytes and Macrophages in Autoimmune Diseases: A Comprehensive Review. Front Immunol. 2019;10:1140. Epub 2019/06/11. doi: 10.3389/fimmu.2019.01140. PubMed PMID: 31178867; PMCID: PMC6543461.

8. Ling K, Wu H, Neish AS, Champion JA. Alginate/chitosan microparticles for gastric passage and intestinal release of therapeutic protein nanoparticles. J Control Release. 2019;295:174-86. Epub 2018/12/18. doi: 10.1016/j.jconrel.2018.12.017. PubMed PMID: 30557649.

9. Jones RM, Wu H, Wentworth C, Luo L, Collier-Hyams L, Neish AS. Salmonella AvrA Coordinates Suppression of Host Immune and Apoptotic Defenses via JNK Pathway Blockade. Cell Host Microbe. 2008;3(4):233-44. Epub 2008/04/15. doi: 10.1016/j.chom.2008.02.016. PubMed PMID: 18407067.

10. Hirahara K, Nakayama T. CD4+ T-cell subsets in inflammatory diseases: beyond the Th1/Th2 paradigm. Int Immunol. 2016;28(4):163-71. Epub 2016/02/14. doi: 10.1093/intimm/dxw006. PubMed PMID: 26874355; PMCID: PMC4889886.

11. Walker JA, McKenzie ANJ. TH2 cell development and function. Nature Reviews Immunology. 2017;18:121. doi: 10.1038/nri.2017.118.

12. Ray A, Cohn L. Th2 cells and GATA-3 in asthma: new insights into the regulation of airway inflammation. J Clin Invest. 1999;104(8):985-93. doi: 10.1172/JCI8204. PubMed PMID: 10525032; PMCID: PMC408864.

13. Bergqvist A, Andersson CK, Hoffmann HJ, Mori M, Shikhagaie M, Krohn IK, Dahl R, Bjermer L, Erjefalt JS. Marked epithelial cell pathology and leukocyte paucity in persistently symptomatic severe asthma. Am J Respir Crit Care Med. 2013;188(12):1475-7. doi: 10.1164/rccm.201308-1444LE. PubMed PMID: 24328780.

14. Pires CF, Rosa FF, Kurochkin I, Pereira CF. Understanding and Modulating Immunity With Cell Reprogramming. Front Immunol. 2019;10:2809. Epub 2020/01/11. doi: 10.3389/fimmu.2019.02809. PubMed PMID: 31921109; PMCID: PMC6917620.

15. Subramanian N, Torabi-Parizi P, Gottschalk RA, Germain RN, Dutta B. Network representations of immune system complexity. Wiley Interdiscip Rev Syst Biol Med. 2015;7(1):13-38. Epub 2015/01/28. doi: 10.1002/wsbm.1288. PubMed PMID: 25625853; PMCID: PMC4339634.

16. Chaplin DD. Overview of the immune response. J Allergy Clin Immunol. 2010;125(2 Suppl 2):S3-23. Epub 2010/03/05. doi: 10.1016/j.jaci.2009.12.980. PubMed PMID: 20176265; PMCID: PMC2923430.

17. Schmidt-Bleek K, Kwee BJ, Mooney DJ, Duda GN. Boon and Bane of Inflammation in Bone Tissue Regeneration and Its Link with Angiogenesis. Tissue Eng Part B Rev. 2015;21(4):354-64. Epub 2015/03/07. doi: 10.1089/ten.TEB.2014.0677. PubMed PMID: 25742724; PMCID: PMC4533093.

18. Koeberle A, Werz O. Multi-target approach for natural products in inflammation. Drug Discov Today. 2014;19(12):1871-82. Epub 2014/08/31. doi: 10.1016/j.drudis.2014.08.006. PubMed PMID: 25172801.

19. Strbo N, Yin N, Stojadinovic O. Innate and Adaptive Immune Responses in Wound Epithelialization. Adv Wound Care (New Rochelle). 2014;3(7):492-501. Epub 2014/07/18. doi: 10.1089/wound.2012.0435. PubMed PMID: 25032069; PMCID: PMC4086194.

20. Avishai E, Yeghiazaryan K, Golubnitschaja O. Impaired wound healing: facts and hypotheses for multi-professional considerations in predictive, preventive and personalised medicine. EPMA J. 2017;8(1):23-33. Epub 2017/06/18. doi: 10.1007/s13167-017-0081-y. PubMed PMID: 28620441; PMCID: PMC5471802.

21. Sen CK, Gordillo GM, Roy S, Kirsner R, Lambert L, Hunt TK, Gottrup F, Gurtner GC, Longaker MT. Human skin wounds: a major and snowballing threat to public health and the economy. Wound Repair Regen. 2009;17(6):763-71. Epub 2009/11/12. doi: 10.1111/j.1524-475X.2009.00543.x. PubMed PMID: 19903300; PMCID: PMC2810192.

22. McCain J. The Disease Burden of the Most Common Autoimmune Diseases. Manag Care. 2016;25(7):28-32. Epub 2017/01/26. PubMed PMID: 28121529.

23. Related titles. In: Ågren MS, editor. Wound Healing Biomaterials: Woodhead Publishing; 2016. p. ii.

24. Woodhead Publishing Series in Biomaterials. In: Ågren MS, editor. Wound Healing Biomaterials: Woodhead Publishing; 2016. p. xvii-xxii.

25. Copyright. In: Ågren MS, editor. Wound Healing Biomaterials: Woodhead Publishing; 2016. p. iv.

26. Front Matter. In: Ågren MS, editor. Wound Healing Biomaterials: Woodhead Publishing; 2016. p. iii.

27. Agostinho Hunt AM, Aguzzi C, Ahmad A, Aramwit P, Barbosa DB, Berretta A, Bonferoni MC, Caramella C, Cerqueira MT, Correlo VM, Cowan LJ, Cutting K, da Silva LP, Davidson BR, Davidson C, Domb AJ, Dong Y, Fernandes GL, Fernandes RA, Ferrari F, Ghadi R, Gorup LF, Grandio D, Haugen HJ, Hsu BB, Jackson CJ, Jain A, James R, Kelly R, Khan W, Kirker KR, Kumbar SG, Kunkel J, Leaper D, Lee CH, Lee Y, Loboa EG, Lyngstadaas SP, Magill LJ, Manoukian OS, Marin C, Marques AP, Mazzocca AD, Meikle ST, Mitchell H, Mobed-Miremadi M, Mohiti-Asli M, Monteiro DR, Morris GA, Moxon S, Nyström A, Ousey K, Phillips PL, Reis RL, Roberts C, Robertson FP, Rodrigues de Camargo E, Rossi S, Saleh K, Sambasivam M, Sandri G, Schultz GS, Smith AM, Smith LE, Sönnergren HH, Viseras C, Wang W, White R, Wolcott RD, Xue M. List of contributors. In: Ågren MS, editor. Wound Healing Biomaterials: Woodhead Publishing; 2016. p. xiii-xvi.

28. Coger V, Million N, Rehbock C, Sures B, Nachev M, Barcikowski S, Wistuba N, Strauss S, Vogt PM. Tissue Concentrations of Zinc, Iron, Copper, and Magnesium During the Phases of Full Thickness Wound Healing in a Rodent Model. Biol Trace Elem Res. 2019;191(1):167-76. Epub 2018/12/16. doi: 10.1007/s12011-018-1600-y. PubMed PMID: 30552609; PMCID: PMC6656798.

29. Wallace HA, Basehore BM, Zito PM. Wound Healing Phases. StatPearls. Treasure Island (FL)2020.

30. Pober JS, Sessa WC. Inflammation and the blood microvascular system. Cold Spring Harb Perspect Biol. 2014;7(1):a016345. Epub 2014/11/11. doi: 10.1101/cshperspect.a016345. PubMed PMID: 25384307; PMCID: PMC4292166.

31. Chen L, Deng H, Cui H, Fang J, Zuo Z, Deng J, Li Y, Wang X, Zhao L. Inflammatory responses and inflammation-associated diseases in organs. Oncotarget. 2018;9(6):7204-18. Epub 2018/02/23. doi: 10.18632/oncotarget.23208. PubMed PMID: 29467962; PMCID: PMC5805548.

32. Zhang N, Wu YP, Qian SJ, Teng C, Chen S, Li H. Research progress in the mechanism of effect of PRP in bone deficiency healing. ScientificWorldJournal.

2013;2013:134582. Epub 2013/05/28. doi: 10.1155/2013/134582. PubMed PMID: 23710132; PMCID: PMC3654280.

33. Canedo-Dorantes L, Canedo-Ayala M. Skin Acute Wound Healing: A Comprehensive Review. Int J Inflam. 2019;2019:3706315. Epub 2019/07/06. doi: 10.1155/2019/3706315. PubMed PMID: 31275545; PMCID: PMC6582859.

34. Pierce GF, Mustoe TA, Lingelbach J, Masakowski VR, Griffin GL, Senior RM, Deuel TF. Platelet-derived growth factor and transforming growth factor-beta enhance tissue repair activities by unique mechanisms. J Cell Biol. 1989;109(1):429-40. Epub 1989/07/01. doi: 10.1083/jcb.109.1.429. PubMed PMID: 2745556; PMCID: PMC2115493.

35. von Bruhl ML, Stark K, Steinhart A, Chandraratne S, Konrad I, Lorenz M, Khandoga A, Tirniceriu A, Coletti R, Kollnberger M, Byrne RA, Laitinen I, Walch A, Brill A, Pfeiler S, Manukyan D, Braun S, Lange P, Riegger J, Ware J, Eckart A, Haidari S, Rudelius M, Schulz C, Echtler K, Brinkmann V, Schwaiger M, Preissner KT, Wagner DD, Mackman N, Engelmann B, Massberg S. Monocytes, neutrophils, and platelets cooperate to initiate and propagate venous thrombosis in mice in vivo. J Exp Med. 2012;209(4):819-35. Epub 2012/03/28. doi: 10.1084/jem.20112322. PubMed PMID: 22451716; PMCID: PMC3328366.

36. Ninan N, Thomas S, Grohens Y. Wound healing in urology. Adv Drug Deliv Rev. 2015;82-83:93-105. Epub 2014/12/17. doi: 10.1016/j.addr.2014.12.002. PubMed PMID: 25500273.

37. Ellis S, Lin EJ, Tartar D. Immunology of Wound Healing. Curr Dermatol Rep. 2018;7(4):350-8. Epub 2018/12/14. doi: 10.1007/s13671-018-0234-9. PubMed PMID: 30524911; PMCID: PMC6244748.

38. Caley MP, Martins VL, O'Toole EA. Metalloproteinases and Wound Healing. Adv Wound Care (New Rochelle). 2015;4(4):225-34. Epub 2015/05/07. doi: 10.1089/wound.2014.0581. PubMed PMID: 25945285; PMCID: PMC4397992.

39. Smith MM, Melrose J. Proteoglycans in Normal and Healing Skin. Adv Wound Care (New Rochelle). 2015;4(3):152-73. Epub 2015/03/19. doi: 10.1089/wound.2013.0464. PubMed PMID: 25785238; PMCID: PMC4352701.

40. Hisamatsu T, Kanai T, Mikami Y, Yoneno K, Matsuoka K, Hibi T. Immune aspects of the pathogenesis of inflammatory bowel disease. Pharmacology & Therapeutics. 2013;137(3):283-97. doi: https://doi.org/10.1016/j.pharmthera.2012.10.008.

41. Sturm A, Dignass AU. Epithelial restitution and wound healing in inflammatory bowel disease. World J Gastroenterol. 2008;14(3):348-53. Epub 2008/01/18. doi: 10.3748/wjg.14.348. PubMed PMID: 18200658; PMCID: PMC2679124.

42. Iizuka M, Konno S. Wound healing of intestinal epithelial cells. World J Gastroenterol. 2011;17(17):2161-71. Epub 2011/06/03. doi: 10.3748/wjg.v17.i17.2161. PubMed PMID: 21633524; PMCID: PMC3092866.

43. Moyer RA, Wendt MK, Johanesen PA, Turner JR, Dwinell MB. Rho activation regulates CXCL12 chemokine stimulated actin rearrangement and restitution in model intestinal epithelia. Lab Invest. 2007;87(8):807-17. Epub 2007/06/19. doi: 10.1038/labinvest.3700595. PubMed PMID: 17572689; PMCID: PMC2693067.

44. El-Assal ON, Besner GE. HB-EGF enhances restitution after intestinal ischemia/reperfusion via PI3K/Akt and MEK/ERK1/2 activation. Gastroenterology. 2005;129(2):609-25. Epub 2005/08/09. doi: 10.1016/j.gastro.2005.05.054. PubMed PMID: 16083716.

45. Sheng H, Shao J, Townsend CM, Jr., Evers BM. Phosphatidylinositol 3-kinase mediates proliferative signals in intestinal epithelial cells. Gut. 2003;52(10):1472-8. Epub 2003/09/13. doi: 10.1136/gut.52.10.1472. PubMed PMID: 12970141; PMCID: PMC1773820.

46. Laukoetter MG, Bruewer M, Nusrat A. Regulation of the intestinal epithelial barrier by the apical junctional complex. Curr Opin Gastroenterol. 2006;22(2):85-9. Epub 2006/02/08. doi: 10.1097/01.mog.0000203864.48255.4f. PubMed PMID: 16462161.

47. Mogensen TH. Pathogen recognition and inflammatory signaling in innate immune defenses. Clin Microbiol Rev. 2009;22(2):240-73, Table of Contents. Epub 2009/04/16. doi: 10.1128/CMR.00046-08. PubMed PMID: 19366914; PMCID: PMC2668232.

48. Chen GY, Nunez G. Sterile inflammation: sensing and reacting to damage. Nat Rev Immunol. 2010;10(12):826-37. Epub 2010/11/23. doi: 10.1038/nri2873. PubMed PMID: 21088683; PMCID: PMC3114424.

49. Mosser DM, Edwards JP. Exploring the full spectrum of macrophage activation. Nat Rev Immunol. 2008;8(12):958-69. Epub 2008/11/26. doi: 10.1038/nri2448. PubMed PMID: 19029990; PMCID: PMC2724991.

50. Ogle ME, Segar CE, Sridhar S, Botchwey EA. Monocytes and macrophages in tissue repair: Implications for immunoregenerative biomaterial design. Exp Biol Med (Maywood). 2016;241(10):1084-97. Epub 2016/05/28. doi: 10.1177/1535370216650293. PubMed PMID: 27229903; PMCID: PMC4898192.

51. Rosales C. Neutrophil: A Cell with Many Roles in Inflammation or Several Cell Types? Front Physiol. 2018;9:113. Epub 2018/03/09. doi: 10.3389/fphys.2018.00113. PubMed PMID: 29515456; PMCID: PMC5826082.

52. Gan Q, Wang T, Cochrane C, McCarron P. Modulation of surface charge, particle size and morphological properties of chitosan-TPP nanoparticles intended for gene delivery. Colloids Surf B Biointerfaces. 2005;44(2-3):65-73. Epub 2005/07/19. doi: 10.1016/j.colsurfb.2005.06.001. PubMed PMID: 16024239.

53. Mayadas TN, Cullere X, Lowell CA. The multifaceted functions of neutrophils. Annu Rev Pathol. 2014;9:181-218. Epub 2013/09/21. doi: 10.1146/annurev-pathol-020712-164023. PubMed PMID: 24050624; PMCID: PMC4277181.

54. Nauseef WM, Borregaard N. Neutrophils at work. Nat Immunol. 2014;15(7):602-11. Epub 2014/06/19. doi: 10.1038/ni.2921. PubMed PMID: 24940954.

55. Scapini P, Cassatella MA. Social networking of human neutrophils within the immune system. Blood. 2014;124(5):710-9. Epub 2014/06/14. doi: 10.1182/blood-2014-03-453217. PubMed PMID: 24923297.

56. Kaplan MJ, Radic M. Neutrophil extracellular traps: double-edged swords of innate immunity. J Immunol. 2012;189(6):2689-95. Epub 2012/09/08. doi: 10.4049/jimmunol.1201719. PubMed PMID: 22956760; PMCID: PMC3439169.

57. Borregaard N. Neutrophils, from marrow to microbes. Immunity. 2010;33(5):657-70. Epub 2010/11/26. doi: 10.1016/j.immuni.2010.11.011. PubMed PMID: 21094463.

58. Chavakis E, Choi EY, Chavakis T. Novel aspects in the regulation of the leukocyte adhesion cascade. Thromb Haemost. 2009;102(2):191-7. Epub 2009/08/05. doi: 10.1160/TH08-12-0844. PubMed PMID: 19652868; PMCID: PMC2722029.

59. Ley K, Laudanna C, Cybulsky MI, Nourshargh S. Getting to the site of inflammation: the leukocyte adhesion cascade updated. Nat Rev Immunol. 2007;7(9):678-89. Epub 2007/08/25. doi: 10.1038/nri2156. PubMed PMID: 17717539.

60. Scott IC, Majithiya JB, Sanden C, Thornton P, Sanders PN, Moore T, Guscott M, Corkill DJ, Erjefalt JS, Cohen ES. Interleukin-33 is activated by allergen- and necrosis-associated proteolytic activities to regulate its alarmin activity during epithelial damage. Sci Rep. 2018;8(1):3363. Epub 2018/02/22. doi: 10.1038/s41598-018-21589-2. PubMed PMID: 29463838; PMCID: PMC5820248.

61. Pittman K, Kubes P. Damage-associated molecular patterns control neutrophil recruitment. J Innate Immun. 2013;5(4):315-23. Epub 2013/03/15. doi: 10.1159/000347132. PubMed PMID: 23486162; PMCID: PMC6741494.

62. McEver RP. Selectins: initiators of leucocyte adhesion and signalling at the vascular wall. Cardiovascular Research. 2015;107(3):331-9. doi: 10.1093/cvr/cvv154.

63. Phillipson M, Kubes P. The neutrophil in vascular inflammation. Nat Med. 2011;17(11):1381-90. Epub 2011/11/09. doi: 10.1038/nm.2514. PubMed PMID: 22064428.

64. Hajishengallis G, Chavakis T. Endogenous modulators of inflammatory cell recruitment. Trends Immunol. 2013;34(1):1-6. Epub 2012/09/07. doi: 10.1016/j.it.2012.08.003. PubMed PMID: 22951309; PMCID: PMC3703146.

65. Sharma SK, Naidu G. The role of danger-associated molecular patterns (DAMPs) in trauma and infections. J Thorac Dis. 2016;8(7):1406-9. Epub 2016/08/09. doi: 10.21037/jtd.2016.05.22. PubMed PMID: 27500853; PMCID: PMC4958879.

66. Wilgus TA, Roy S, McDaniel JC. Neutrophils and Wound Repair: Positive Actions and Negative Reactions. Adv Wound Care (New Rochelle). 2013;2(7):379-88. Epub 2014/02/15. doi: 10.1089/wound.2012.0383. PubMed PMID: 24527354; PMCID: PMC3763227.

67. Jorch SK, Kubes P. An emerging role for neutrophil extracellular traps in noninfectious disease. Nat Med. 2017;23(3):279-87. Epub 2017/03/08. doi: 10.1038/nm.4294. PubMed PMID: 28267716.

68. Knight JS, Carmona-Rivera C, Kaplan MJ. Proteins derived from neutrophil extracellular traps may serve as self-antigens and mediate organ damage in autoimmune diseases. Front Immunol. 2012;3:380. Epub 2012/12/19. doi: 10.3389/fimmu.2012.00380. PubMed PMID: 23248629; PMCID: PMC3521997.

69. Burgueno JF, Fritsch J, Santander AM, Brito N, Fernandez I, Pignac-Kobinger J, Conner GE, Abreu MT. Intestinal Epithelial Cells Respond to Chronic Inflammation and Dysbiosis by Synthesizing H2O2. Front Physiol. 2019;10:1484. Epub 2019/12/25. doi: 10.3389/fphys.2019.01484. PubMed PMID: 31871440; PMCID: PMC6921703.

70. Wera O, Lancellotti P, Oury C. The Dual Role of Neutrophils in Inflammatory Bowel Diseases. J Clin Med. 2016;5(12). Epub 2016/12/22. doi: 10.3390/jcm5120118. PubMed PMID: 27999328; PMCID: PMC5184791.

71. Buell MG, Berin MC. Neutrophil-independence of the initiation of colonic injury. Comparison of results from three models of experimental colitis in the rat. Dig Dis Sci. 1994;39(12):2575-88. Epub 1994/12/01. doi: 10.1007/bf02087693. PubMed PMID: 7995182.

72. Natsui M, Kawasaki K, Takizawa H, Hayashi SI, Matsuda Y, Sugimura K, Seki K, Narisawa R, Sendo F, Asakura H. Selective depletion of neutrophils by a monoclonal antibody, RP-3, suppresses dextran sulphate sodium-induced colitis in rats. J Gastroenterol Hepatol. 1997;12(12):801-8. Epub 1998/03/21. doi: 10.1111/j.1440-1746.1997.tb00375.x. PubMed PMID: 9504889.

73. Rivera A, Siracusa MC, Yap GS, Gause WC. Innate cell communication kick-starts pathogen-specific immunity. Nat Immunol. 2016;17(4):356-63. Epub 2016/03/24. doi: 10.1038/ni.3375. PubMed PMID: 27002843; PMCID: PMC4949486.

74. Corliss BA, Azimi MS, Munson JM, Peirce SM, Murfee WL. Macrophages: An Inflammatory Link Between Angiogenesis and Lymphangiogenesis. Microcirculation. 2016;23(2):95-121. Epub 2015/11/29. doi: 10.1111/micc.12259. PubMed PMID: 26614117; PMCID: PMC4744134.

75. Laskin DL, Sunil VR, Gardner CR, Laskin JD. Macrophages and tissue injury: agents of defense or destruction? Annu Rev Pharmacol Toxicol. 2011;51:267-88. Epub 2010/10/05. doi: 10.1146/annurev.pharmtox.010909.105812. PubMed PMID: 20887196; PMCID: PMC3670679.

76. Sansbury BE, Spite M. Resolution of Acute Inflammation and the Role of Resolvins in Immunity, Thrombosis, and Vascular Biology. Circ Res. 2016;119(1):113-30. Epub 2016/06/25. doi: 10.1161/CIRCRESAHA.116.307308. PubMed PMID: 27340271; PMCID: PMC5260827.

77. Krzyszczyk P, Schloss R, Palmer A, Berthiaume F. The Role of Macrophages in Acute and Chronic Wound Healing and Interventions to Promote Pro-wound Healing Phenotypes. Front Physiol. 2018;9:419. Epub 2018/05/17. doi: 10.3389/fphys.2018.00419. PubMed PMID: 29765329; PMCID: PMC5938667.

78. Roszer T. Understanding the Mysterious M2 Macrophage through Activation Markers and Effector Mechanisms. Mediators Inflamm. 2015;2015:816460. Epub 2015/06/20. doi: 10.1155/2015/816460. PubMed PMID: 26089604; PMCID: PMC4452191.

79. Papadakis KA, Targan SR. The Role of Chemokines and Chemokine Receptors in Mucosal Inflammation. Inflammatory Bowel Diseases. 2000;6(4):303-13. doi: 10.1097/00054725-200011000-00007.

80. Navegantes KC, de Souza Gomes R, Pereira PAT, Czaikoski PG, Azevedo CHM, Monteiro MC. Immune modulation of some autoimmune diseases: the critical role of macrophages and neutrophils in the innate and adaptive immunity. J Transl Med. 2017;15(1):36. Epub 2017/02/17. doi: 10.1186/s12967-017-1141-8. PubMed PMID: 28202039; PMCID: PMC5312441.

81. Janeway CA Jr TP, Walport M, et al. Immunobiology: The Immune System in Health and Disease.: New York: Garland Science; 2001.

82. Dunkelberger JR, Song W-C. Complement and its role in innate and adaptive immune responses. Cell Research. 2010;20(1):34-50. doi: 10.1038/cr.2009.139.

83. Oakes RS, Froimchuk E, Jewell CM. Engineering Biomaterials to Direct Innate Immunity. Adv Ther (Weinh). 2019;2(6). Epub 2019/06/27. doi: 10.1002/adtp.201800157. PubMed PMID: 31236439; PMCID: PMC6590522.

84. Germain RN. T-cell development and the CD4-CD8 lineage decision. Nat Rev Immunol. 2002;2(5):309-22. Epub 2002/05/30. doi: 10.1038/nri798. PubMed PMID: 12033737.

85. Kaiko GE, Horvat JC, Beagley KW, Hansbro PM. Immunological decision-making: how does the immune system decide to mount a helper T-cell response? Immunology. 2008;123(3):326-38. Epub 2007/11/07. doi: 10.1111/j.1365-2567.2007.02719.x. PubMed PMID: 17983439; PMCID: PMC2433332.

86. Krebs CF, Steinmetz OM. CD4(+) T Cell Fate in Glomerulonephritis: A Tale of Th1, Th17, and Novel Treg Subtypes. Mediators Inflamm. 2016;2016:5393894. Epub 2016/12/16. doi: 10.1155/2016/5393894. PubMed PMID: 27974866; PMCID: PMC5126430.

87. Betts MR, Brenchley JM, Price DA, De Rosa SC, Douek DC, Roederer M, Koup RA. Sensitive and viable identification of antigen-specific CD8+ T cells by a flow cytometric assay for degranulation. J Immunol Methods. 2003;281(1-2):65-78. Epub 2003/10/29. doi: 10.1016/s0022-1759(03)00265-5. PubMed PMID: 14580882.

88. Reiser J, Banerjee A. Effector, Memory, and Dysfunctional CD8(+) T Cell Fates in the Antitumor Immune Response. J Immunol Res. 2016;2016:8941260. Epub 2016/06/18. doi: 10.1155/2016/8941260. PubMed PMID: 27314056; PMCID: PMC4893440.

89. Kondelkova K, Vokurkova D, Krejsek J, Borska L, Fiala Z, Ctirad A. Regulatory T cells (TREG) and their roles in immune system with respect to immunopathological disorders. Acta Medica (Hradec Kralove). 2010;53(2):73-7. Epub 2010/08/03. doi: 10.14712/18059694.2016.63. PubMed PMID: 20672742.

90. Gol-Ara M, Jadidi-Niaragh F, Sadria R, Azizi G, Mirshafiey A. The role of different subsets of regulatory T cells in immunopathogenesis of rheumatoid arthritis. Arthritis. 2012;2012:805875. Epub 2012/11/08. doi: 10.1155/2012/805875. PubMed PMID: 23133752; PMCID: PMC3486158.

91. Ligocki AJ, Niederkorn JY. Advances on Non-CD4 + Foxp3+ T Regulatory Cells: CD8+, Type 1, and Double Negative T Regulatory Cells in Organ Transplantation. Transplantation. 2015;99(8):1553-9. Epub 2015/07/21. doi: 10.1097/TP.0000000000000813. PubMed PMID: 26193065; PMCID: PMC4551577.

92. Zhao H, Liao X, Kang Y. Tregs: Where We Are and What Comes Next? Frontiers in Immunology. 2017;8:1578.

93. Huang Y, Chen Z. Inflammatory bowel disease related innate immunity and adaptive immunity. Am J Transl Res. 2016;8(6):2490-7. Epub 2016/07/12. PubMed PMID: 27398134; PMCID: PMC4931145.

94. Jung C, Hugot JP, Barreau F. Peyer's Patches: The Immune Sensors of the Intestine. Int J Inflam. 2010;2010:823710. Epub 2010/12/29. doi: 10.4061/2010/823710. PubMed PMID: 21188221; PMCID: PMC3004000.

95. Cuadrado E, Alonso M, de Juan MD, Echaniz P, Arenas JI. Regulatory T cells in patients with inflammatory bowel diseases treated with adacolumn granulocytapheresis. World J Gastroenterol. 2008;14(10):1521-7. Epub 2008/03/12. doi: 10.3748/wjg.14.1521. PubMed PMID: 18330941; PMCID: PMC2693745.

96. Folkman J, Long DM. The Use of Silicone Rubber as a Carrier for Prolonged Drug Therapy. J Surg Res. 1964;4:139-42. Epub 1964/03/01. doi: 10.1016/s0022-4804(64)80040-8. PubMed PMID: 14130164.

97. Li J, Mooney DJ. Designing hydrogels for controlled drug delivery. Nat Rev Mater. 2016;1(12). Epub 2016/12/01. doi: 10.1038/natrevmats.2016.71. PubMed PMID: 29657852; PMCID: PMC5898614.

98. Buckles RG. Biomaterials for drug delivery systems. J Biomed Mater Res. 1983;17(1):109-28. Epub 1983/01/01. doi: 10.1002/jbm.820170110. PubMed PMID: 6826569.

99. Liu L, Yao W, Rao Y, Lu X, Gao J. pH-Responsive carriers for oral drug delivery: challenges and opportunities of current platforms. Drug Delivery. 2017;24(1):569-81. doi: 10.1080/10717544.2017.1279238.

100. Folkman J. How the field of controlled-release technology began, and its central role in the development of angiogenesis research. Biomaterials. 1990;11(9):615-8. Epub 1990/11/01. doi: 10.1016/0142-9612(90)90017-k. PubMed PMID: 1708683.

101. Grisham MB. Oxidants and free radicals in inflammatory bowel disease. Lancet. 1994;344(8926):859-61. Epub 1994/09/24. doi: 10.1016/s0140-6736(94)92831-2. PubMed PMID: 7916405.

102. Hanauer SB, Baert F. Medical therapy of inflammatory bowel disease. Med Clin North Am. 1994;78(6):1413-26. Epub 1994/11/01. doi: 10.1016/s0025-7125(16)30108-0. PubMed PMID: 7967917.

103. Rider P, Carmi Y, Cohen I. Biologics for Targeting Inflammatory Cytokines, Clinical Uses, and Limitations. Int J Cell Biol. 2016;2016:9259646. Epub 2017/01/14. doi: 10.1155/2016/9259646. PubMed PMID: 28083070; PMCID: PMC5204077 publication of this paper.

104. Pithadia AB, Jain S. Treatment of inflammatory bowel disease (IBD). Pharmacol Rep. 2011;63(3):629-42. Epub 2011/08/23. doi: 10.1016/s1734-1140(11)70575-8. PubMed PMID: 21857074.

105. Homayun B, Lin X, Choi HJ. Challenges and Recent Progress in Oral Drug Delivery Systems for Biopharmaceuticals. Pharmaceutics. 2019;11(3). Epub 2019/03/22. doi: 10.3390/pharmaceutics11030129. PubMed PMID: 30893852; PMCID: PMC6471246.

106. Varum FJ, McConnell EL, Sousa JJ, Veiga F, Basit AW. Mucoadhesion and the gastrointestinal tract. Crit Rev Ther Drug Carrier Syst. 2008;25(3):207-58. Epub 2008/06/11. doi: 10.1615/critrevtherdrugcarriersyst.v25.i3.10. PubMed PMID: 18540839.

107. Ransford RA, Langman MJ. Sulphasalazine and mesalazine: serious adverse reactions re-evaluated on the basis of suspected adverse reaction reports to the Committee on Safety of Medicines. Gut. 2002;51(4):536-9. Epub 2002/09/18. doi: 10.1136/gut.51.4.536. PubMed PMID: 12235076; PMCID: PMC1773410.

108. Rutgeerts P, Sandborn WJ, Feagan BG, Reinisch W, Olson A, Johanns J, Travers S, Rachmilewitz D, Hanauer SB, Lichtenstein GR, de Villiers WJS, Present D, Sands BE,

Colombel JF. Infliximab for Induction and Maintenance Therapy for Ulcerative Colitis. New England Journal of Medicine. 2005;353(23):2462-76. doi: 10.1056/NEJMoa050516.

109. Lautenschlager C, Schmidt C, Lehr CM, Fischer D, Stallmach A. PEG-functionalized microparticles selectively target inflamed mucosa in inflammatory bowel disease. Eur J Pharm Biopharm. 2013;85(3 Pt A):578-86. Epub 2013/10/03. doi: 10.1016/j.ejpb.2013.09.016. PubMed PMID: 24084650.

110. Turner JR. Intestinal mucosal barrier function in health and disease. Nature Reviews Immunology. 2009;9(11):799-809. doi: 10.1038/nri2653.

111. Schmitz H, Barmeyer C, Fromm M, Runkel N, Foss H-D, Bentzel CJ, Riecken E-O, Schulzke J-D. Altered tight junction structure contributes to the impaired epithelial barrier function in ulcerative colitis. Gastroenterology. 1999;116(2):301-9. doi: https://doi.org/10.1016/S0016-5085(99)70126-5.

112. McGuckin MA, Eri R, Simms LA, Florin THJ, Radford-Smith G. Intestinal Barrier Dysfunction in Inflammatory Bowel Diseases. Inflammatory Bowel Diseases. 2008;15(1):100-13. doi: 10.1002/ibd.20539.

113. McAlindon ME, Gray T, Galvin A, Sewell HF, Podolsky DK, Mahida YR. Differential lamina propria cell migration via basement membrane pores of inflammatory bowel disease mucosa. Gastroenterology. 1998;115(4):841-8. doi: https://doi.org/10.1016/S0016-5085(98)70255-0.

114. Tibbitt MW, Anseth KS. Hydrogels as extracellular matrix mimics for 3D cell culture. Biotechnol Bioeng. 2009;103(4):655-63. Epub 2009/05/28. doi: 10.1002/bit.22361. PubMed PMID: 19472329; PMCID: PMC2997742.

115. Richter A, Paschew G, Klatt S, Lienig J, Arndt KF, Adler HP. Review on Hydrogel-based pH Sensors and Microsensors. Sensors (Basel). 2008;8(1):561-81. Epub 2008/01/25. doi: 10.3390/s8010561. PubMed PMID: 27879722; PMCID: PMC3668326.

116. Yang Z, Xu B. Supramolecular hydrogels based on biofunctional nanofibers of self-assembled small molecules. Journal of Materials Chemistry. 2007;17(23):2385-93. doi: 10.1039/B702493B.

117. Lee KY, Mooney DJ. Hydrogels for tissue engineering. Chem Rev. 2001;101(7):1869-79. Epub 2001/11/17. doi: 10.1021/cr000108x. PubMed PMID: 11710233.

118. Dreifke MB, Jayasuriya AA, Jayasuriya AC. Current wound healing procedures and potential care. Mater Sci Eng C Mater Biol Appl. 2015;48:651-62. Epub 2015/01/13. doi: 10.1016/j.msec.2014.12.068. PubMed PMID: 25579968; PMCID: PMC4443476.

119. De Angelis B, D'Autilio M, Orlandi F, Pepe G, Garcovich S, Scioli MG, Orlandi A, Cervelli V, Gentile P. Wound Healing: In Vitro and In Vivo Evaluation of a Bio-Functionalized Scaffold Based on Hyaluronic Acid and Platelet-Rich Plasma in Chronic

Ulcers. J Clin Med. 2019;8(9). Epub 2019/09/22. doi: 10.3390/jcm8091486. PubMed PMID: 31540446; PMCID: PMC6780765.

120. Wu R-X, Xu X-Y, Wang J, He X-T, Sun H-H, Chen F-M. Biomaterials for endogenous regenerative medicine: Coaxing stem cell homing and beyond. Applied Materials Today. 2018;11:144-65. doi: https://doi.org/10.1016/j.apmt.2018.02.004.

121. Chen FM, Liu X. Advancing biomaterials of human origin for tissue engineering. Prog Polym Sci. 2016;53:86-168. Epub 2016/03/30. doi: 10.1016/j.progpolymsci.2015.02.004. PubMed PMID: 27022202; PMCID: PMC4808059.

122. Allen TM, Cullis PR. Liposomal drug delivery systems: from concept to clinical applications. Adv Drug Deliv Rev. 2013;65(1):36-48. Epub 2012/10/06. doi: 10.1016/j.addr.2012.09.037. PubMed PMID: 23036225.

123. Laroui H, Theiss AL, Yan Y, Dalmasso G, Nguyen HT, Sitaraman SV, Merlin D. Functional TNFalpha gene silencing mediated by polyethyleneimine/TNFalpha siRNA nanocomplexes in inflamed colon. Biomaterials. 2011;32(4):1218-28. Epub 2010/10/26. doi: 10.1016/j.biomaterials.2010.09.062. PubMed PMID: 20970849; PMCID: PMC2992601.

124. Kriegel C, Amiji M. Oral TNF-alpha gene silencing using a polymeric microsphere-based delivery system for the treatment of inflammatory bowel disease. J Control Release. 2011;150(1):77-86. Epub 2010/10/21. doi: 10.1016/j.jconrel.2010.10.002. PubMed PMID: 20959130; PMCID: PMC3033993.

125. Hua S. Orally administered liposomal formulations for colon targeted drug delivery. Front Pharmacol. 2014;5:138. Epub 2014/06/25. doi: 10.3389/fphar.2014.00138. PubMed PMID: 24959147; PMCID: PMC4050429.

126. De S, Robinson D. Polymer relationships during preparation of chitosan-alginate and poly-l-lysine-alginate nanospheres. J Control Release. 2003;89(1):101-12. Epub 2003/04/16. doi: 10.1016/s0168-3659(03)00098-1. PubMed PMID: 12695066.

127. Florence AT. The oral absorption of micro- and nanoparticulates: neither exceptional nor unusual. Pharm Res. 1997;14(3):259-66. Epub 1997/03/01. doi: 10.1023/a:1012029517394. PubMed PMID: 9098866.

128. Mizrahy S, Peer D. Polysaccharides as building blocks for nanotherapeutics. Chem Soc Rev. 2012;41(7):2623-40. Epub 2011/11/17. doi: 10.1039/c1cs15239d. PubMed PMID: 22085917.

129. Lee JW, Park JH, Robinson JR. Bioadhesive-based dosage forms: the next generation. J Pharm Sci. 2000;89(7):850-66. Epub 2000/06/22. doi: 10.1002/1520-6017(200007)89:7<850::AID-JPS2>3.0.CO;2-G. PubMed PMID: 10861586.

130. Li J, Cai C, Li J, Li J, Li J, Sun T, Wang L, Wu H, Yu G. Chitosan-Based Nanomaterials for Drug Delivery. Molecules. 2018;23(10). Epub 2018/10/20. doi: 10.3390/molecules23102661. PubMed PMID: 30332830; PMCID: PMC6222903.

131. Donati I, Paoletti S. Material Properties of Alginates. In: Rehm BHA, editor. Alginates: Biology and Applications. Berlin, Heidelberg: Springer Berlin Heidelberg; 2009. p. 1-53.

132. Kravanja G, Primozic M, Knez Z, Leitgeb M. Chitosan-based (Nano)materials for Novel Biomedical Applications. Molecules. 2019;24(10). Epub 2019/05/24. doi: 10.3390/molecules24101960. PubMed PMID: 31117310; PMCID: PMC6572373.

133. Ahmed TA, Aljaeid BM. Preparation, characterization, and potential application of chitosan, chitosan derivatives, and chitosan metal nanoparticles in pharmaceutical drug delivery. Drug Des Devel Ther. 2016;10:483-507. Epub 2016/02/13. doi: 10.2147/DDDT.S99651. PubMed PMID: 26869768; PMCID: PMC4734734.

134. Gierszewska M, Ostrowska-Czubenko J, Chrzanowska E. pH-responsive chitosan/alginate polyelectrolyte complex membranes reinforced by tripolyphosphate. European Polymer Journal. 2018;101:282-90. doi: https://doi.org/10.1016/j.eurpolymj.2018.02.031.

135. Chen T, Li S, Zhu W, Liang Z, Zeng Q. Self-assembly pH-sensitive chitosan/alginate coated polyelectrolyte complexes for oral delivery of insulin. Journal of Microencapsulation. 2019;36(1):96-107. doi: 10.1080/02652048.2019.1604846.

136. Murata Y, Jinno D, Liu D, Isobe T, Kofuji K, Kawashima S. The drug release profile from calcium-induced alginate gel beads coated with an alginate hydrolysate. Molecules. 2007;12(11):2559-66. Epub 2007/12/11. doi: 10.3390/12112559. PubMed PMID: 18065958; PMCID: PMC6149178.

137. Shi J, Alves NM, Mano JF. Chitosan coated alginate beads containing poly(N-isopropylacrylamide) for dual-stimuli-responsive drug release. J Biomed Mater Res B Appl Biomater. 2008;84(2):595-603. Epub 2007/07/10. doi: 10.1002/jbm.b.30907. PubMed PMID: 17618514.

138. Matricardi P, Meo CD, Coviello T, Alhaique F. Recent advances and perspectives on coated alginate microspheres for modified drug delivery. Expert Opin Drug Deliv. 2008;5(4):417-25. Epub 2008/04/23. doi: 10.1517/17425247.5.4.417. PubMed PMID: 18426383.

139. Sosnik A. Alginate Particles as Platform for Drug Delivery by the Oral Route: State-of-the-Art. ISRN Pharm. 2014;2014:926157. Epub 2014/08/08. doi: 10.1155/2014/926157. PubMed PMID: 25101184; PMCID: PMC4004034.

140. Urbanska AM, Karagiannis ED, Guajardo G, Langer RS, Anderson DG. Therapeutic effect of orally administered microencapsulated oxaliplatin for colorectal

cancer. Biomaterials. 2012;33(18):4752-61. Epub 2012/04/05. doi: 10.1016/j.biomaterials.2012.03.023. PubMed PMID: 22472433; PMCID: PMC3586541.

141. Zarate J, Virdis L, Orive G, Igartua M, Hernandez RM, Pedraz JL. Design and characterization of calcium alginate microparticles coated with polycations as protein delivery system. J Microencapsul. 2011;28(7):614-20. Epub 2011/07/12. doi: 10.3109/02652048.2011.599439. PubMed PMID: 21740107.

142. Feng Y, Kopplin G, Sato K, Draget KI, Vårum KM. Alginate gels with a combination of calcium and chitosan oligomer mixtures as crosslinkers. Carbohydrate Polymers. 2017;156:490-7. doi: https://doi.org/10.1016/j.carbpol.2016.09.006.

143. Khong TT, Aarstad OA, Skjåk-Bræk G, Draget KI, Vårum KM. Gelling Concept Combining Chitosan and Alginate—Proof of Principle. Biomacromolecules. 2013;14(8):2765-71. doi: 10.1021/bm400610b.

144. Laroui H, Dalmasso G, Nguyen HT, Yan Y, Sitaraman SV, Merlin D. Drug-loaded nanoparticles targeted to the colon with polysaccharide hydrogel reduce colitis in a mouse model. Gastroenterology. 2010;138(3):843-53 e1-2. Epub 2009/11/17. doi: 10.1053/j.gastro.2009.11.003. PubMed PMID: 19909746.

145. Bhavsar MD, Amiji MM. Development of novel biodegradable polymeric nanoparticles-in-microsphere formulation for local plasmid DNA delivery in the gastrointestinal tract. AAPS PharmSciTech. 2008;9(1):288-94. Epub 2008/05/01. doi: 10.1208/s12249-007-9021-9. PubMed PMID: 18446494; PMCID: PMC2976886.

146. Hua S, Marks E, Schneider JJ, Keely S. Advances in oral nano-delivery systems for colon targeted drug delivery in inflammatory bowel disease: Selective targeting to diseased versus healthy tissue. Nanomedicine: Nanotechnology, Biology and Medicine. 2015;11(5):1117-32. doi: https://doi.org/10.1016/j.nano.2015.02.018.

147. Kumar A, Montemagno C, Choi H-J. Smart Microparticles with a pH-responsive Macropore for Targeted Oral Drug Delivery. Scientific Reports. 2017;7(1):3059. doi: 10.1038/s41598-017-03259-x.

148. Cruz-Acuna R, Quiros M, Farkas AE, Dedhia PH, Huang S, Siuda D, Garcia-Hernandez V, Miller AJ, Spence JR, Nusrat A, Garcia AJ. Synthetic hydrogels for human intestinal organoid generation and colonic wound repair. Nat Cell Biol. 2017;19(11):1326-35. Epub 2017/10/24. doi: 10.1038/ncb3632. PubMed PMID: 29058719; PMCID: PMC5664213.

149. Harris JM, Zalipsky S, American Chemical Society. Division of Polymer Chemistry., American Chemical Society. Meeting. Poly(ethylene glycol) : chemistry and biological applications. Washington, DC: American Chemical Society; 1997. xii, 489 p. p.

150. Harris JM. Poly(ethylene glycol) chemistry : biotechnical and biomedical applications. New York: Plenum Press; 1992. xxi, 385 p. p.

151. Zalipsky S. Functionalized poly(ethylene glycol) for preparation of biologically relevant conjugates. Bioconjug Chem. 1995;6(2):150-65. Epub 1995/03/01. doi: 10.1021/bc00032a002. PubMed PMID: 7599259.

152. Davis FF. The origin of pegnology. Adv Drug Deliv Rev. 2002;54(4):457-8. Epub 2002/06/08. doi: 10.1016/s0169-409x(02)00021-2. PubMed PMID: 12052708.

153. Sawhney AS, Pathak CP, Hubbell JA. Bioerodible hydrogels based on photopolymerized poly(ethylene glycol)-co-poly(.alpha.-hydroxy acid) diacrylate macromers. Macromolecules. 1993;26(4):581-7. doi: 10.1021/ma00056a005.

154. West JL, Hubbell JA. Polymeric Biomaterials with Degradation Sites for Proteases Involved in Cell Migration. Macromolecules. 1999;32(1):241-4. doi: 10.1021/ma981296k.

155. Patterson J, Hubbell JA. Enhanced proteolytic degradation of molecularly engineered PEG hydrogels in response to MMP-1 and MMP-2. Biomaterials. 2010;31(30):7836-45. doi: 10.1016/j.biomaterials.2010.06.061.

156. Elbert DL, Hubbell JA. Conjugate Addition Reactions Combined with Free-Radical Cross-Linking for the Design of Materials for Tissue Engineering. Biomacromolecules. 2001;2(2):430-41. doi: 10.1021/bm0056299.

157. Hermanson GT. Bioconjugate techniques. Third edition. ed. London ; Waltham, MA: Elsevier/AP; 2013. xvii, 1146 pages p.

158. Phelps EA, Enemchukwu NO, Fiore VF, Sy JC, Murthy N, Sulchek TA, Barker TH, Garcia AJ. Maleimide cross-linked bioactive PEG hydrogel exhibits improved reaction kinetics and cross-linking for cell encapsulation and in situ delivery. Adv Mater. 2012;24(1):64-70, 2. Epub 2011/12/17. doi: 10.1002/adma.201103574. PubMed PMID: 22174081; PMCID: PMC3517145.

159. Krishnaswamy S, Spitzer MH, Mingueneau M, Bendall SC, Litvin O, Stone E, Pe'er D, Nolan GP. Systems biology. Conditional density-based analysis of T cell signaling in single-cell data. Science. 2014;346(6213):1250689. Epub 2014/10/25. doi: 10.1126/science.1250689. PubMed PMID: 25342659; PMCID: PMC4334155.

160. Chattopadhyay PK, Price DA, Harper TF, Betts MR, Yu J, Gostick E, Perfetto SP, Goepfert P, Koup RA, De Rosa SC, Bruchez MP, Roederer M. Quantum dot semiconductor nanocrystals for immunophenotyping by polychromatic flow cytometry. Nat Med. 2006;12(8):972-7. Epub 2006/07/25. doi: 10.1038/nm1371. PubMed PMID: 16862156.

161. Lu Y, Xue Q, Eisele MR, Sulistijo ES, Brower K, Han L, Amir el AD, Pe'er D, Miller-Jensen K, Fan R. Highly multiplexed profiling of single-cell effector functions reveals deep functional heterogeneity in response to pathogenic ligands. Proc Natl Acad Sci U S A. 2015;112(7):E607-15. Epub 2015/02/04. doi: 10.1073/pnas.1416756112. PubMed PMID: 25646488; PMCID: PMC4343126.

162. Qiu P, Simonds EF, Bendall SC, Gibbs KD, Jr., Bruggner RV, Linderman MD, Sachs K, Nolan GP, Plevritis SK. Extracting a cellular hierarchy from high-dimensional cytometry data with SPADE. Nat Biotechnol. 2011;29(10):886-91. Epub 2011/10/04. doi: 10.1038/nbt.1991. PubMed PMID: 21964415; PMCID: PMC3196363.

163. Qiu P. Computational prediction of manually gated rare cells in flow cytometry data. Cytometry A. 2015;87(7):594-602. Epub 2015/03/11. doi: 10.1002/cyto.a.22654. PubMed PMID: 25755118; PMCID: PMC4483162.

164. Irish JM, Myklebust JH, Alizadeh AA, Houot R, Sharman JP, Czerwinski DK, Nolan GP, Levy R. B-cell signaling networks reveal a negative prognostic human lymphoma cell subset that emerges during tumor progression. Proc Natl Acad Sci U S A. 2010;107(29):12747-54. Epub 2010/06/15. doi: 10.1073/pnas.1002057107. PubMed PMID: 20543139; PMCID: PMC2919949.

165. Qiu P. Inferring phenotypic properties from single-cell characteristics. PLoS One. 2012;7(5):e37038. Epub 2012/06/05. doi: 10.1371/journal.pone.0037038. PubMed PMID: 22662133; PMCID: PMC3360688.

166. Herzenberg LA, Tung J, Moore WA, Herzenberg LA, Parks DR. Interpreting flow cytometry data: a guide for the perplexed. Nat Immunol. 2006;7(7):681-5. Epub 2006/06/21. doi: 10.1038/ni0706-681. PubMed PMID: 16785881.

167. Maecker HT, Rinfret A, D'Souza P, Darden J, Roig E, Landry C, Hayes P, Birungi J, Anzala O, Garcia M, Harari A, Frank I, Baydo R, Baker M, Holbrook J, Ottinger J, Lamoreaux L, Epling CL, Sinclair E, Suni MA, Punt K, Calarota S, El-Bahi S, Alter G, Maila H, Kuta E, Cox J, Gray C, Altfeld M, Nougarede N, Boyer J, Tussey L, Tobery T, Bredt B, Roederer M, Koup R, Maino VC, Weinhold K, Pantaleo G, Gilmour J, Horton H, Sekaly RP. Standardization of cytokine flow cytometry assays. BMC Immunol. 2005;6:13. Epub 2005/06/28. doi: 10.1186/1471-2172-6-13. PubMed PMID: 15978127; PMCID: PMC1184077.

168. Kay AW, Strauss-Albee DM, Blish CA. Application of Mass Cytometry (CyTOF) for Functional and Phenotypic Analysis of Natural Killer Cells. Methods Mol Biol. 2016;1441:13-26. Epub 2016/05/15. doi: 10.1007/978-1-4939-3684-7_2. PubMed PMID: 27177653; PMCID: PMC5304457.

169. Pyne S, Hu X, Wang K, Rossin E, Lin T-I, Maier LM, Baecher-Allan C, McLachlan GJ, Tamayo P, Hafler DA, De Jager PL, Mesirov JP. Automated high-dimensional flow cytometric data analysis. Proceedings of the National Academy of Sciences. 2009;106(21):8519-24. doi: 10.1073/pnas.0903028106.

170. Amir E-aD, Davis KL, Tadmor MD, Simonds EF, Levine JH, Bendall SC, Shenfeld DK, Krishnaswamy S, Nolan GP, Pe'er D. viSNE enables visualization of high dimensional single-cell data and reveals phenotypic heterogeneity of leukemia. Nature Biotechnology. 2013;31(6):545-52. doi: 10.1038/nbt.2594.

171. Qiu P. Toward deterministic and semiautomated SPADE analysis. Cytometry Part A. 2017;91(3):281-9. doi: 10.1002/cyto.a.23068.

172. Gossez M, Rimmelé T, Andrieu T, Debord S, Bayle F, Malcus C, Poitevin-Later F, Monneret G, Venet F. Proof of concept study of mass cytometry in septic shock patients reveals novel immune alterations. Scientific Reports. 2018;8(1):17296. doi: 10.1038/s41598-018-35932-0.

173. Samusik N, Good Z, Spitzer MH, Davis KL, Nolan GP. Automated mapping of phenotype space with single-cell data. Nat Methods. 2016;13(6):493-6. Epub 2016/05/18. doi: 10.1038/nmeth.3863. PubMed PMID: 27183440; PMCID: PMC4896314.

174. Fruchterman TMJ, Reingold EM. Graph drawing by force-directed placement. Software: Practice and Experience. 1991;21(11):1129-64. doi: 10.1002/spe.4380211102.

175. Larouche J, Sheoran S, Maruyama K, Martino MM. Immune Regulation of Skin Wound Healing: Mechanisms and Novel Therapeutic Targets. Adv Wound Care (New Rochelle). 2018;7(7):209-31. Epub 2018/07/10. doi: 10.1089/wound.2017.0761. PubMed PMID: 29984112; PMCID: PMC6032665.

176. Sorg H, Tilkorn DJ, Hager S, Hauser J, Mirastschijski U. Skin Wound Healing: An Update on the Current Knowledge and Concepts. European Surgical Research. 2017;58(1-2):81-94. doi: 10.1159/000454919.

177. Godwin JW, Pinto AR, Rosenthal NA. Chasing the recipe for a pro-regenerative immune system. Semin Cell Dev Biol. 2017;61:71-9. Epub 2016/08/16. doi: 10.1016/j.semcdb.2016.08.008. PubMed PMID: 27521522; PMCID: PMC5338634.

178. Eming SA, Martin P, Tomic-Canic M. Wound repair and regeneration: mechanisms, signaling, and translation. Sci Transl Med. 2014;6(265):265sr6. Epub 2014/12/05. doi: 10.1126/scitranslmed.3009337. PubMed PMID: 25473038; PMCID: PMC4973620.

179. Serhan CN, Petasis NA. Resolvins and protectins in inflammation resolution. Chem Rev. 2011;111(10):5922-43. Epub 2011/07/20. doi: 10.1021/cr100396c. PubMed PMID: 21766791; PMCID: PMC3192290.

180. Barron L, Wynn TA. Fibrosis is regulated by Th2 and Th17 responses and by dynamic interactions between fibroblasts and macrophages. Am J Physiol Gastrointest Liver Physiol. 2011;300(5):G723-8. Epub 2011/02/05. doi: 10.1152/ajpgi.00414.2010. PubMed PMID: 21292997; PMCID: PMC3302189.

181. Sok MCP, Tria MC, Olingy CE, San Emeterio CL, Botchwey EA. Aspirin-Triggered Resolvin D1-modified materials promote the accumulation of pro-regenerative immune cell subsets and enhance vascular remodeling. Acta Biomater. 2017;53:109-22. Epub 2017/02/19. doi: 10.1016/j.actbio.2017.02.020. PubMed PMID: 28213094; PMCID: PMC5512001.

182. Martinez FO, Sica A, Mantovani A, Locati M. Macrophage activation and polarization. Front Biosci. 2008;13:453-61. Epub 2007/11/06. PubMed PMID: 17981560.

183. Wang S, Liu R, Yu Q, Dong L, Bi Y, Liu G. Metabolic reprogramming of macrophages during infections and cancer. Cancer Lett. 2019;452:14-22. Epub 2019/03/25. doi: 10.1016/j.canlet.2019.03.015. PubMed PMID: 30905817.

184. Bohlson SS, O'Conner SD, Hulsebus HJ, Ho MM, Fraser DA. Complement, c1q, and c1q-related molecules regulate macrophage polarization. Front Immunol. 2014;5:402. Epub 2014/09/06. doi: 10.3389/fimmu.2014.00402. PubMed PMID: 25191325; PMCID: PMC4139736.

185. Leibovich SJ, Ross R. The role of the macrophage in wound repair. A study with hydrocortisone and antimacrophage serum. Am J Pathol. 1975;78(1):71-100. Epub 1975/01/01. PubMed PMID: 1109560; PMCID: PMC1915032.

186. Mackay IR. Science, medicine, and the future: Tolerance and autoimmunity. BMJ. 2000;321(7253):93-6. Epub 2000/07/07. doi: 10.1136/bmj.321.7253.93. PubMed PMID: 10884262; PMCID: PMC1127768.

187. Mbongue J, Nicholas D, Firek A, Langridge W. The role of dendritic cells in tissue-specific autoimmunity. J Immunol Res. 2014;2014:857143. Epub 2014/05/31. doi: 10.1155/2014/857143. PubMed PMID: 24877157; PMCID: PMC4022068.

188. van Eden W, Jansen MAA, de Wolf ACMT, Ludwig IS, Leufkens P, Broere F. The Immunomodulatory Potential of tolDCs Loaded with Heat Shock Proteins. Frontiers in Immunology. 2017;8:1690.

189. Iyer SS, Cheng G. Role of interleukin 10 transcriptional regulation in inflammation and autoimmune disease. Crit Rev Immunol. 2012;32(1):23-63. Epub 2012/03/21. PubMed PMID: 22428854; PMCID: PMC3410706.

190. King A, Balaji S, Le LD, Crombleholme TM, Keswani SG. Regenerative Wound Healing: The Role of Interleukin-10. Adv Wound Care (New Rochelle). 2014;3(4):315-23. Epub 2014/04/24. doi: 10.1089/wound.2013.0461. PubMed PMID: 24757588; PMCID: PMC3985521.

191. Kushwah R, Hu J. Role of dendritic cells in the induction of regulatory T cells. Cell Biosci. 2011;1(1):20. Epub 2011/06/30. doi: 10.1186/2045-3701-1-20. PubMed PMID: 21711933; PMCID: PMC3125210.

192. Maldonado RA, von Andrian UH. How tolerogenic dendritic cells induce regulatory T cells. Adv Immunol. 2010;108:111-65. Epub 2010/11/09. doi: 10.1016/B978-0-12-380995-7.00004-5. PubMed PMID: 21056730; PMCID: PMC3050492.

193. Ito T, Hanabuchi S, Wang YH, Park WR, Arima K, Bover L, Qin FX, Gilliet M, Liu YJ. Two functional subsets of FOXP3+ regulatory T cells in human thymus and

periphery. Immunity. 2008;28(6):870-80. Epub 2008/06/03. doi: 10.1016/j.immuni.2008.03.018. PubMed PMID: 18513999; PMCID: PMC2709453.

194. Atri C, Guerfali FZ, Laouini D. Role of Human Macrophage Polarization in Inflammation during Infectious Diseases. Int J Mol Sci. 2018;19(6). Epub 2018/06/21. doi: 10.3390/ijms19061801. PubMed PMID: 29921749; PMCID: PMC6032107.

195. van Amerongen MJ, Harmsen MC, van Rooijen N, Petersen AH, van Luyn MJ. Macrophage depletion impairs wound healing and increases left ventricular remodeling after myocardial injury in mice. Am J Pathol. 2007;170(3):818-29. doi: 10.2353/ajpath.2007.060547. PubMed PMID: 17322368; PMCID: PMC1864893.

196. Crane MJ, Daley JM, van Houtte O, Brancato SK, Henry WL, Jr., Albina JE. The monocyte to macrophage transition in the murine sterile wound. PLoS One. 2014;9(1):e86660. Epub 2014/01/28. doi: 10.1371/journal.pone.0086660. PubMed PMID: 24466192; PMCID: PMC3899284.

197. Varga T, Mounier R, Horvath A, Cuvellier S, Dumont F, Poliska S, Ardjoune H, Juban G, Nagy L, Chazaud B. Highly Dynamic Transcriptional Signature of Distinct Macrophage Subsets during Sterile Inflammation, Resolution, and Tissue Repair. The Journal of Immunology. 2016. doi: 10.4049/jimmunol.1502490.

198. Gordon S, Pluddemann A, Martinez Estrada F. Macrophage heterogeneity in tissues: phenotypic diversity and functions. Immunol Rev. 2014;262(1):36-55. Epub 2014/10/17. doi: 10.1111/imr.12223. PubMed PMID: 25319326; PMCID: PMC4231239.

199. Anzai A, Anzai T, Nagai S, Maekawa Y, Naito K, Kaneko H, Sugano Y, Takahashi T, Abe H, Mochizuki S, Sano M, Yoshikawa T, Okada Y, Koyasu S, Ogawa S, Fukuda K. Regulatory role of dendritic cells in postinfarction healing and left ventricular remodeling. Circulation. 2012;125(10):1234-45. Epub 2012/02/07. doi: 10.1161/CIRCULATIONAHA.111.052126. PubMed PMID: 22308302.

200. Domogalla MP, Rostan PV, Raker VK, Steinbrink K. Tolerance through Education: How Tolerogenic Dendritic Cells Shape Immunity. Front Immunol. 2017;8:1764. Epub 2018/01/30. doi: 10.3389/fimmu.2017.01764. PubMed PMID: 29375543; PMCID: PMC5770648.

201. Geissmann F, Manz MG, Jung S, Sieweke MH, Merad M, Ley K. Development of monocytes, macrophages, and dendritic cells. Science. 2010;327(5966):656-61. doi: 10.1126/science.1178331. PubMed PMID: 20133564; PMCID: PMC2887389.

202. Banchereau J, Briere F, Caux C, Davoust J, Lebecque S, Liu YJ, Pulendran B, Palucka K. Immunobiology of dendritic cells. Annu Rev Immunol. 2000;18:767-811. Epub 2000/06/03. doi: 10.1146/annurev.immunol.18.1.767. PubMed PMID: 10837075.

203. Zhang C, Li L, Feng K, Fan D, Xue W, Lu J. 'Repair' Treg Cells in Tissue Injury. Cell Physiol Biochem. 2017;43(6):2155-69. Epub 2017/10/27. doi: 10.1159/000484295. PubMed PMID: 29069643.

204. Auffray C, Fogg D, Garfa M, Elain G, Join-Lambert O, Kayal S, Sarnacki S, Cumano A, Lauvau G, Geissmann F. Monitoring of blood vessels and tissues by a population of monocytes with patrolling behavior. Science. 2007;317(5838):666-70. doi: 10.1126/science.1142883. PubMed PMID: 17673663.

205. Lammermann T, Bader BL, Monkley SJ, Worbs T, Wedlich-Soldner R, Hirsch K, Keller M, Forster R, Critchley DR, Fassler R, Sixt M. Rapid leukocyte migration by integrin-independent flowing and squeezing. Nature. 2008;453(7191):51-5. doi: 10.1038/nature06887. PubMed PMID: 18451854.

206. Churlaud G, Pitoiset F, Jebbawi F, Lorenzon R, Bellier B, Rosenzwajg M, Klatzmann D. Human and Mouse CD8(+)CD25(+)FOXP3(+) Regulatory T Cells at Steady State and during Interleukin-2 Therapy. Front Immunol. 2015;6:171. Epub 2015/05/01. doi: 10.3389/fimmu.2015.00171. PubMed PMID: 25926835; PMCID: PMC4397865.

207. Chaput N, Louafi S, Bardier A, Charlotte F, Vaillant JC, Menegaux F, Rosenzwajg M, Lemoine F, Klatzmann D, Taieb J. Identification of CD8+CD25+Foxp3+ suppressive T cells in colorectal cancer tissue. Gut. 2009;58(4):520-9. Epub 2008/11/22. doi: 10.1136/gut.2008.158824. PubMed PMID: 19022917.

208. Brimnes J, Allez M, Dotan I, Shao L, Nakazawa A, Mayer L. Defects in CD8+ regulatory T cells in the lamina propria of patients with inflammatory bowel disease. J Immunol. 2005;174(9):5814-22. Epub 2005/04/22. doi: 10.4049/jimmunol.174.9.5814. PubMed PMID: 15843585.

209. Scallan E, Hoekstra RM, Angulo FJ, Tauxe RV, Widdowson MA, Roy SL, Jones JL, Griffin PM. Foodborne illness acquired in the United States--major pathogens. Emerg Infect Dis. 2011;17(1):7-15. Epub 2011/01/05. doi: 10.3201/eid1701.P11101. PubMed PMID: 21192848; PMCID: PMC3375761.

210. Rescigno M, Rotta G, Valzasina B, Ricciardi-Castagnoli P. Dendritic cells shuttle microbes across gut epithelial monolayers. Immunobiology. 2001;204(5):572-81. Epub 2002/02/16. doi: 10.1078/0171-2985-00094. PubMed PMID: 11846220.

211. Rescigno M, Urbano M, Valzasina B, Francolini M, Rotta G, Bonasio R, Granucci F, Kraehenbuhl JP, Ricciardi-Castagnoli P. Dendritic cells express tight junction proteins and penetrate gut epithelial monolayers to sample bacteria. Nat Immunol. 2001;2(4):361-7. Epub 2001/03/29. doi: 10.1038/86373. PubMed PMID: 11276208.

212. Tam MA, Rydstrom A, Sundquist M, Wick MJ. Early cellular responses to Salmonella infection: dendritic cells, monocytes, and more. Immunol Rev. 2008;225:140-62. Epub 2008/10/08. doi: 10.1111/j.1600-065X.2008.00679.x. PubMed PMID: 18837781.

213. El Qaidi S, Scott NE, Hays MP, Geisbrecht BV, Watkins S, Hardwidge PR. An intra-bacterial activity for a T3SS effector. Sci Rep. 2020;10(1):1073. Epub 2020/01/25. doi: 10.1038/s41598-020-58062-y. PubMed PMID: 31974499; PMCID: PMC6978387.

214. Jones RM, Luo L, Moberg KH. Aeromonas salmonicida-secreted protein AopP is a potent inducer of apoptosis in a mammalian and a Drosophila model. Cell Microbiol. 2012;14(2):274-85. Epub 2011/11/02. doi: 10.1111/j.1462-5822.2011.01717.x. PubMed PMID: 22040305; PMCID: PMC3267377.

215. Hardt WD, Galan JE. A secreted Salmonella protein with homology to an avirulence determinant of plant pathogenic bacteria. Proc Natl Acad Sci U S A. 1997;94(18):9887-92. Epub 1997/09/02. doi: 10.1073/pnas.94.18.9887. PubMed PMID: 9275221; PMCID: PMC23287.

216. Orth K, Palmer LE, Bao ZQ, Stewart S, Rudolph AE, Bliska JB, Dixon JE. Inhibition of the mitogen-activated protein kinase kinase superfamily by a Yersinia effector. Science. 1999;285(5435):1920-3. Epub 1999/09/18. doi: 10.1126/science.285.5435.1920. PubMed PMID: 10489373.

217. Mukherjee S, Hao YH, Orth K. A newly discovered post-translational modification--the acetylation of serine and threonine residues. Trends Biochem Sci. 2007;32(5):210-6. Epub 2007/04/07. doi: 10.1016/j.tibs.2007.03.007. PubMed PMID: 17412595.

218. Wu H, Jones RM, Neish AS. The Salmonella effector AvrA mediates bacterial intracellular survival during infection in vivo. Cell Microbiol. 2012;14(1):28-39. Epub 2011/09/09. doi: 10.1111/j.1462-5822.2011.01694.x. PubMed PMID: 21899703; PMCID: PMC3240734.

219. Dahlhamer JM, Zammitti EP, Ward BW, Wheaton AG, Croft JB. Prevalence of Inflammatory Bowel Disease Among Adults Aged >/=18 Years - United States, 2015. MMWR Morb Mortal Wkly Rep. 2016;65(42):1166-9. Epub 2016/10/28. doi: 10.15585/mmwr.mm6542a3. PubMed PMID: 27787492.

220. Molodecky NA, Soon IS, Rabi DM, Ghali WA, Ferris M, Chernoff G, Benchimol EI, Panaccione R, Ghosh S, Barkema HW, Kaplan GG. Increasing incidence and prevalence of the inflammatory bowel diseases with time, based on systematic review. Gastroenterology. 2012;142(1):46-54 e42; quiz e30. Epub 2011/10/18. doi: 10.1053/j.gastro.2011.10.001. PubMed PMID: 22001864.

221. Neurath MF. Current and emerging therapeutic targets for IBD. Nat Rev Gastroenterol Hepatol. 2017;14(5):269-78. Epub 2017/02/02. doi: 10.1038/nrgastro.2016.208. PubMed PMID: 28144028.

222. Neish AS, Gewirtz AT, Zeng H, Young AN, Hobert ME, Karmali V, Rao AS, Madara JL. Prokaryotic regulation of epithelial responses by inhibition of IkappaB-alpha ubiquitination. Science. 2000;289(5484):1560-3. Epub 2000/09/01. doi: 10.1126/science.289.5484.1560. PubMed PMID: 10968793.

223. Shams T, Illangakoon UE, Parhizkar M, Harker AH, Edirisinghe S, Orlu M, Edirisinghe M. Electrosprayed microparticles for intestinal delivery of prednisolone. J R

Soc Interface. 2018;15(145). Epub 2018/08/31. doi: 10.1098/rsif.2018.0491. PubMed PMID: 30158187; PMCID: PMC6127171.

224. Meissner Y, Lamprecht A. Alternative drug delivery approaches for the therapy of inflammatory bowel disease. J Pharm Sci. 2008;97(8):2878-91. Epub 2007/10/24. doi: 10.1002/jps.21216. PubMed PMID: 17948914.

225. Salatin S, Jelvehgari M, Maleki-Dizaj S, Adibkia K. A sight on protein-based nanoparticles as drug/gene delivery systems. Ther Deliv. 2015;6(8):1017-29. Epub 2015/08/26. doi: 10.4155/tde.15.28. PubMed PMID: 26305428.

226. Ulbrich W, Lamprecht A. Targeted drug-delivery approaches by nanoparticulate carriers in the therapy of inflammatory diseases. J R Soc Interface. 2010;7 Suppl 1:S55-66. Epub 2009/11/27. doi: 10.1098/rsif.2009.0285.focus. PubMed PMID: 19940000; PMCID: PMC2843985.

227. Herrera Estrada L, Wu H, Ling K, Zhang G, Sumagin R, Parkos CA, Jones RM, Champion JA, Neish AS. Bioengineering Bacterially Derived Immunomodulants: A Therapeutic Approach to Inflammatory Bowel Disease. ACS Nano. 2017;11(10):9650-62. doi: 10.1021/acsnano.7b03239.

228. Yoshida T, Lai TC, Kwon GS, Sako K. pH- and ion-sensitive polymers for drug delivery. Expert Opin Drug Deliv. 2013;10(11):1497-513. Epub 2013/08/13. doi: 10.1517/17425247.2013.821978. PubMed PMID: 23930949; PMCID: PMC3912992.

229. Cook MT, Tzortzis G, Charalampopoulos D, Khutoryanskiy VV. Production and Evaluation of Dry Alginate-Chitosan Microcapsules as an Enteric Delivery Vehicle for Probiotic Bacteria. Biomacromolecules. 2011;12(7):2834-40. doi: 10.1021/bm200576h.

230. Chavarri M, Maranon I, Ares R, Ibanez FC, Marzo F, Villaran Mdel C. Microencapsulation of a probiotic and prebiotic in alginate-chitosan capsules improves survival in simulated gastro-intestinal conditions. Int J Food Microbiol. 2010;142(1-2):185-9. Epub 2010/07/28. doi: 10.1016/j.ijfoodmicro.2010.06.022. PubMed PMID: 20659775.

231. Goh CH, Heng PWS, Chan LW. Alginates as a useful natural polymer for microencapsulation and therapeutic applications. Carbohydrate Polymers. 2012;88(1):1-12. doi: https://doi.org/10.1016/j.carbpol.2011.11.012.

232. Murua A, Portero A, Orive G, Hernandez RM, de Castro M, Pedraz JL. Cell microencapsulation technology: towards clinical application. J Control Release. 2008;132(2):76-83. Epub 2008/09/16. doi: 10.1016/j.jconrel.2008.08.010. PubMed PMID: 18789985.

233. George M, Abraham TE. Polyionic hydrocolloids for the intestinal delivery of protein drugs: alginate and chitosan--a review. J Control Release. 2006;114(1):1-14. Epub 2006/07/11. doi: 10.1016/j.jconrel.2006.04.017. PubMed PMID: 16828914.

234. Lee KY, Mooney DJ. Alginate: properties and biomedical applications. Prog Polym Sci. 2012;37(1):106-26. Epub 2011/11/30. doi: 10.1016/j.progpolymsci.2011.06.003. PubMed PMID: 22125349; PMCID: PMC3223967.

235. El Maghraby GM, Arafa MF. Chapter 15 - Alginate-chitosan combinations in controlled drug delivery. In: Hasnain MS, Nayak AK, editors. Natural Polysaccharides in Drug Delivery and Biomedical Applications: Academic Press; 2019. p. 339-61.

236. Monack DM, Hersh D, Ghori N, Bouley D, Zychlinsky A, Falkow S. Salmonella exploits caspase-1 to colonize Peyer's patches in a murine typhoid model. J Exp Med. 2000;192(2):249-58. Epub 2000/07/19. doi: 10.1084/jem.192.2.249. PubMed PMID: 10899911; PMCID: PMC2193260.

237. Weber C, Coester C, Kreuter J, Langer K. Desolvation process and surface characterisation of protein nanoparticles. Int J Pharm. 2000;194(1):91-102. Epub 1999/12/22. doi: 10.1016/s0378-5173(99)00370-1. PubMed PMID: 10601688.

238. McCormick BA, Colgan SP, Delp-Archer C, Miller SI, Madara JL. Salmonella typhimurium attachment to human intestinal epithelial monolayers: transcellular signalling to subepithelial neutrophils. J Cell Biol. 1993;123(4):895-907. Epub 1993/11/01. doi: 10.1083/jcb.123.4.895. PubMed PMID: 8227148; PMCID: PMC2200157.

239. Madara JL, Patapoff TW, Gillece-Castro B, Colgan SP, Parkos CA, Delp C, Mrsny RJ. 5'-adenosine monophosphate is the neutrophil-derived paracrine factor that elicits chloride secretion from T84 intestinal epithelial cell monolayers. J Clin Invest. 1993;91(5):2320-5. Epub 1993/05/01. doi: 10.1172/JCI116462. PubMed PMID: 8486793; PMCID: PMC288238.

240. Parkos CA. Neutrophil-Epithelial Interactions: A Double-Edged Sword. Am J Pathol. 2016;186(6):1404-16. Epub 2016/04/17. doi: 10.1016/j.ajpath.2016.02.001. PubMed PMID: 27083514; PMCID: PMC4901132.

241. Andreasen AS, Krabbe KS, Krogh-Madsen R, Taudorf S, Pedersen BK, Moller K. Human endotoxemia as a model of systemic inflammation. Curr Med Chem. 2008;15(17):1697-705. Epub 2008/08/05. doi: 10.2174/092986708784872393. PubMed PMID: 18673219.

242. Hurley JC. Endotoxemia: methods of detection and clinical correlates. Clin Microbiol Rev. 1995;8(2):268-92. Epub 1995/04/01. PubMed PMID: 7621402; PMCID: PMC172859.

243. Haagsma JA, Havelaar AH, Janssen BM, Bonsel GJ. Disability adjusted life years and minimal disease: application of a preference-based relevance criterion to rank enteric pathogens. Popul Health Metr. 2008;6:7. Epub 2008/12/31. doi: 10.1186/1478-7954-6-7. PubMed PMID: 19114007; PMCID: PMC2655281.

244. Lefrançois L, Lycke N. Isolation of Mouse Small Intestinal Intraepithelial Lymphocytes, Peyer's Patch, and Lamina Propria Cells. Current Protocols in Immunology. 1996;17(1):3.19.1-3..6. doi: 10.1002/0471142735.im0319s17.

245. Mayassi T, Jabri B. Human intraepithelial lymphocytes. Mucosal Immunol. 2018;11(5):1281-9. Epub 2018/04/21. doi: 10.1038/s41385-018-0016-5. PubMed PMID: 29674648; PMCID: PMC6178824.

246. Beagley KW, Fujihashi K, Lagoo AS, Lagoo-Deenadaylan S, Black CA, Murray AM, Sharmanov AT, Yamamoto M, McGhee JR, Elson CO, et al. Differences in intraepithelial lymphocyte T cell subsets isolated from murine small versus large intestine. J Immunol. 1995;154(11):5611-9. Epub 1995/06/01. PubMed PMID: 7751614.

247. Neutra MR, Mantis NJ, Kraehenbuhl JP. Collaboration of epithelial cells with organized mucosal lymphoid tissues. Nat Immunol. 2001;2(11):1004-9. Epub 2001/10/31. doi: 10.1038/ni1101-1004. PubMed PMID: 11685223.

248. Barreau F, Meinzer U, Chareyre F, Berrebi D, Niwa-Kawakita M, Dussaillant M, Foligne B, Ollendorff V, Heyman M, Bonacorsi S, Lesuffleur T, Sterkers G, Giovannini M, Hugot JP. CARD15/NOD2 is required for Peyer's patches homeostasis in mice. PLoS One. 2007;2(6):e523. Epub 2007/06/15. doi: 10.1371/journal.pone.0000523. PubMed PMID: 17565376; PMCID: PMC1885825.

249. Iwasaki A, Kelsall BL. Localization of distinct Peyer's patch dendritic cell subsets and their recruitment by chemokines macrophage inflammatory protein (MIP)-3alpha, MIP-3beta, and secondary lymphoid organ chemokine. J Exp Med. 2000;191(8):1381-94. Epub 2000/04/19. doi: 10.1084/jem.191.8.1381. PubMed PMID: 10770804; PMCID: PMC2193144.

250. Willer Y, Müller B, Bumann D. Intestinal Inflammation Responds to Microbial Tissue Load Independent of Pathogen/Non-Pathogen Discrimination. PLOS ONE. 2012;7(5):e35992. doi: 10.1371/journal.pone.0035992.

251. Clark MA, Blair H, Liang L, Brey RN, Brayden D, Hirst BH. Targeting polymerised liposome vaccine carriers to intestinal M cells. Vaccine. 2001;20(1-2):208-17. Epub 2001/09/25. doi: 10.1016/s0264-410x(01)00258-4. PubMed PMID: 11567766.

252. Gebert A, Rothkotter HJ, Pabst R. M cells in Peyer's patches of the intestine. Int Rev Cytol. 1996;167:91-159. Epub 1996/01/01. doi: 10.1016/s0074-7696(08)61346-7. PubMed PMID: 8768493.

253. Bachhav SS, Dighe VD, Devarajan PV. Exploring Peyer's Patch Uptake as a Strategy for Targeted Lung Delivery of Polymeric Rifampicin Nanoparticles. Mol Pharm. 2018;15(10):4434-45. Epub 2018/08/15. doi: 10.1021/acs.molpharmaceut.8b00382. PubMed PMID: 30106591.

254. Leppkes M, Roulis M, Neurath MF, Kollias G, Becker C. Pleiotropic functions of TNF-α in the regulation of the intestinal epithelial response to inflammation. International Immunology. 2014;26(9):509-15. doi: 10.1093/intimm/dxu051.

255. Hanninen A, Maksimow M, Alam C, Morgan DJ, Jalkanen S. Ly6C supports preferential homing of central memory CD8+ T cells into lymph nodes. Eur J Immunol. 2011;41(3):634-44. Epub 2011/02/11. doi: 10.1002/eji.201040760. PubMed PMID: 21308682.

256. Kusaka Y, Kajiwara C, Shimada S, Ishii Y, Miyazaki Y, Inase N, Standiford TJ, Tateda K. Potential Role of Gr-1+ CD8+ T Lymphocytes as a Source of Interferon-gamma and M1/M2 Polarization during the Acute Phase of Murine Legionella pneumophila Pneumonia. J Innate Immun. 2018;10(4):328-38. Epub 2018/07/19. doi: 10.1159/000490585. PubMed PMID: 30021216; PMCID: PMC6757147.

257. Au - Radulovic K, Au - Mak'Anyengo R, Au - Kaya B, Au - Steinert A, Au - Niess JH. Injections of Lipopolysaccharide into Mice to Mimic Entrance of Microbial-derived Products After Intestinal Barrier Breach. JoVE. 2018(135):e57610. doi: doi:10.3791/57610.

258. Elzoghby AO, Samy WM, Elgindy NA. Protein-based nanocarriers as promising drug and gene delivery systems. J Control Release. 2012;161(1):38-49. Epub 2012/05/09. doi: 10.1016/j.jconrel.2012.04.036. PubMed PMID: 22564368.

259. Couter CJ, Surana NK. Isolation and Flow Cytometric Characterization of Murine Small Intestinal Lymphocytes. J Vis Exp. 2016(111). Epub 2016/05/24. doi: 10.3791/54114. PubMed PMID: 27213538; PMCID: PMC4942069.

260. Tada T. The immune system as a supersystem. Annu Rev Immunol. 1997;15:1-13. Epub 1997/01/01. doi: 10.1146/annurev.immunol.15.1.1. PubMed PMID: 9143679.

261. Vivier E, Malissen B. Innate and adaptive immunity: specificities and signaling hierarchies revisited. Nature Immunology. 2005;6(1):17-21. doi: 10.1038/ni1153.

262. Nakayama T, Hirahara K, Onodera A, Endo Y, Hosokawa H, Shinoda K, Tumes DJ, Okamoto Y. Th2 Cells in Health and Disease. Annu Rev Immunol. 2017;35:53-84. Epub 2016/12/04. doi: 10.1146/annurev-immunol-051116-052350. PubMed PMID: 27912316.

263. Mosmann TR, Sad S. The expanding universe of T-cell subsets: Th1, Th2 and more. Immunol Today. 1996;17(3):138-46. Epub 1996/03/01. PubMed PMID: 8820272.

264. Tindemans I, Serafini N, Di Santo JP, Hendriks RW. GATA-3 function in innate and adaptive immunity. Immunity. 2014;41(2):191-206. Epub 2014/08/26. doi: 10.1016/j.immuni.2014.06.006. PubMed PMID: 25148023.

265. Zhu J, Min B, Hu-Li J, Watson CJ, Grinberg A, Wang Q, Killeen N, Urban JF, Jr., Guo L, Paul WE. Conditional deletion of Gata3 shows its essential function in T(H)1-

T(H)2 responses. Nat Immunol. 2004;5(11):1157-65. Epub 2004/10/12. doi: 10.1038/ni1128. PubMed PMID: 15475959.

266. Yamashita M, Ukai-Tadenuma M, Kimura M, Omori M, Inami M, Taniguchi M, Nakayama T. Identification of a conserved GATA3 response element upstream proximal from the interleukin-13 gene locus. J Biol Chem. 2002;277(44):42399-408. Epub 2002/09/03. doi: 10.1074/jbc.M205876200. PubMed PMID: 12205084.

267. Popp V, Gerlach K, Mott S, Turowska A, Garn H, Atreya R, Lehr HA, Ho IC, Renz H, Weigmann B, Neurath MF. Rectal Delivery of a DNAzyme That Specifically Blocks the Transcription Factor GATA3 and Reduces Colitis in Mice. Gastroenterology. 2017;152(1):176-92 e5. Epub 2016/09/19. doi: 10.1053/j.gastro.2016.09.005. PubMed PMID: 27639807.

268. Wenzel SE. Asthma phenotypes: the evolution from clinical to molecular approaches. Nat Med. 2012;18(5):716-25. doi: 10.1038/nm.2678. PubMed PMID: 22561835.

269. Bateman ED, Hurd SS, Barnes PJ, Bousquet J, Drazen JM, FitzGerald M, Gibson P, Ohta K, O'Byrne P, Pedersen SE, Pizzichini E, Sullivan SD, Wenzel SE, Zar HJ. Global strategy for asthma management and prevention: GINA executive summary. Eur Respir J. 2008;31(1):143-78. doi: 10.1183/09031936.00138707. PubMed PMID: 18166595.

270. Egbuonu F, Antonio FA, Edavalath M. Effect of inhaled corticosteroids on glycemic status. Open Respir Med J. 2014;8:101-5. doi: 10.2174/1874306401408010101. PubMed PMID: 25674180; PMCID: PMC4319206.

271. Woodruff PG, Modrek B, Choy DF, Jia G, Abbas AR, Ellwanger A, Koth LL, Arron JR, Fahy JV. T-helper type 2-driven inflammation defines major subphenotypes of asthma. Am J Respir Crit Care Med. 2009;180(5):388-95. doi: 10.1164/rccm.200903-0392OC. PubMed PMID: 19483109; PMCID: PMC2742757.

272. Winandy S, Brown M. No DL1 Notch ligand? GATA be a mast cell. Nat Immunol. 2007;8(8):796-8. doi: 10.1038/ni0807-796. PubMed PMID: 17641659.

273. Sadat MA, Kumatori A, Suzuki S, Yamaguchi Y, Tsuji Y, Nakamura M. GATA-3 represses gp91phox gene expression in eosinophil-committed HL-60-C15 cells. FEBS Lett. 1998;436(3):390-4. PubMed PMID: 9801155.

274. Gauvreau GM, Boulet LP, Postma DS, Kawayama T, Watson RM, Duong M, Deschesnes F, De Monchy JG, O'Byrne PM. Effect of low-dose ciclesonide on allergen-induced responses in subjects with mild allergic asthma. J Allergy Clin Immunol. 2005;116(2):285-91. doi: 10.1016/j.jaci.2005.05.021. PubMed PMID: 16083781.

275. Holgate ST. Trials and tribulations in identifying new biologic treatments for asthma. Trends Immunol. 2012;33(5):238-46. doi: 10.1016/j.it.2012.02.003. PubMed PMID: 22436378.

276. Zhang DH, Yang L, Cohn L, Parkyn L, Homer R, Ray P, Ray A. Inhibition of allergic inflammation in a murine model of asthma by expression of a dominant-negative mutant of GATA-3. Immunity. 1999;11(4):473-82. PubMed PMID: 10549629.

277. Krug N, Hohlfeld JM, Kirsten AM, Kornmann O, Beeh KM, Kappeler D, Korn S, Ignatenko S, Timmer W, Rogon C, Zeitvogel J, Zhang N, Bille J, Homburg U, Turowska A, Bachert C, Werfel T, Buhl R, Renz J, Garn H, Renz H. Allergen-induced asthmatic responses modified by a GATA3-specific DNAzyme. N Engl J Med. 2015;372(21):1987-95. doi: 10.1056/NEJMoa1411776. PubMed PMID: 25981191.

278. Homburg U, Renz H, Timmer W, Hohlfeld JM, Seitz F, Luer K, Mayer A, Wacker A, Schmidt O, Kuhlmann J, Turowska A, Roller J, Kutz K, Schluter G, Krug N, Garn H. Safety and tolerability of a novel inhaled GATA3 mRNA targeting DNAzyme in patients with TH2-driven asthma. J Allergy Clin Immunol. 2015;136(3):797-800. doi: 10.1016/j.jaci.2015.02.018. PubMed PMID: 25842286.

279. Danese S, Fiocchi C. Ulcerative colitis. N Engl J Med. 2011;365(18):1713-25. Epub 2011/11/04. doi: 10.1056/NEJMra1102942. PubMed PMID: 22047562.

280. Baumgart DC, Sandborn WJ. Crohn's disease. Lancet. 2012;380(9853):1590-605. Epub 2012/08/24. doi: 10.1016/S0140-6736(12)60026-9. PubMed PMID: 22914295.

281. Osterman MT, Lichtenstein GR. Infliximab vs Adalimumab for UC: Is There A Difference? Clinical Gastroenterology and Hepatology. 2017;15(8):1197-9. doi: 10.1016/j.cgh.2017.04.036.

282. Nguyen VQ, Ulrik CS. Measures to reduce maintenance therapy with oral corticosteroid in adults with severe asthma. Allergy Asthma Proc. 2016;37(6):125-39. PubMed PMID: 27931289.

283. Kim HL, Leigh R, Becker A. Omalizumab: Practical considerations regarding the risk of anaphylaxis. Allergy Asthma Clin Immunol. 2010;6(1):32. doi: 10.1186/1710-1492-6-32. PubMed PMID: 21129189; PMCID: PMC3006370.

284. Crooke ST, Geary RS. Clinical pharmacological properties of mipomersen (Kynamro), a second generation antisense inhibitor of apolipoprotein B. Br J Clin Pharmacol. 2013;76(2):269-76. Epub 2012/09/28. doi: 10.1111/j.1365-2125.2012.04469.x. PubMed PMID: 23013161; PMCID: PMC3731601.

285. Guvakova MA, Yakubov LA, Vlodavsky I, Tonkinson JL, Stein CA. Phosphorothioate oligodeoxynucleotides bind to basic fibroblast growth factor, inhibit its binding to cell surface receptors, and remove it from low affinity binding sites on extracellular matrix. J Biol Chem. 1995;270(6):2620-7. PubMed PMID: 7852327.

286. Popescu FD, Popescu F. A review of antisense therapeutic interventions for molecular biological targets in asthma. Biologics. 2007;1(3):271-83. PubMed PMID: 19707336; PMCID: PMC2721314.

287. Mehta M, Deeksha, Tewari D, Gupta G, Awasthi R, Singh H, Pandey P, Chellappan DK, Wadhwa R, Collet T, Hansbro PM, Kumar SR, Thangavelu L, Negi P, Dua K, Satija S. Oligonucleotide therapy: An emerging focus area for drug delivery in chronic inflammatory respiratory diseases. Chemico-Biological Interactions. 2019;308:206-15. doi: https://doi.org/10.1016/j.cbi.2019.05.028.

288. Pratt AJ, MacRae IJ. The RNA-induced silencing complex: a versatile gene-silencing machine. J Biol Chem. 2009;284(27):17897-901. Epub 2009/04/04. doi: 10.1074/jbc.R900012200. PubMed PMID: 19342379; PMCID: PMC2709356.

289. Grimm D, Streetz KL, Jopling CL, Storm TA, Pandey K, Davis CR, Marion P, Salazar F, Kay MA. Fatality in mice due to oversaturation of cellular microRNA/short hairpin RNA pathways. Nature. 2006;441(7092):537-41. doi: 10.1038/nature04791. PubMed PMID: 16724069.

290. Santoro SW, Joyce GF. A general purpose RNA-cleaving DNA enzyme. Proc Natl Acad Sci U S A. 1997;94(9):4262-6. Epub 1997/04/29. doi: 10.1073/pnas.94.9.4262. PubMed PMID: 9113977; PMCID: PMC20710.

291. Liu H, Yu X, Chen Y, Zhang J, Wu B, Zheng L, Haruehanroengra P, Wang R, Li S, Lin J, Li J, Sheng J, Huang Z, Ma J, Gan J. Crystal structure of an RNA-cleaving DNAzyme. Nat Commun. 2017;8(1):2006. Epub 2017/12/10. doi: 10.1038/s41467-017-02203-x. PubMed PMID: 29222499; PMCID: PMC5722873.

292. Sel S, Wegmann M, Dicke T, Sel S, Henke W, Yildirim AO, Renz H, Garn H. Effective prevention and therapy of experimental allergic asthma using a GATA-3-specific DNAzyme. J Allergy Clin Immunol. 2008;121(4):910-6 e5. doi: 10.1016/j.jaci.2007.12.1175. PubMed PMID: 18325571.

293. Zon LI, Yamaguchi Y, Yee K, Albee EA, Kimura A, Bennett JC, Orkin SH, Ackerman SJ. Expression of mRNA for the GATA-binding proteins in human eosinophils and basophils: potential role in gene transcription. Blood. 1993;81(12):3234-41. Epub 1993/06/15. PubMed PMID: 8507862.

294. Alexopoulou L, Holt AC, Medzhitov R, Flavell RA. Recognition of double-stranded RNA and activation of NF-kappaB by Toll-like receptor 3. Nature. 2001;413(6857):732-8. Epub 2001/10/19. doi: 10.1038/35099560. PubMed PMID: 11607032.

295. Hemmi H, Takeuchi O, Kawai T, Kaisho T, Sato S, Sanjo H, Matsumoto M, Hoshino K, Wagner H, Takeda K, Akira S. A Toll-like receptor recognizes bacterial DNA. Nature. 2000;408(6813):740-5. Epub 2000/12/29. doi: 10.1038/35047123. PubMed PMID: 11130078.

296. Fuhst R, Runge F, Buschmann J, Ernst H, Praechter C, Hansen T, von Erichsen J, Turowska A, Hoymann HG, Muller M, Pohlmann G, Sewald K, Ziemann C, Schluter G, Garn H. Toxicity profile of the GATA-3-specific DNAzyme hgd40 after inhalation

exposure. Pulm Pharmacol Ther. 2013;26(2):281-9. doi: 10.1016/j.pupt.2012.12.005. PubMed PMID: 23266273.

297. Narayan SP, Choi CH, Hao L, Calabrese CM, Auyeung E, Zhang C, Goor OJ, Mirkin CA. The Sequence-Specific Cellular Uptake of Spherical Nucleic Acid Nanoparticle Conjugates. Small. 2015;11(33):4173-82. Epub 2015/06/23. doi: 10.1002/smll.201500027. PubMed PMID: 26097111; PMCID: PMC4560454.

298. Zhu XD, Zhuang Y, Ben JJ, Qian LL, Huang HP, Bai H, Sha JH, He ZG, Chen Q. Caveolae-dependent endocytosis is required for class A macrophage scavenger receptor-mediated apoptosis in macrophages. J Biol Chem. 2011;286(10):8231-9. Epub 2011/01/06. doi: 10.1074/jbc.M110.145888. PubMed PMID: 21205827; PMCID: PMC3048709.

299. Yehl K, Joshi JP, Greene BL, Dyer RB, Nahta R, Salaita K. Catalytic deoxyribozyme-modified nanoparticles for RNAi-independent gene regulation. ACS Nano. 2012;6(10):9150-7. doi: 10.1021/nn3034265. PubMed PMID: 22966955; PMCID: PMC3482470.

300. Somasuntharam I, Yehl K, Carroll SL, Maxwell JT, Martinez MD, Che PL, Brown ME, Salaita K, Davis ME. Knockdown of TNF-alpha by DNAzyme gold nanoparticles as an anti-inflammatory therapy for myocardial infarction. Biomaterials. 2016;83:12-22. Epub 2016/01/17. doi: 10.1016/j.biomaterials.2015.12.022. PubMed PMID: 26773660; PMCID: PMC5564214.

301. Rai M, Ingle AP, Birla S, Yadav A, Santos CA. Strategic role of selected noble metal nanoparticles in medicine. Crit Rev Microbiol. 2016;42(5):696-719. doi: 10.3109/1040841X.2015.1018131. PubMed PMID: 26089024.

302. James LR, Xu ZQ, Sluyter R, Hawksworth EL, Kelso C, Lai B, Paterson DJ, de Jonge MD, Dixon NE, Beck JL, Ralph SF, Dillon CT. An investigation into the interactions of gold nanoparticles and anti-arthritic drugs with macrophages, and their reactivity towards thioredoxin reductase. J Inorg Biochem. 2015;142:28-38. doi: 10.1016/j.jinorgbio.2014.09.013. PubMed PMID: 25306263.

303. Rambanapasi C, Zeevaart JR, Buntting H, Bester C, Kotze D, Hayeshi R, Grobler A. Bioaccumulation and Subchronic Toxicity of 14 nm Gold Nanoparticles in Rats. Molecules. 2016;21(6). doi: 10.3390/molecules21060763. PubMed PMID: 27294904.

304. Zolnik BS, Gonzalez-Fernandez A, Sadrieh N, Dobrovolskaia MA. Nanoparticles and the immune system. Endocrinology. 2010;151(2):458-65. doi: 10.1210/en.2009-1082. PubMed PMID: 20016026; PMCID: PMC2817614.

305. Santoro SW, Joyce GF. Mechanism and utility of an RNA-cleaving DNA enzyme. Biochemistry. 1998;37(38):13330-42. Epub 1998/09/28. doi: 10.1021/bi9812221. PubMed PMID: 9748341.

306. Sun LQ, Cairns MJ, Gerlach WL, Witherington C, Wang L, King A. Suppression of smooth muscle cell proliferation by a c-myc RNA-cleaving deoxyribozyme. J Biol Chem. 1999;274(24):17236-41. Epub 1999/06/08. PubMed PMID: 10358082.

307. Hill HD, Mirkin CA. The bio-barcode assay for the detection of protein and nucleic acid targets using DTT-induced ligand exchange. Nat Protoc. 2006;1(1):324-36. doi: 10.1038/nprot.2006.51. PubMed PMID: 17406253.

308. Martin TR, Frevert CW. Innate immunity in the lungs. Proc Am Thorac Soc. 2005;2(5):403-11. Epub 2005/12/03. doi: 10.1513/pats.200508-090JS. PubMed PMID: 16322590; PMCID: PMC2713330.

309. Bosnjak B, Stelzmueller B, Erb KJ, Epstein MM. Treatment of allergic asthma: modulation of Th2 cells and their responses. Respir Res. 2011;12:114. Epub 2011/08/27. doi: 10.1186/1465-9921-12-114. PubMed PMID: 21867534; PMCID: PMC3179723.

310. De Vooght V, Vanoirbeek JA, Haenen S, Verbeken E, Nemery B, Hoet PH. Oropharyngeal aspiration: an alternative route for challenging in a mouse model of chemical-induced asthma. Toxicology. 2009;259(1-2):84-9. Epub 2009/05/12. doi: 10.1016/j.tox.2009.02.007. PubMed PMID: 19428947.

311. Lakatos HF, Burgess HA, Thatcher TH, Redonnet MR, Hernady E, Williams JP, Sime PJ. Oropharyngeal aspiration of a silica suspension produces a superior model of silicosis in the mouse when compared to intratracheal instillation. Exp Lung Res. 2006;32(5):181-99. Epub 2006/08/16. doi: 10.1080/01902140600817465. PubMed PMID: 16908446.

312. Foster WM, Walters DM, Longphre M, Macri K, Miller LM. Methodology for the measurement of mucociliary function in the mouse by scintigraphy. J Appl Physiol (1985). 2001;90(3):1111-7. Epub 2001/02/22. doi: 10.1152/jappl.2001.90.3.1111. PubMed PMID: 11181627.

313. Oberdörster G, Stone V, Donaldson K. Toxicology of nanoparticles: A historical perspective. Nanotoxicology. 2007;1(1):2-25. doi: 10.1080/17435390701314761.

314. Heyder J. Deposition of Inhaled Particles in the Human Respiratory Tract and Consequences for Regional Targeting in Respiratory Drug Delivery. Proceedings of the American Thoracic Society. 2004;1(4):315-20. doi: 10.1513/pats.200409-046ta. PubMed PMID: pub.1011446450.

315. Azarmi S, Roa WH, Lobenberg R. Targeted delivery of nanoparticles for the treatment of lung diseases. Adv Drug Deliv Rev. 2008;60(8):863-75. Epub 2008/03/01. doi: 10.1016/j.addr.2007.11.006. PubMed PMID: 18308418.

316. Laroui H, Sitaraman SV, Merlin D. A method to target bioactive compounds to specific regions of the gastrointestinal tract: double gavage using polysaccharide hydrogels2009.

317. Sibille Y, Reynolds HY. Macrophages and polymorphonuclear neutrophils in lung defense and injury. Am Rev Respir Dis. 1990;141(2):471-501. Epub 1990/02/01. doi: 10.1164/ajrccm/141.2.471. PubMed PMID: 2405761.

318. Jorgensen LG, Fredholm L, Hyltoft Petersen P, Hey H, Munkholm P, Brandslund I. How accurate are clinical activity indices for scoring of disease activity in inflammatory bowel disease (IBD)? Clin Chem Lab Med. 2005;43(4):403-11. Epub 2005/05/19. doi: 10.1515/CCLM.2005.073. PubMed PMID: 15899657.

319. Kim HY, DeKruyff RH, Umetsu DT. The many paths to asthma: phenotype shaped by innate and adaptive immunity. Nat Immunol. 2010;11(7):577-84. Epub 2010/06/22. doi: 10.1038/ni.1892. PubMed PMID: 20562844; PMCID: PMC3114595.

320. Cates EC, Fattouh R, Wattie J, Inman MD, Goncharova S, Coyle AJ, Gutierrez-Ramos JC, Jordana M. Intranasal exposure of mice to house dust mite elicits allergic airway inflammation via a GM-CSF-mediated mechanism. J Immunol. 2004;173(10):6384-92. Epub 2004/11/06. PubMed PMID: 15528378.

321. Gregory LG, Lloyd CM. Orchestrating house dust mite-associated allergy in the lung. Trends Immunol. 2011;32(9):402-11. Epub 2011/07/26. doi: 10.1016/j.it.2011.06.006. PubMed PMID: 21783420; PMCID: PMC3381841.

322. Piyadasa H, Altieri A, Basu S, Schwartz J, Halayko AJ, Mookherjee N. Biosignature for airway inflammation in a house dust mite-challenged murine model of allergic asthma. Biol Open. 2016;5(2):112-21. Epub 2016/01/08. doi: 10.1242/bio.014464. PubMed PMID: 26740570; PMCID: PMC4823983.

323. Strober W, Fuss IJ. Proinflammatory cytokines in the pathogenesis of inflammatory bowel diseases. Gastroenterology. 2011;140(6):1756-67. Epub 2011/05/03. doi: 10.1053/j.gastro.2011.02.016. PubMed PMID: 21530742; PMCID: PMC3773507.

324. Breese E, Braegger CP, Corrigan CJ, Walker-Smith JA, MacDonald TT. Interleukin-2- and interferon-gamma-secreting T cells in normal and diseased human intestinal mucosa. Immunology. 1993;78(1):127-31. Epub 1993/01/01. PubMed PMID: 8436398; PMCID: PMC1421783.

325. Fuss IJ, Heller F, Boirivant M, Leon F, Yoshida M, Fichtner-Feigl S, Yang Z, Exley M, Kitani A, Blumberg RS, Mannon P, Strober W. Nonclassical CD1d-restricted NK T cells that produce IL-13 characterize an atypical Th2 response in ulcerative colitis. J Clin Invest. 2004;113(10):1490-7. Epub 2004/05/18. doi: 10.1172/JCI19836. PubMed PMID: 15146247; PMCID: PMC406524.

326. Sanchez-Munoz F, Dominguez-Lopez A, Yamamoto-Furusho JK. Role of cytokines in inflammatory bowel disease. World J Gastroenterol. 2008;14(27):4280-8. Epub 2008/07/31. PubMed PMID: 18666314; PMCID: PMC2731177.

327. Hohenberger M, Cardwell LA, Oussedik E, Feldman SR. Interleukin-17 inhibition: role in psoriasis and inflammatory bowel disease. Journal of Dermatological Treatment. 2018;29(1):13-8. doi: 10.1080/09546634.2017.1329511.

328. Scheinman EJ, Avni O. Transcriptional regulation of GATA3 in T helper cells by the integrated activities of transcription factors downstream of the interleukin-4 receptor and T cell receptor. J Biol Chem. 2009;284(5):3037-48. Epub 2008/12/06. doi: 10.1074/jbc.M807302200. PubMed PMID: 19056736.

329. Ouyang W, Lohning M, Gao Z, Assenmacher M, Ranganath S, Radbruch A, Murphy KM. Stat6-independent GATA-3 autoactivation directs IL-4-independent Th2 development and commitment. Immunity. 2000;12(1):27-37. Epub 2000/02/08. PubMed PMID: 10661403.

330. Usui T, Nishikomori R, Kitani A, Strober W. GATA-3 suppresses Th1 development by downregulation of Stat4 and not through effects on IL-12Rbeta2 chain or T-bet. Immunity. 2003;18(3):415-28. Epub 2003/03/22. PubMed PMID: 12648458.

331. Boirivant M, Fuss IJ, Chu A, Strober W. Oxazolone colitis: A murine model of T helper cell type 2 colitis treatable with antibodies to interleukin 4. J Exp Med. 1998;188(10):1929-39. Epub 1998/11/17. PubMed PMID: 9815270; PMCID: PMC2212414.

332. Ohtani K, Ohtsuka Y, Ikuse T, Baba Y, Yamakawa Y, Aoyagi Y, Fujii T, Kudo T, Nagata S, Shimizu T. Increased mucosal expression of GATA-3 and STAT-4 in pediatric ulcerative colitis. Pediatr Int. 2010;52(4):584-9. Epub 2009/12/25. doi: 10.1111/j.1442-200X.2009.03019.x. PubMed PMID: 20030749.

333. Laroui H, Sitaraman SV, Merlin D. Gastrointestinal delivery of anti-inflammatory nanoparticles. Methods Enzymol. 2012;509:101-25. Epub 2012/05/10. doi: 10.1016/B978-0-12-391858-1.00006-X. PubMed PMID: 22568903.

334. Misharin AV, Morales-Nebreda L, Mutlu GM, Budinger GR, Perlman H. Flow cytometric analysis of macrophages and dendritic cell subsets in the mouse lung. Am J Respir Cell Mol Biol. 2013;49(4):503-10. Epub 2013/05/16. doi: 10.1165/rcmb.2013-0086MA. PubMed PMID: 23672262; PMCID: PMC3824047.

335. Vanoirbeek JA, Rinaldi M, De Vooght V, Haenen S, Bobic S, Gayan-Ramirez G, Hoet PH, Verbeken E, Decramer M, Nemery B, Janssens W. Noninvasive and invasive pulmonary function in mouse models of obstructive and restrictive respiratory diseases. Am J Respir Cell Mol Biol. 2010;42(1):96-104. Epub 2009/04/07. doi: 10.1165/rcmb.2008-0487OC. PubMed PMID: 19346316.

336. Cruz MJ, Olle-Monge M, Vanoirbeek JA, Assialioui A, Gomez-Olles S, Munoz X. Persistence of respiratory and inflammatory responses after dermal sensitization to persulfate salts in a mouse model of non-atopic asthma. Allergy Asthma Clin Immunol. 2016;12:26. Epub 2016/05/26. doi: 10.1186/s13223-016-0131-3. PubMed PMID: 27222656; PMCID: PMC4878079.

337. Loots MA, Lamme EN, Zeegelaar J, Mekkes JR, Bos JD, Middelkoop E. Differences in cellular infiltrate and extracellular matrix of chronic diabetic and venous ulcers versus acute wounds. J Invest Dermatol. 1998;111(5):850-7. Epub 1998/11/06. doi: 10.1046/j.1523-1747.1998.00381.x. PubMed PMID: 9804349.

338. Miao M, Niu Y, Xie T, Yuan B, Qing C, Lu S. Diabetes-impaired wound healing and altered macrophage activation: a possible pathophysiologic correlation. Wound Repair Regen. 2012;20(2):203-13. Epub 2012/03/03. doi: 10.1111/j.1524-475X.2012.00772.x. PubMed PMID: 22380690.

339. Sindrilaru A, Peters T, Wieschalka S, Baican C, Baican A, Peter H, Hainzl A, Schatz S, Qi Y, Schlecht A, Weiss JM, Wlaschek M, Sunderkotter C, Scharffetter-Kochanek K. An unrestrained proinflammatory M1 macrophage population induced by iron impairs wound healing in humans and mice. J Clin Invest. 2011;121(3):985-97. Epub 2011/02/15. doi: 10.1172/JCI44490. PubMed PMID: 21317534; PMCID: PMC3049372.

340. Patel S, Maheshwari A, Chandra A. Biomarkers for wound healing and their evaluation. J Wound Care. 2016;25(1):46-55. Epub 2016/01/15. doi: 10.12968/jowc.2016.25.1.46. PubMed PMID: 26762498.

341. Couper KN, Blount DG, Riley EM. IL-10: The Master Regulator of Immunity to Infection. The Journal of Immunology. 2008;180(9):5771. doi: 10.4049/jimmunol.180.9.5771.

342. Baert F, Noman M, Vermeire S, Van Assche G, G DH, Carbonez A, Rutgeerts P. Influence of immunogenicity on the long-term efficacy of infliximab in Crohn's disease. N Engl J Med. 2003;348(7):601-8. Epub 2003/02/14. doi: 10.1056/NEJMoa020888. PubMed PMID: 12584368.

343. Levine AG, Arvey A, Jin W, Rudensky AY. Continuous requirement for the TCR in regulatory T cell function. Nat Immunol. 2014;15(11):1070-8. Epub 2014/09/30. doi: 10.1038/ni.3004. PubMed PMID: 25263123; PMCID: PMC4205268.

344. Mosser DM, Edwards JP. Exploring the full spectrum of macrophage activation. Nature Reviews Immunology. 2008;8(12):958-69. doi: 10.1038/nri2448.

345. Gordon S. The macrophage: past, present and future. Eur J Immunol. 2007;37 Suppl 1:S9-17. Epub 2007/11/01. doi: 10.1002/eji.200737638. PubMed PMID: 17972350.

346. Koch SD, Uss E, van Lier RA, ten Berge IJ. Alloantigen-induced regulatory CD8+CD103+ T cells. Hum Immunol. 2008;69(11):737-44. Epub 2008/09/30. doi: 10.1016/j.humimm.2008.08.281. PubMed PMID: 18822329.

347. Oderup C, Cederbom L, Makowska A, Cilio CM, Ivars F. Cytotoxic T lymphocyte antigen-4-dependent down-modulation of costimulatory molecules on dendritic cells in CD4+ CD25+ regulatory T-cell-mediated suppression. Immunology. 2006;118(2):240-9. Epub 2006/06/15. doi: 10.1111/j.1365-2567.2006.02362.x. PubMed PMID: 16771859; PMCID: PMC1782280.